Ministry of Higher Education
and Scientific Research
Diyala University
College of Science
Department of Chemistry

Removal of Eosin dye from aqueous solutions using Nano surfaces

A Thesis
Submitted to Council of the College of Science, University of
Diyala In Partial Fulfillment of the Requirements for the
Degree of Master in Chemistry Sciences
by

DONIA AHMED ABDULATEEF

B. Sc. in the Science Chemistry/ Diyala University 2015

Supervised by

Prof. Dr. Amir Fadhil Dawood
Assist. Prof. Dr. Ghalib Adris Atiya

2018 A.D 1439 A.H

بِسْمِ اللَّهِ الرَّحْمَنِ الرَّحِيم

وَلِيَعۡلَمَ ٱلَّذِينَ أُوتُواْ ٱلۡعِلۡمَ أَنَّهُ ٱلۡحَقُّ مِن رَّبِّكَ فَيُؤۡمِنُواْ بِهِۦ فَتُخۡبِتَ لَهُۥ قُلُوبُهُمۡۗ وَإِنَّ ٱللَّهَ لَهَادِ ٱلَّذِينَ ءَامَنُوٓاْ إِلَىٰ صِرَٰطٖ مُّسۡتَقِيمٖ ٥٤

صدق الله العظيم

(سورة الحج- الاية 54)

Certification

We certify that this thesis was prepared under our supervision at the university of Diyala / College of Science / Department of Chemistry as partial requirements for the Degree Master of Science in Chemistry.

Signature :

Name : Dr. Amir Fadhil Dawood

Title : Professor

Date : / / 2018

Signature :

Name : Dr. Ghalib Adris Atiya

Title : Assistant Professor

Date : / / 2018

Head of the Department of Chemistry

In view of the available recommendation, i forward this thesis for debate by the examining committee.

Signature :

Name : Dr.Ahmed Najem Abd

Title : Professor

Date : / / 2018

Scientific Amendment

I certify that the thesis entitled "**Removal of Eosin dye from aqueous solutions using Nano surfaces** " presented by (DONIA AHMED ABDULATEEF) has been evaluated scientifically; therefore, it is suitable for debate by examining committee.

Signature :

Name : Dr. Sameer. H. Kareem

Title : Assistant Professor

Date : / / 2018

Linguistic Amendment

I certify that the thesis entitled " **Removal of Eosin dye from aqueous solutions using Nano surfaces** " presented by (DONIA AHMED ABDULATEEF) has been corrected linguistically, therefore, it is suitable for debate by examining committee.

Signature :

Name : Nizar Hussein Wali

Title : Lecturer

Date : / / 2018

Examination Committee Discussion

We certify that we have read this thesis entitled **"Removal of Eosin dye from aqueous solutions using Nano surfaces"** and we examined the student "DONIA AHMED ABDULATEEF" on its content and in what is related with it, and in our opinion it meets the standard of a thesis for the degree of Master of Science in Chemistry.

Signature :
Name : Dr. Taki A. Himdan Ahmed
Title : Professor
Date : / / 2018
(Chairman)

Signature :
Name : Dr.Ahmed Najem Abd
Title : Professor
Date : / / 2018
(Member)

Signature :
Name : Dr. Abdullah. S. Khazeal
Title : Assistant Professor
Date : / / 2018
(Member)

Signature :
Name : Dr. Amir Fadhil Dawood
Title : Professor
Date : / / 2018
(supervisor)

Signature :
Name : Dr. Ghalib Adris Atiya
Title : Assistant Professor
Date : / / 2018
(supervisor)

Approved by the dean of the college of Science / University of Diyala.

Signature
Name: Dr. Tahseen H. Mubarak
Title: professor
Date: / / 2018

DEDICATION

To...

My parents, brothers, and sisters.

To my friends.

With

Love and Respect

Acknowledgment

First and foremost, I would like to thank Allah. And I would like to express my sincere gratitude to **Prof. Dr. Amir Fadhil Dawood** for suggesting the project, help, great support and valuable opinions throughout this research.

I also wish to express my special thanks to **Asst. Prof. Dr. Ghalib Adris Atiya** Dean of the College of education for pure Sciences, the University of Diyala for providing some advice in this research.

I am glad to acknowledge the staff of chemistry department in College of education for pure sciences /Diyala University especially the head of the Chemistry Department, **Asst. Prof. Dr. Fires Habeb Abdulrazzak** for their help and support during this research.

Exceptional thanks are stretched out to the Dean, Chairman, and the staff of the Chemistry Department, College of science, Diyala University for their help.

Finally, I wish to acknowledge the support and encouragement of my parent, brothers, and relatives during long days and weeks of work required for providing this research.

Donia2017

ABSTRACT

In this study, the nano – (ZnO) and (CuO) have been prepared via process of precipitation by means of the techniques (AFM, FTIR, XRD, SEM, BET) have been diagnosed. Moreover, the X - ray diffraction (XRD) has been used to characterize the crystallization of the nano – oxides. As for the size of particles, it has been calculated by using the Debye-Scherer's equation. Accordingly, the sizes of the (ZnO) and (CuO) are estimated at (23.4, 47.8) nano –meter respectively at the calcination temperature, i.e. 400 °C. This, however, fits in with the techniques (SEM, AFM, BET, and FTIR). To characterize the composition of oxides, the (SEM) as well as the (AFM) have been utilized. As for the surface area, it is estimated at (35, 635, and 6,704) m^2/g for oxides (ZnO and CuO) respectively.

The prepared nano – oxides have been used to remove the Eosin dye from its aqueous solutions. The research also touches upon the study of the factors affecting the process of adsorption. It involves the elementary effect of concentration for the dye, i.e. (2-20) ppm as well as pH (1-10) the equilibrium time (10- 140) minutes, the weight of the adsorbent is (0.09- 0.01) g at a temperature of (20 -40) °C.

The isotherms of adsorption, kinetics and thermodynamic functions of adsorption of the Eosin dye have been investigated at a fixed concentration (10) ppm. The typical weight of the adsorbent surface (0.04) g and pH (7) at variant temperatures (20 – 40) °C .The results show that the best equilibrium time for the surface CuO is (50) minutes and for the surface ZnO is (120) minutes . The percentage estimated for the removal of the Eosin dye has increased in proportion to the increase of the equilibrium time. This tantamount to the percentage of the Eosin pigment on the surface of CuO, i.e. (91 .05) while on the surface ZnO, it amounts to (40 .82%).

The results of effects of adsorption on the Eosin dye on the adsorbent surfaces have been analysed by using the isotherms by Langmuir, Freundlich, Dubinin Kaganer – Radushkevich and Temkin. These results have shown that there is a linear relation and high correlation co efficient for Dubinin's isotherm for the surface CuO. The isotherm of Freundlich, though, fits in with the surface ZnO. All this is done by taking into consideration the results being arrived at through the study of adsorption at variant temperatures.

The thermodynamic function values (ΔG, ΔH, ΔS) have been calculated through the application of Vant – Hoff's equation for the adsorption of the Eosin dye on the adsorption surfaces used. The negative values (ΔG) of the surface ZnO and CuO indicate that the adsorption takes place thermodynamically spontaneous. It is to be noted that (ΔH) values are negative for both surfaces. I.e. the adsorption is a exothermic and an indicator that the adsorption is physical as its values are less than 40 k g /mol. beside the values of ($E<8$) kg /mol indicate the fact that the physical forces affect adsorption whereas (ΔS) values are negative for the surface ZnO, i.e. the adsorbed particles of the Eosin dye align on the surface more than the solution. ΔS values are negative for the surface CuO, i.e. the particles are unbound and still in continuous motion on the surface.

A study of the Kinetics of adsorption by the application of the pseudo-first-order by using Langmuir's model as well as by the application of the pseudo –second –order has been conducted. The results have shown high correlation coefficients for the pseudo –second-order and an adsorption of the Eosin dye on both surfaces following the dynamicity of the pseudo-second –order.

List of Contents

No.	*Subjects*	Page
	Chapter One	
1	General Introduction	1
1.1	Pollution	1
1.3	Methods Treatment of Water Pollution	2
1.2.1	Chemical oxidation	2
1.2.2	Reverse osmosis	2
1.2.3	Ion exchange	3
1.2.4	Filtration	3
1.2.5	Adsorption	3
1.3	Types of Adsorption	5
1.3.1	Physical adsorption	5
1.3.2	Chemical adsorption	5
1.4	Factors Affecting on Adsorption	7
1.4.1	Nature of adsorbate	7
1.4.2	Nature of adsorbent	7
1.4.3	Temperature effect	8
1.4.4	Effect of pH	8
1.4.5	Solvent effect and Traube’s rule	9
1.4.6	Particle size of the adsorbent effect	10
1.4.7	Size of the pores	10
1.5	Nanomaterials	11
1.6	Zinc Oxide Nanoparticles (ZnO)	12

1.6.1	Crystal structure of ZnO nanoparticles	12
1.6.2	Chemical properties	13
1.7	Copper (II) oxide nanoparticles (CuO)	14
1.7.1	Crystal structure	15
1.8	Adsorption Isotherms	15
1.9	Theory of Adsorption	18
1.9.1	Langmuir isotherm	19
1.9.2	Freundlich isotherm	20
1.9.3	Dubinin-Kaganer-Radushkevich isotherm (DKR)	22
1.9.4	Temkin and pyzhev isotherm	23
1.10	Adsorption Kinetics	24
1.11	Thermodynamic Adsorption	25
1.12	Dyes	26
1.12.1	Acid dye	27
1.13	Literature Survey	30
1.14	The Aim of the Present Study	41

Chapter Two

2	Experiment study	42
2.1	Instruments	42
2.2	The Chemical Material	43
2.3	The Adsorbate	43
2.4	The Adsorbent	44
2.5	Preparation zinc oxide nanoparticles	44
2.5.1	Preparation of solution	44
2.5.2	Precipitation procedure	44
2.6	Preparation copper oxide nanoparticles	46

2.6.1	Preparation of solution	46
2.6.2	Precipitation procedure	46
2.7	Characterization of (ZnO ,CuO) nanoparticles	47
2.7.1	Fourier Transform Infrared Spectrophotometer (FT-IR)	47
2.7.2	X-ray diffraction (XRD)	47
2.7.3	The Surface area (BET)	48
2.7.4	The Scanning Electron Microscope (SEM)	49
2.7.5	Atomic Force Microscopy (AFM)	50
2.8	Preparation of Standard Solutions for Eosin dye	51
2.9	Determination of λmax and Calibration curve for Eosin dye	51
2.10	Optimum conditions for adsorption	53
2.10.1	Determination of Equilibrium Time	53
2.10.2	Determination of Adsorbent Weight	54
2.10.3	Study Effect of concentration adsorption	54
2.10.4	Adsorption Kinetics	55
2.10.5	Effect of temperature	55
2.10.6	Calculation of Thermodynamic function	56
2.10.7	Determination of Adsorption Isotherm	56
2.10.8	Effect of pH	57

Chapter Three

3.1	Characterization of ZnO and CuO Nanoparticles	58
3.1.1	Fourier transform infrared spectrum analysis (FTIR)	58
3.1.2	X-ray diffraction (XRD)	59
3.1.2.1	Structural XRD pattern of CuO nanoparticles	59
3.1.2.2	Structural XRD pattern of ZnO nanoparticles	61
3.1.3	The surface area (BET)	63

3.1.4	Scanning electron microscopy analysis (SEM)	64
3.1.4.1	SEM of CuO nanoparticles	64
3.1.4.2	SEM of ZnO nanoparticles	64
3.1.5	Atomic Force Microscopy (AFM)	65
3.2	Optimum conditions for adsorption	68
3.2.1	Determination of Equilibrium Time of adsorption	68
3.2.2	Adsorbent Weight	70
3.2.3	Study Effect of concentration on adsorption	72
3.2.4	Effect of pH	73
3.2.5	Effect of temperature on adsorption and calculation of thermodynamic functions	78
3.2.6	Adsorption Kinetics	83
3.2.7	Adsorption Isotherm	89
3.3	Conclusions	103
3.4	Recommendations	105
References		106

List of Figures

No.	*Subjects*	Page
Chapter One		
1.1	Shows the transmission of adsorption from physical to chemical with increasing the temperature. (1) Physical adsorption. (2) Chemical adsorption. (3) Transition region.	6
1.2	Traube's Rule a. Adsorption isotherm of fatty acids in aqueous solution on carbon. b. Adsorption isotherm of fatty acids in toluene on silica gel.	10
1.3	Hexagonal wurtzite structures of ZnO.	12

1.4	The crystal structure of CuO.	15
1.5	Giles classification of adsorption isotherms.	17
1.6	Classification Brunauer for adsorption.	18
1.7	(a) Langmuir isotherm. (b) The linear form of Langmuir isotherm	20
1.8	The linear relationship of Freundlich isotherm.	22

Chapter Two

2.1	Steps of process ZnO preparation.	45
2.2	Fourier transforms infrared spectrophotometer (FT-IR).	47
2.3	X-ray diffraction (XRD).	48
2.4	Surface area (BET).	49
2.5	Scanning electron microscope (SEM).	50
2.6	Atomic force microscopy (AFM).	51
2.7	The scan spectrum curve of Eosin dye.	52
2.8	The calibration curve for Eosin dye at the pH different and temperature 25 °C.	53

Chapter Three

3.1	FTIR spectra of ZnO nanoparticles.	58
3.2	FTIR spectra of CuO nanoparticles.	59
3.3	XRD pattern of CuO nanoparticles.	60
3.4	XRD pattern of ZnO nanoparticles.	62
3.5	SEM image of CuO nanoparticles.	64
3.6	SEM image of ZnO nanoparticles.	65
3.7	AFM images of CuO nanoparticles.	66

3.8	Particle size distribution of CuO nanoparticles.	66
3.9	AFM images of ZnO nanoparticles.	67
3.10	Particle size distribution of ZnO nanoparticles.	68
3.11	Effect of equilibrium time for adsorption of Eosin dye at temperature =25 ^{o}C and C_o=10 ppm on (a) CuO nanoparticles. (b) ZnO nanoparticles.	69
3.12	Effect of adsorbents weight on the adsorption of Eosin dye at temperature =25 ^{o}C; and C_o=10 ppm on (a) CuO nanoparticles. (b) ZnO nanoparticles.	71
3.13	Effect of adsorbates concentration on adsorption of Eosin dye at temperature =25 ^{o}C and C_o=10 ppm on (a) CuO nanoparticles. (b) ZnO nanoparticles.	73
3.14	Effect of pH on the adsorption of Eosin dye on CuO nanoparticles at 25 ^{o}C.	74
3.15	Effect of pH on the adsorption of Eosin dye on ZnO nanoparticles at 25 ^{o}C.	75
3.16	Effect of change the pH on the amount adsorbate of Eosin dye on (CuO, ZnO) nanoparticles at 25 ^{o}C.	77
3.17	Effect of temperature change on the adsorption of the Eosin dye on CuO nanoparticles.	79
3.18	The effect of temperature change on the adsorption of the Eosin dye on ZnO nanoparticles.	80
3.19	Values of greatest amounts adsorbed (ln X_m) for Eosin dye on (CuO, ZnO) nanoparticles at different temperatures (293-318 K).	81
3.20	The Pseudo-First Order Model of Eosin dye on CuO nanoparticles.	84
3.21	The Pseudo –Second Order Model of Eosin dye on CuO nanoparticles.	84
3.22	The Pseudo-First Order Model of Eosin dye on ZnO nanoparticles.	88
3.23	The Pseudo –Second Order Model of Eosin dye on ZnO nanoparticles.	88
3.24	Effect of temperature change on the adsorption of the Eosin dye on CuO nanoparticles.	90
3.25	Effect of temperature change on the adsorption of Eosin dye on ZnO nanoparticles.	91
3.26	Isotherm Langmuir for Eosin dye at different concentrations (2-20) ppm; and temperature (20, 25, 30, 35, 40) ^{o}C on CuO nanoparticles.	93

3.27	Isotherm Langmuir for Eosin dyes on ZnO nanoparticles at different temperature (20, 25, 30, 35, 40) °C.	94
3.28	Isotherm Freundlich for Eosin dyes at different concentrations and temperature on CuO nanoparticles.	95
3.29	Isotherm Freundlich for Eosin dyes at the different concentrations and temperature 25 °C on CuO nanoparticles.	96
3.30	Isotherm Freundlich for Eosin dyes at different concentrations and temperature on ZnO nanoparticles.	97
3.31	Isotherm Dubinin (DKR) for Eosin dyes at different concentrations and temperature on CuO nanoparticles.	98
3.32	Isotherm Dubinin (DKR) for Eosin dye at different concentrations and temperature on ZnO nanoparticles.	99
3.33	Isotherm Temkin for Eosin dye at different concentrations and temperature on CuO nanoparticles.	101
3.34	Isotherm Temkin for Eosin dye at different concentrations and temperature on ZnO nanoparticles.	102

List of Tables

No.	***Subjects***	**Page**
	Chapter One	
1.1	Properties of ZnO.	13
1.2	Properties of CuO.	14
1.3	Properties of Eosin dye.	29
	Chapter Two	
2.1	List of instruments.	42
2.2	Chemicals, purity and suppliers.	43
2.3	Chemical and physical properties of the Eosin dye.	43
2.4	Values of concentrations and absorbance for calibration curve at the pH different and temperature 25 °C.	53

Chapter Three

3.1	Strongest three peaks in XRD of CuO nanoparticles.	61
3.2	Strongest three peaks in XRD of ZnO nanoparticles.	63
3.3	Effect of equilibrium time for adsorption of Eosin dye at temperature =25 ^{o}C; and C_o=10 ppm on (CuO, ZnO) nanoparticles.	69
3.4	Effect of adsorbents weight on the adsorption of Eosin dye at temperature =25 ^{o}C and C_o=10 ppm on (CuO, ZnO) nanoparticles.	71
3.5	Effect of adsorbates concentration on adsorption of Eosin dye at temperature =25 ^{o}C; and C_o=10 ppm on (CuO, ZnO) nanoparticles.	72
3.6	Effect of pH on the adsorption of Eosin dye on CuO nanoparticles at 25 ^{o}C.	74
3.7	Effect of pH on the adsorption of Eosin dye on ZnO nanoparticles at 25 ^{o}C.	75
3.8	Effect of change the pH on the amount adsorbate of Eosin dye on (CuO, ZnO) nanoparticles at 25 ^{o}C.	77
3.9	Effect of temperature change on the adsorption of the Eosin dye on CuO nanoparticles.	79
3.10	Effect of temperature change on the adsorption of the Eosin dye on ZnO nanoparticles.	80
3.11	Values of greatest amounts adsorbed (ln X_m) for Eosin dye on (CuO, ZnO) nanoparticles at different temperatures (20-40 ^{o}C) and K.	81
3.12	Values of thermodynamic functions for adsorption Eosin dye on (CuO, ZnO) nanoparticles.	82
3.13	Values of the Pseudo-Second Order Model for adsorption of Eosin dye on CuO nanoparticles.	83
3.14	Adsorption Kinetics Constants of Eosin dye on CuO nanoparticles	85
3.15	Values of the Pseudo-Second Order Model for adsorption of Eosin dye on ZnO nanoparticles.	85
3.16	Adsorption Kinetics Constants of Eosin dye on ZnO nanoparticles	87
3.17	Effect of temperature change on the adsorption of the Eosin dye on CuO nanoparticles.	90

3.18	Effect of temperature change on the adsorption of the Eosin dye on ZnO nanoparticles.	90
3.19	Isotherm Langmuir for Eosin dye at different concentrations (2-20) ppm; and temperature (20-40) °C on CuO nanoparticles.	92
3.20	Isotherm Freundlich for Eosin dyes at different concentrations and temperature on CuO nanoparticles.	93
3.21	Isotherm Dubinin (DKR) for Eosin dyes at different concentrations and temperature on CuO nanoparticles.	95
3.22	Isotherm Temkin for Eosin dyes at different concentrations and temperature on CuO nanoparticles.	97
3.23	The calculated adsorption parameters of the four used isotherms for CuO nanoparticles.	98
3.24	Isotherm Langmuir for Eosin dye at different concentrations and temperature on ZnO nanoparticles.	99
3.25	Isotherm Freundlich for Eosin dyes at different concentrations and temperature on ZnO nanoparticles.	100
3.26	Isotherm Dubinin (DKR) for Eosin dyes at different concentrations and temperature on ZnO nanoparticles.	101
3.27	Isotherm Temkin for Eosin dyes at different concentrations and temperature on ZnO nanoparticles.	102
3.29	The calculated adsorption parameters of the four used isotherms for ZnO nanoparticles.	103

List of Abbreviation and Symbols

Abbreviations or symbols	***Full Name***
AFM	Atomic Force Microscopy
% Adsorption	Percentage adsorption
BET	Branuuer-Emmett-Teller
B	Constant which is related to the heat of adsorption
β	Constant related to the adsorption energy (mol^2/kJ^2)
C_e	Equilibrium concentration of solute (mg/L)
C_o	Initial concentration of solute (mg/L)
D	Crystallite size
ε	Polanyi potential which is related to the equilibrium concentration
FT-IR	Fourier Transform-Infra Red

ΔG	Free energy change
ΔH	Enthalpy change
K_T	Equilibrium binding constant (L/mg)
K_1	Rate constant of pseudo-first-order (min^{-1})
K_2	Rate constant of pseudo-second-order (g.mg-1min^{-1})
K	Constant of Van’t Hoff equation
K_F	Freundlich Constant
K_L	Langmuir equilibrium constant (L/mg)
λ_{max}	Maximum Absorbance
$\ln X_m$	Natural logarithm for greatest amount adsorbed (mg/g)
m	Mass of adsorbent (g)
n	Intensity of adsorption
θ	Diffraction angle
Q_e	Amount of solute adsorbed per unit weight of adsorbent (mg/g)
q_{max}	Maximum adsorption capacity (mg/g)
q_t	Amount of solute adsorbed per unit weight of adsorbent at any time (mg/g).
R	Universal gas constant
R^2	Correlation Coefficient
SEM	Scanning Electron Microscope
ΔS	Entropy change
UV-ViS	Ultra-Violet Spectrophotometer
$V_{sol.}$	Volume of solution (L)
XRD	X-Ray Diffraction

CHAPTER ONE

Introduction

1. General Introduction

1.1. Pollution

Pollution is a problem of the required knowledge of how to get rid of it; this problem is becoming more serious because of the obvious role which man plays in exacerbating [1].

One of its types is environmental pollution which includes soil pollution because of chemicals or acid rain [2]. As well as, this air pollution caused toxic volatile compound, and pollution of groundwater because of organic and inorganic compounds which leaked to the water.

Pollution of groundwater and wastewater, it also comes from public institutions [3]. Both have him bad and negative effects on human health, where it can cause diarrhea and many diseases [4].

The problem of environmental pollution is increasing in developing countries and advanced industrially and especially the problem of wastewater pollution and according to humanitarian and global organizations considered it a source of concern and from industries that increase pollution problem wastewater, are industries dye textile, leather, wood and plastic materials which use dyes to color their products many drinks of water is used, so it produces many colors in water of small amounts of dyes, this is very clear and undesirable [5].

The annual production of yarn dyes and textile is more than (8×106 tones) in a year (1990) of which (10%) they are discharged as liquid waste [6]. It was noted that many of these dyes are carcinogenic and toxic and cause birth defects [7].

The carcinogens are chemicals that cause cancer it is an abnormal growth in the organism, there are several ways to treat water pollution including reverse osmosis, ion exchange, chemical oxidation, filtration and adsorption which will be mentioned later, adsorption is easy, safe and effective in water treatment using activated carbon it is one of the adsorbents and the most widespread because carbon has a high porosity [8].

1.2. Methods of Treatment for Water Pollution

The purpose of treatment of contaminated water is the removal of contaminants and floats and make water content stable and free from contaminants and the pollution treatment process is divided into three stages are the primary treatment stage includes removal of easily separable materials such as oils, floating solids, or quickly settling solids and the secondary treatment stage are biological treatment such as biological filtration and the use of vital processes depend on the microorganisms such as a bacteria to analyze organic impurities and the two previous phases are incapable for remove dissolved organic matter so used the tertiary treatment stage it is an advanced stage of treatment on water produced by the secondary stage on a chemo-physical basis and reach to high quality and at lower cost [9]. The most important methods of water treatment are**:-**

1.2.1. Chemical oxidation

Chemical oxidation is a method for treating of the polluted water by oxidation using strong oxidants agents such as potassium permanganate, hydrogen peroxide, manganese dioxide [10] and ozone, oxidants agents are often treated with hydrated lime or caustic soda solution in order to precipitate mineral salts in the polluted water [11].

1.2.2. Reverse osmosis

Osmosis is a natural phenomenon in which water passes through a semipermeable (no solute flow) membrane from the side with lower solute concentration to the higher solute concentration side until equilibrium of solvent (water) chemical potential is restored. At equilibrium the pressure difference between the two sides of the membrane is equal to the osmotic pressure difference. To reverse the flow of water, a pressure difference greater than the osmotic pressure difference is applied; as a result, separation of water from solutions becomes possible. This phenomenon is termed reverse osmosis. It has also been termed hyperfiltration [12, 13].

1.2.3. Ion exchange

Ion Exchange is a chemical process where ion exchange occurs. This method relies on the use of resins (polymer easy to its penetrate or gel) to remove contaminated organic substances that ionic nature as well as to remove phosphorus and ammonia, it also uses zeolites, and clay in the ion exchange process [14] .The ion exchange process are affected by the values of each of the acidic function pH and temperature. This method is low despite the use of high capacity in selectivity and the removal of various materials and the reason is due to limited production on specific sources and as well high cost.

1.2.4. Filtration

Filtration is a description of a number of biological processes, mechanical and physical processes of through the separation of solids about liquid using porous membrane called the filter , and allowed for the liquid to pass through it , and solid materials are not allowed to pass. It was therefore used to remove unwanted material in wastewater [15].

1.2.5. Adsorption

Adsorption is one of the methods used in the treatment of industrial water pollution especially organic compounds, toxic compounds that cannot be separated in a way of liquidation such as filtration, sterilization and others. Adsorption is the phenomenon of the accumulation of atoms or molecules of matter on the surface of liquid or solid as a result of this accumulation will form a layer on the surface [16]. Adsorption can also be defined as the binding of atoms or molecules from a liquid or gas state on the solid surface is called the substance that is adsorbed, the (adsorbate) and the surface that adsorbs this substance is called (adsorbent) [17].The surfaces used in the adsorption it has high porosity and high surface area such as activated charcoal and zeolites [18] silica gel [19, 20] or zeolite complex – polymer urea formaldehyde [21]. In a bulk material, all the bonding requirements (be they ionic, covalent, or metallic) of the constituent atoms of the material are filled by other atoms in the material. However, atoms on the (clean) surface of the and therefore can attract adsorbents, such as what happens with the catalyst where activates the catalyst, reaction of materials on the surface of the adsorbent [22]. The process of adsorption for solution includes contact two surfaces of solid and liquid with each other, where be the liquid surface is pure or contains material one or more dissolved in it, the adsorption process is usually accompanied by a decrease in free energy (ΔG), and but that the process of adsorption will be spontaneous and gets decrease in entropy (ΔS) because restricted material on the surface and accompanied by a decrease in enthalpy (ΔH) according to the following **Equation (1.1)** [23].

$$\Delta G = \Delta H - T\Delta S \quad \text{.......} \quad (1.1)$$

Where

ΔG: Free energy change ($kJ.mol^{-1}$).

ΔH: Enthalpy change ($kJ.mol^{-1}$).

ΔS: Entropy change ($J.mol^{-1}. K^{-1}$).

T: Temperature in Kelvin.

There are two types of adsorption are physical adsorption and chemical adsorption. And reverse the adsorption process is desorption and it is a reverse process for adsorption where the atoms or molecules are separated from the solid surface. This process is accompanied by liberalization of energy resulting breaking the bonds and return it to the system, it can be a rate of operation desorption an appropriate guide to know the type of interference between the adsorbate and the adsorbent.

1.3. Types of Adsorption

Adsorption can be classified .It based on type of correlation between atoms or molecules or ions the adsorbate on the surface of the absorbent into two types, namely:-

1.3.1. Physical adsorption

In physisorption or physical adsorption is associated the molecules or atoms or ions the adsorbate with the surface of the adsorbent by Vander Waals forces (weak intermolecular). Adsorption occurs on the surface in this type of through the natural forces of attraction along the lines of the forces causing the diffraction of real gases about the ideal laws that are on the pattern of forces that cause liquefying gases. This type of adsorption can occur at temperatures less than boiling point the adsorbate where the heat of adsorption estimated (25 $KJ.mol^{-1}$) and needs to energy low activation. It notes in this type of adsorption that there are no selective in material selection, and in this type of adsorption, the adsorbed layer can be removed by raising temperatures. It is said that the process is reversible and be adsorption a number of layers and the surfaces which happens on it such as this type of adsorption be inert because of electronic saturation for its atoms [24].

1.3.2. Chemical adsorption

In chemical adsorption is associated the molecules or atoms or ions the adsorbate with the surface of the adsorbent by chemical bonds unlike the Vander Waals forces causing physical adsorption. This adsorption is the first step in the chemical reaction so it needs energy high activation and need the adsorbate (chemical adsorption) to fixed activation energy for the surface of the homogenized, can vary the activation energy value from one location to another on the surface of adsorbent its same, when it is non-homogeneous in energy, this type of adsorption occurs at temperatures higher than the boiling point the adsorbate and the adsorption temperature is estimated (80 $KJ.mol^{-1}$) [25]. This type of adsorption is characterized by specificity, as it happens under a certain conditions of temperature and certain pressure. It is noted here that the adsorbed layer can’t be removed, that means the process is irreversible. Adsorption is monolayer and the surfaces obtained by adsorption are active because of the none its saturation electronically.

The temperature can play an important role in adsorption; physical adsorption can occur at low temperatures and turn into chemical adsorption at high temperature, as the case of hydrogen gas adsorption on the surface of nickel metal, and is shown in **Figure (1.1)** [26].

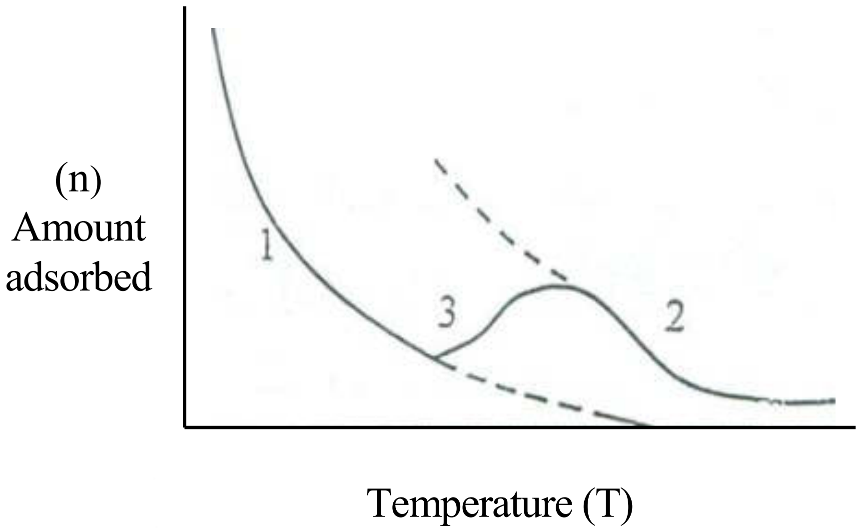

Figure (1.1): *Shows the transmission of adsorption from physical to chemical with increasing the temperature.* ***(1)*** *Physical adsorption.* ***(2)*** *Chemical adsorption.* ***(3)*** *Transition region [26].*

1.4. Factors Affecting on Adsorption

1.4.1. Nature of adsorbate

Adsorption is affected by the nature of the adsorbate when interference between the adsorbent surface and adsorbate particles, it affected by the nature, size and the concentration of the adsorbate, on the polar group and increasing the weight of the molecules and that interference difference between the adsorbent surface and adsorbate particles at the surface makes from the adsorption process selective as it has been concluded that the vacuum structure for the adsorbate had a clear effect on the orientation on the surface [27]. As noted (Robert Thomas) that the pesticide (Baraqut) has scalability adsorption high on clays compared to other pesticides this was interpreted on this high polar for (Baraqut) which gives organic ions cation have a high tendency to correlation with the clays surfaces negatively charged [28].

1.4.2. Nature of adsorbent

Play the characteristics or nature of the adsorbent such as chemical composition and dimensions of the pores and the distribution charge an important role in adsorption [29].The effect of the porosity for the adsorbent depends on the relationship between the dimensions the pores adsorbent [30]. It is noted that the increase in the surface area will increase number of adsorption sites on the surface and thus increasing the capacity the adsorption, adsorption is affected by the surface polarity and the charge distribution where observed (Sparkman) that the amount of adsorption of most organic compounds on a surface (α - Alumina) higher compared to the surface (silica) and (kaolin) and this is because the alumina surface positively charged either the surface of clay and silica they are negatively charged [31].

1.4.3. Temperature effect

Affected each of type adsorption and the nature of both adsorbent and adsorbate by the temperature, and as previously mentioned can knowledge the type of adsorption by the temperature. The physical adsorption occurs at low temperatures while chemical adsorption needs high temperatures, and the adsorption is reduced or increased with temperature depending on the type of interference forces between the adsorbate molecules and the surface molecules adsorbent. And the process of adsorption can be endothermic [32] so increasing the system temperature leads to an increase quantity (Q_e) adsorption and usually adsorption process is exothermic by relying on the principle of (Le-chateliers) low the system temperature leads to increased concentration (C_e) adsorption such as the physical adsorption [33].

1.4.4. Effect of pH

Effect of pH is the measurement that determines whether the liquid is acidic, basic or neutral. The liquids that $pH < 7$ acids, and the liquids that $pH > 7$ alkaline solutions or bases either $pH = 7$ be neutral and is equal to acidic the water pure at 25 °C. Can knowledge the acidic degree for any solution by using the pH indicator. That the increase or decrease of the acidic function has a clear effect on adsorption and this effect varies depending on the adsorption system. The changes in acidic function lead to an increase solubility the adsorbate molecules reduce the amount of adsorption unlike the changes that result in a decrease in the solubility the adsorbate molecules .There are several changes have a role in the process of acidic function change is the nature of the chemical sites for the adsorbent surface, and the adsorbate as well as solvent the chemical situation lead to the weakening or strengthening of adsorption [34].

1.4.5. Solvent effect and Traube's rule

The effect of the solvent is the important factor in the control on the extent of adsorption where the solvent interfere with the solute in the solution, also interferes the solvent with the adsorbent surface, the interference depends on the chemical composition of both of them and the solvent is interfere with the dissolved material in the layer the adsorbate on the adsorbent surface. Generally, an inverse relationship between the extent of adsorption of a species and its solubility in the solvent used. When other effect is not present, for a given solvent, the less soluble solutes are generally more strongly adsorbed than the more soluble solute [35]. The rule is that polar adsorbent will preferentially adsorb the more polar component of a non-polar solvent; polarity is used here in the general sense of ability to engage hydrogen bonding or dipole-dipole type interactions as opposed to nonspecific dispersion interactions. A semi-quantitative extension of the above is known as Traubel's rule, which was given by Freundlich states "The adsorption of an organic substance from aqueous solution increase strongly and regularly as the homologous series is ascended".

Data illustrating Traube's rule is shown in **Figure (1.2a)** in which it is seen that the quantity adsorbed on carbon from aqueous solution increase in the following order**:-**

Butyric acid > propionic acid > acetic acid > formic acid.

The reverse sequence was indeed observed in **Figure (1.2b)** for fatty acids adsorbed on a polar adsorbent (silica gel) from non-polar solvent (toluene). In addition, this reversal occurred with silica gel even if aqueous solutions were used [36].

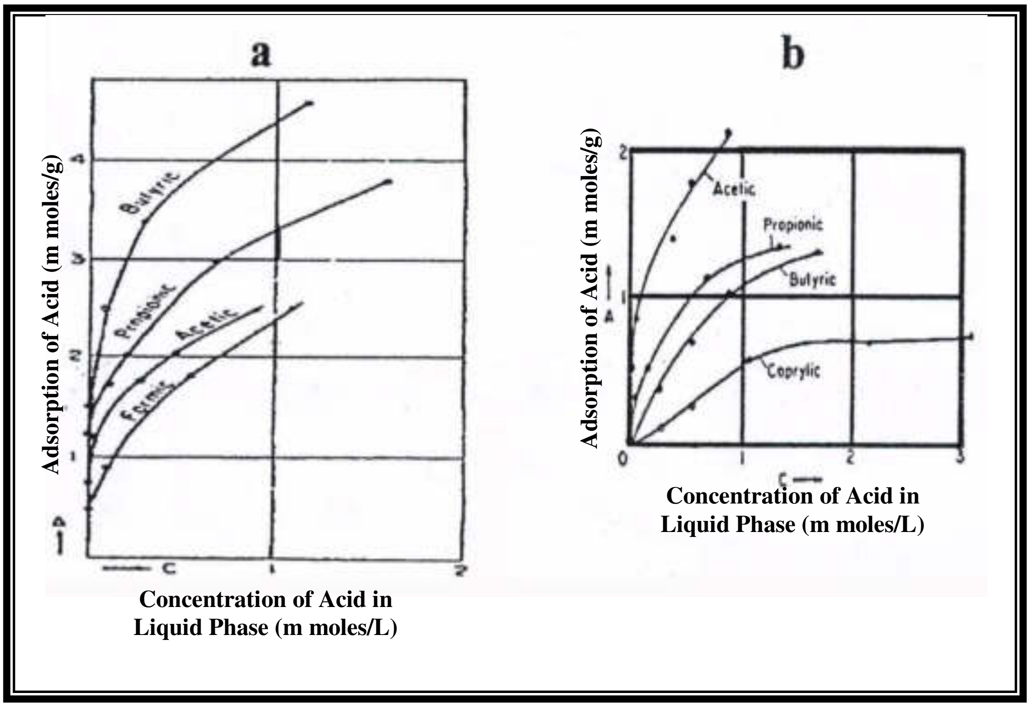

Figure (1.2): *Traube's Rule*

a. *Adsorption isotherm of fatty acids in aqueous solution on carbon.*

b. *Adsorption isotherm of fatty acids in toluene on silica gel [36].*

1.4.6. Particle size of the adsorbent effect

The penetration of large molecules is different from the penetration of small molecules where affects the size of molecules the adsorbent on the adsorption process .The adsorbent surface area increases whenever they are the molecules are small and thus lead at increase adsorption [37].

1.4.7. Size of the pores

The size of the molecule with respect to size of the pores. Large molecules may be too large to enter small pores. This may reduce adsorption independently of other causes [38].

1.5. Nanomaterials

Nano material is defined as a physical substance with one dimension at the lowest between (1-100 nm), (1nm=10^{-9} m) have received considerable interest because of the unique properties different from their bulk counterparts [39].

Nanomaterials research takes a materials science based approach to nanotechnology, leveraging advances in materials metrology and synthesis which have been developed in support of micro fabrication research. Materials with structure at the nanoscale often have unique optical, electronic, or mechanical properties [40]. They are slowly becoming commercialized [41] and beginning to appear as commodities [42]. Inorganic nanomaterial's such as quantum dots, nanowires and nanorods because of their interesting optical and electrical properties, could be used in optoelectronics [43].

Nanparticles or Nancrystals made of metals, semiconductors, or oxides are of particular interest for their mechanical, electrical, magnetic, optical, chemical and other properties [44, 45]. They have been used as quantum dots and as chemical catalysts such as nonmaterial based catalysts, lately, a range of nanoparticles are extensively investigated for biomedical applications including tissue engineering, drug delivery, and biosensor [46]. Nanoparticles can exhibit size-related properties significantly different from those of either fine particles or bulk materials [47].

1.6. Zinc Oxide Nanoparticles (ZnO)

Zinc oxide is a new types of inorganic materials its formula (ZnO). It appears as a white powder, approximately insoluble in water. The powder is extensively used as an additive in numerous substance and products inclusive of rubbers, plastics, ceramics, glass, cement, and lubricants [48]. ZnO is a wide band gap semiconductor of the (II-VI) semiconductor group. The native doping of the semiconductor due to oxygen vacancies or zinc interstitials is (n-type). This semiconductor has several favorable properties, including good transparency, high electron mobility, wide band gap, and strong room-temperature luminescence. Those properties are valuable in emerging applications for the transparent electrodes in liquid crystal displays, energy saving or heat protecting windows, and electronics as thin-film transistors and light emitting diodes [49].

1.6.1. Crystal structure of ZnO nanoparticles

Zinc oxide crystallizes have three forms:-

- Hexagonal wurtzite.
- Cubic zincblende.
- Cubic rock salt

The wurtzite structure is most stable and thus most common at ambient conditions [50], and is shown in **Figure (1.3)**.

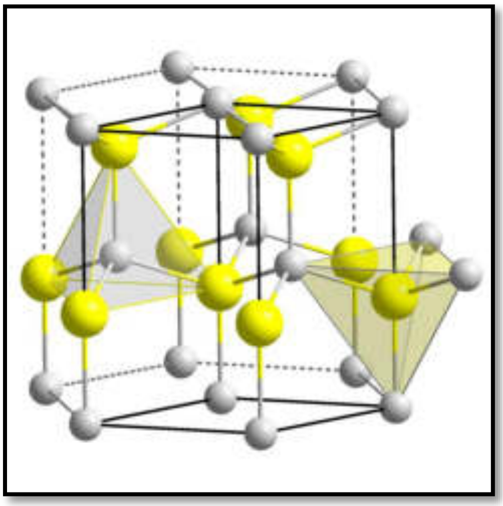

Figure (1.3): *Hexagonal wurtzite structures of ZnO [51].*

In this hexagonal wurtzite structure has a point group (C_{6v}) and the space group is (C_{6v}^{4}) or ($P6_3 mc$) with two lattice constants are a = 3.25 Å and c = 5.2 Å. The ratio of c/a is 1.60, close to the ideal value 1.633 for a hexagonal unit cell [52]. Either the bonding in ZnO is greatly ionic ($Zn^{2+}– O^{2−}$), and which interpret its strong piezoelectric. Because of this iconicity, zinc and oxygen planes hold electric charge (positive and negative, respectively). So to maintain electrical neutrality, those plane reconstruct at atomic level in most relative materials, however not in ZnO, its surfaces are atomically flat, stable and exhibit no reconstruction. This anomaly of ZnO is not fully interpreting [53].

1.6.2. Chemical properties

Zinc oxide be as the white powder usually known as white zinc and which the mineral usually contains a certain amount of manganese and other pollutant that give a yellow to red color [54]. Crystalline zinc oxide is thermo-chromic where changing from white to yellow when heated and in air reverting to the white on cooling [55]. This color change is caused by a small loss of oxygen to the environment at high temperatures to form the non stoichiometric $Zn_{1+x}O$, where at 800 °C, x = 0.00007 [56]. **Table (1.1)** shows ZnO properties.

Table (1.1): *Properties of ZnO [57].*

Molecular formula	**ZnO**
Molar mass	**81.408 g/mol**
Appearance	**White solid**
Odor	**Odorless**
Density	**5.606 g/cm^3**
Melting point	**1975 °C (decomposes)**
Boiling point	**2360 °C**
Solubility in water	**0.16 mg/100 ml at (30°C)**
Band gap	**3.3 eV (direct)**
Refractive index (nD)	**2.0041**

1.7. Copper (II) oxide nanoparticles (CuO)

Copper (II) oxide or cupric oxide is the inorganic compound with the formula CuO. It appears as a black to brown powder, and it is of stable copper oxides. As a mineral, it is known as tenorite and paramelaconite. Copper (II) oxide is a p-type semiconductor, with a narrow band gap of (1.2 eV). It is a product of copper mining and the precursor to many other copper containing products and chemical compounds, as a significant product of copper mining. Cupric oxide (CuO) is used as a pigment in ceramics to produce blue, red, and green, and sometimes gray, pink, or black glazes and can be it used to produce dry cell batteries [58]. It be insoluble in water and no in the bases and can get it from the oxidation of metallic copper [59]. There are two types of copper oxide: copper (I) oxide and copper (II) oxide. CuO and Cu_2O materials are known to be (p-type) semiconductors in general and hence potential useful for constructing junction devices such as junction diodes [60]. **Table (1.2)** shows CuO properties.

Table (1.2): *Properties of CuO [61].*

Molecular formula	**CuO**
Molar mass	**79.545 g/mol**
Appearance	**black to brown powder**
Melting point	**1326 °C**
Boiling point	**2000 °C**
Solubility in water	**Insoluble**
Band gap	**1.2 eV (direct)**
Refractive index (nD)	**2.63**

1.7.1. Crystal structure

Copper (II) oxide belongs to the monoclinic crystal system, with a crystallographic point group of 2/ m or C_{2h}. The space group of its unit cell is C_2/c, and its lattice parameters are a = 4.6837, b = 3.4226, c= 5.1288, α = 90°, β = 99.54°, γ = 90°. The copper atom is coordinated by 4 oxygen atoms in an approximately square planar configuration [62] as shown in **Figure (1.4)** below.

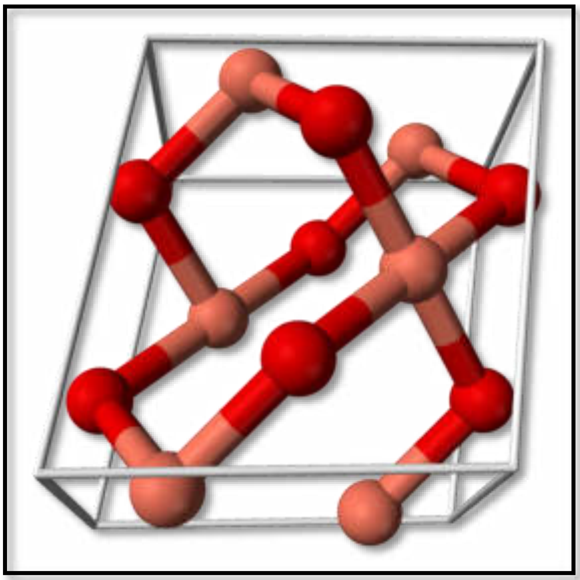

Figure (1.4): *The crystal structure of CuO [63].*

1.8. Adsorption Isotherms

Adsorption isotherms is designed to measure the concentration of the adsorbate in the medium before and after adsorption, at a fixed temperature which represents the relationship between the amount of the adsorbate at a certain surface and concentration of the material or the pressure of the adsorbate at equilibrium by fixed temperature to study the interaction between the adsorbate and the surface of the adsorbent and to know about the structure of the adsorbed layer [64], it is measured isotherms by drawing between the amount of the solute adsorbate on the solid surface and the concentration of solute at equilibrium [65], and the solute concentration at equilibrium or (equilibrium concentration) is the solute concentration in the liquid phase after reaching the equilibrium with solid surface connected to it [66]. Adsorption isotherms by the world Giles, was classified as in the **Figure (1.5)** to (S.L.H.C) by depending on their initial sections plotted when the solution is very dilute. These classes include subclasses (1, 2, and 3 to the max) by depending on the increase in the solute concentration.

Giles tried to explain the mechanism of adsorption and how to guide the molecules of the adsorbate and other factors affecting adsorption and interpretation as follows**:-**

i. **S-curves,** indicative of vertical or flat orientation of adsorbed, there is strong inter-molecular attraction within the adsorbed layer, and the adsorbate is monofunctional. In the initial part of an S-curve, the more solute is already adsorbed, the easier it is for additional amounts to become fixed.
ii. **L-curves,** where the sites are few and widely separated and a monolayer adsorption is formed, so as this type refers to as normal Langmuir isotherms indicative of molecules adsorbed flat on the surface like carbon series or cyclic hydrocarbons. The solute is adsorbed; the harder it is for additional amounts to become fixed.
iii. **H-curves,** is that attained when there is high adsorption affinity as in the case of high molecular weight compounds like: proteins and polymer, this isotherm can be observed even if the solution is very dilute..
iv. **C-curves,** constant-partition linear curves given by substances, which penetrate into the adsorbent more readily than the solvent does [67, 68].

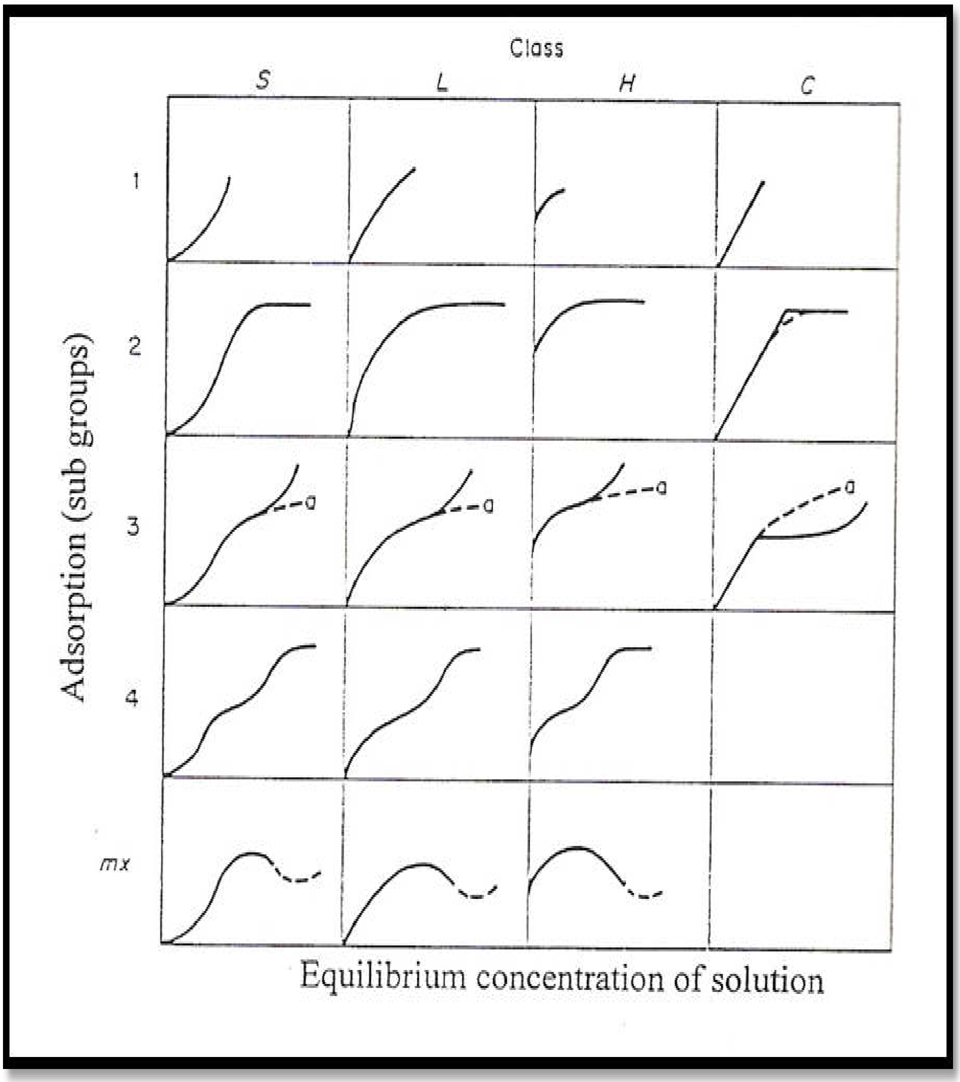

Figure (1.5): *Giles classification of adsorption isotherm.*

Brunauer class and his group [69] adsorption isotherms to five classes as illustrated in **Figure (1.6)**, the class (I) it is the adsorption of the type (L) according to classification Giles, either the class (II) it is according to what is expected from the approximation (B.E.T) when multi-layer adsorption occurs which often occurs when adsorption of gases, indicating that adsorption is nearing infinity when gas intensification begins.

Either the class (III) notes when there is an interfere between the second layer and the first layer, and the class (IV) it is similar to a class (I) but there are two limits to the amount of adsorbate instead of a single limit.

And the class (V) is between the two classes (I, II) .The chemical adsorption occurs within the class (I) only physical adsorption occurs in any one of the classes four other.

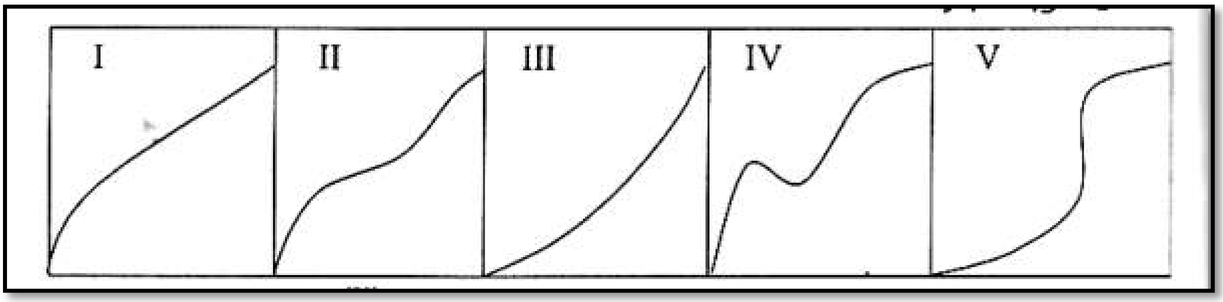

Figure (1.6): Classification Brunauer for adsorption.

1.9. Theory of Adsorption

The adsorption of molecules can be described by the following chemical reaction:

$$A + B \rightarrow A.B \quad \ldots\ldots (1.2)$$

Where (A) is the adsorbate, (B) is the adsorbent and (AB) is the adsorbed compound. Adsorbates are associated on the surface by different types of chemical forces such as Van der Waals forces, dipole-dipole interactions and hydrogen bonds. The molecules continue to accumulate on the surface until the rate of the forward reaction (adsorption) equals the rate of the reverse reaction (desorption). When this condition exists, equilibrium has been reached [70], this kind of technique to know concentration of adsorbate and to know mass of adsorbent. After the arrival of the solution and the solid surface to equilibrium, (at a constant temperature) and know ratio solid to solution then measure the solution concentration from the difference between the initial concentration and final equilibrium concentration to the solution volume and assumed to be the amount of adsorption per unit mass of adsorbent as in the **Equation (1.3)** [71]:-

$$Q_e = \frac{C_o - C_e}{m} . V_{sol.} \quad \ldots\ldots (1.3)$$

Q_e: Amount of solute adsorbed per unit weight of adsorbent (mg/g).

C_e: Equilibrium concentration of solute (mg/L).

$V_{sol.}$: Volume of solution (L).

m: Mass of adsorbent (g).

C_o: Initial concentration of solute (mg/L).

1.9.1. Langmuir isotherm

The basis of progress the theory associated with the adsorption phenomenon had passed in (1916) when he proposed to Langmuir an equation to explain the adsorption of the type (L) according to classification Giles. It is supposed to occur adsorption for monomolecular on surface of adsorbent to exclude occurrence of interactions between minutes the adsorbed in low coverage for surface, the adsorbate quantity increases rapidly at first and then gradually stabilizes due to increased coverage on surface, and active site occupancy and increased competition for remaining sites. The Langmuir model assumes that molecules chemically adsorb on fixed number of well-known sites on the surface of adsorbent, these sites be equivalent in energy. Each site holding one molecule of adsorbate only and adsorbed molecules on the adsorbent surface do not interfere with one another or with other molecules in solution. Thus, monolayer of the adsorbed molecule will form on the adsorbent surface and represent the following by **Equation (1.4) or (1.5)** [72]:-

$$\frac{C_{eq}}{q_{eq}} = \frac{1}{bQ} + \frac{C_{eq}}{Q} \quad \dots\dots\dots\dots\dots\dots\dots\dots\dots\dots\dots\dots\dots\dots (1.4)$$

or

$$\frac{C_e}{Q_e} = \frac{1}{q_{max}k_L} + \frac{C_e}{q_{max}} \quad \dots\dots\dots\dots\dots\dots\dots\dots\dots\dots\dots\dots\dots (1.5)$$

This is the **Equation** for the Langmuir isotherm [73].

Where

Q_e: Amount of solute adsorbed per unit weight of adsorbent (mg/g).

C_e: Equilibrium concentration of solute (mg/L).

q_{max}: Maximum adsorption capacity (mg/g).

K_L: Langmuir equilibrium constant (L/mg).

The parameter $\mathbf{q_{max}}$ and $\mathbf{K_L}$ can be found by plotting ($\frac{C_e}{Q_e}$) versus (C_e) which yields a straight line with a slope of ($\frac{1}{q_{max}}$) **and an intercept of** ($\frac{1}{q_{max K_L}}$) as in **Figure (1.7)**.

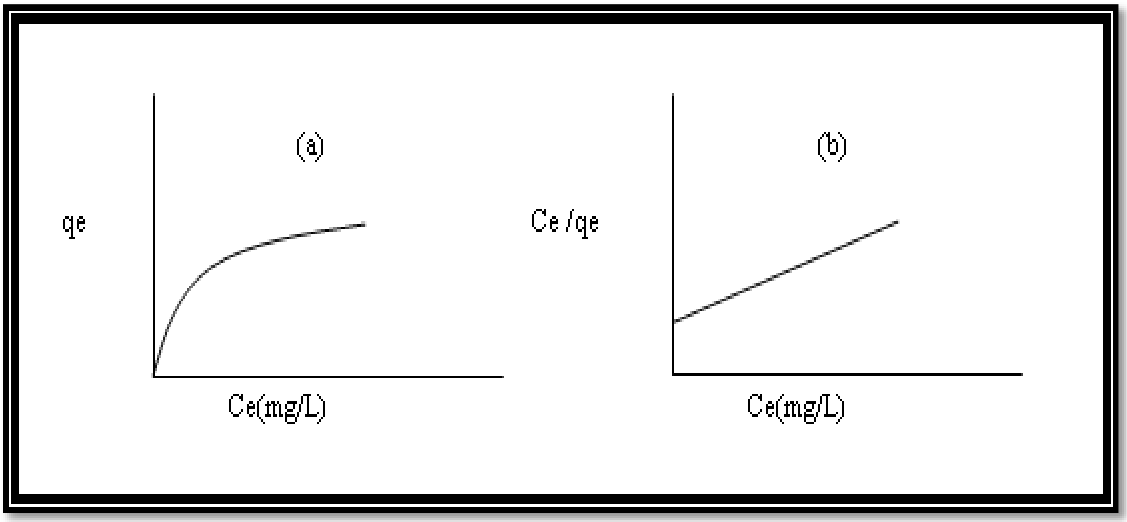

Figure (1.7):

(a) Langmuir isotherm.

(b) The linear form of Langmuir isotherm.

1.9.2. Freundlich isotherm

Place the Freundlich isotherm represent the change in the amount adsorbate on the unit area or the mass of adsorbent with equilibrium concentration. Freundlich, a German physical Chemist, presented adsorption isotherm for non-ideal system [74]. In the derivation of Langmuir isotherm, it has been assumed that there is independence and similarity in binding energy at each adsorption site this linear relationship is obeyed by many but not all adsorbates at low concentration [75].

In (1926), Freundlich had proposed an empirical equation for adsorption in solution; his proposal was based on the experimental measurements. Freundlich adsorption isotherm equation may be derived assuming a heterogeneous surface with adsorption on each class of sites obeying the Langmuir equation [76].the heterogeneous adsorption sites have different potential energies and different geometrical shapes on the surface, so the affinity from site to site toward the same molecule is different [77]. Freundlich proposed that such isotherm could be represented by **Equations (1.6), (1.7):-**

$$\frac{X}{m} = K_F(C_e)^{1/n} \quad \ldots\ldots\ldots\ldots\ldots\ldots\ldots\ldots\ldots (1.6)$$

$$Q_e = \frac{X}{m}$$

$$Q_e = K_F(C_e)^{1/n} \quad \ldots\ldots\ldots\ldots\ldots\ldots\ldots\ldots\ldots (1.7)$$

$K_{F,}$ n are the constants Freundlich which depend on the nature both of adsorbate, adsorbent surface and the temperature [78]. It has been shown mathematically that n can be regarded as a measure of heterogeneity of adsorption sites [79].

For example, surface site heterogeneity increases as n approaches 0 [80]. When; n > 1, bond energies increase with surface density; n < 1, bond energies decrease with surface density; and n=1, all surface sites are equivalent [81].

The adsorption energy is decrease logarithmically whenever the covered surface increased, but in the Langmuir equation, the adsorption energy is uniform and independent of surface area and it **Equations (1.8), (1.9):-**

$$\ln Q_e = \ln K_F + \frac{1}{n}\ln C_e \quad \ldots\ldots\ldots\ldots\ldots\ldots\ldots\ldots\ldots (1.8)$$

$$\log Q_e = \log K_F + \frac{1}{n}\log C_e \quad \ldots\ldots\ldots\ldots\ldots\ldots\ldots\ldots\ldots (1.9)$$

Also influenced by the behavior of the constants Freundlich by the electric double layer and the amphoteric behavior of the surface . The Freundlich equation does not predict the maximum value of the capacity of adsorption and plot $\ln Q_e$ against $\ln C_e$, a straight line is obtained with slope equals $1/n$, and the intercept equals $\ln K_F$ as in **Figure (1.8)** [82].

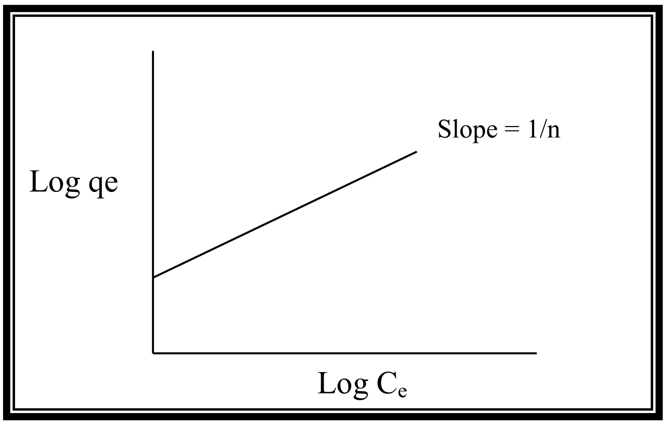

Figure (1.8): *The linear relationship of Freundlich isotherm*

.

1.9.3. Dubinin-Kaganer-Radushkevich isotherm (DKR)

This isotherm is more important from Langmuir and Freundlich on the surface is heterogeneous [83, 84] and it **Equation (1.10)**.

$$\ln Q_e = \ln q_{max} - \beta\varepsilon^2 \quad \ldots\ldots\ldots\ldots\ldots\ldots\ldots\ldots\ldots\ldots \quad (1.10)$$

Q_e: Amount of solute adsorbed per unit weight of adsorbent (mg/g).

q_{max}: maximum adsorption capacity (mg/g).

β: A constant related to the adsorption energy (mol^2/kJ^2).

ε: Polanyi potential which is related to the equilibrium concentration as **Equation (1.11):-**

$$\varepsilon = RT\ln\left(1 + \frac{1}{C_e}\right) \quad \ldots\ldots\ldots\ldots\ldots\ldots\ldots\ldots\ldots\ldots \quad (1.11)$$

R: Universal gas constant ($8.314.10^{-3}$ KJ $mol^{-1}K^{-1}$).

T: Temperature in Kelvin [85].

The main energy of adsorption **E** is calculated by using the following **Equation (1.12)** [86]:

$$\mathbf{E} = (-2\boldsymbol{\beta})^{0.5} \quad \ldots\ldots\ldots\ldots\ldots\ldots\ldots\ldots\ldots\ldots\ldots\ldots\ldots\ldots\ldots\ldots\ldots\ldots\ldots\ldots\ldots\ldots\ldots\ldots\ldots\ldots\ldots\ldots\ldots\ldots\ldots\ldots\ldots\ldots\ldots\ldots\ldots (\mathbf{1.12})$$

The energy equation gives us a perception of the adsorption mechanism, E < 8 KJ /mol indicates that the physical forces influence adsorption and that E> 16 KJ/mol indicates the spread of molecules and when **E** is between (8-16) indicates that adsorption is directed by chemical ion exchange.

1.9.4. Temkin and Pyzhev isotherm

This isotherm assumes that the adsorption heat for all layers is linearly reduced with increasing coverage because of the interfere the adsorbate and the adsorbent surface. Adsorption is characterized by the uniform distribution of the bond energy and the following **Equation (1.13):-**

$$\mathbf{Q_e = Bln(K_T.C_e)} \quad \ldots\ldots\ldots\ldots\ldots\ldots\ldots\ldots\ldots\ldots\ldots\ldots\ldots\ldots\ldots\ldots\ldots\ldots\ldots\ldots\ldots\ldots\ldots\ldots\ldots\ldots\ldots\ldots\ldots\ldots\ldots (\mathbf{1.13})$$

And **Equation (1.14)** for Temkin isotherm is [87]**:-**

$$\mathbf{Q_e = BlnK_T + BlnC_e} \quad \ldots\ldots\ldots\ldots\ldots\ldots\ldots\ldots\ldots\ldots\ldots\ldots\ldots\ldots\ldots\ldots\ldots\ldots\ldots\ldots\ldots\ldots\ldots\ldots\ldots\ldots\ldots\ldots\ldots\ldots (\mathbf{1.14})$$

B= $\frac{\mathbf{R.T}}{\mathbf{b}}$ **:** Constant which is related to the heat of adsorption.

R: Universal gas constant ($8.314.10^{-3}$ J mol^{-1} K^{-1}).

T: Temperature at 293, 298, 303, 308 and 318 K.

B: Variation of sorption energy (J/mol).

K_T: Equilibrium binding constant (L/mg).

Q_e: Amount of solute adsorbed per unit weight of adsorbent (mg/g).

C_e: Equilibrium concentration of solute (mg/L).

1.10. Adsorption Kinetics

Adsorption kinetic is to describe the rate of the amount of the adsorbate and it is clear that this rate is the controlling step [88]. In (1898) Largergreen [89] suggested a pseudo first order equation for the adsorption of a liquid/solid system based on the solid capacity. This model supposed that the change rate for adsorption the solute with time is directly proportional with the difference in saturated concentration and solids adsorption with time [90].

The Pseudo- first order is described by the following **Equations (1.15):-**

$$\frac{d_{q_t}}{d_t} = K_1(q_e - q_t) \quad \dots\dots\dots\dots\dots\dots\dots\dots\dots\dots\dots\dots\dots\dots\dots\dots\dots.\dots\dots\dots\dots\dots\dots\dots\dots (1.15)$$

When t = 0 to t = t and qt = 0 to qt = qt the **Equation (1.16)** becomes**: -**

$$\ln(q_e - q_t) = \ln q_e - K_1 t \quad \dots\dots\dots\dots\dots\dots\dots\dots\dots\dots\dots\dots\dots\dots\dots\dots\dots\dots\dots\dots\dots\dots (1.16)$$

q_t: Amount of solute adsorbed per unit weight of adsorbent at any time (mg/g).

q_e: Amount of solute adsorbed per unit weight of adsorbent (mg/g).

K_1: Rate constant of pseudo-first-order (min^{-1}).

When plotting **$\ln(q_e$-$q_t)$** versus t can get the slope on **K_1** and from the intersection on **$\ln q_e$.**

The pseudo-second order is described by the following **Equations** [91, 92].

When t = 0 to t = t and qt = 0 to qt = qt the **Equation (1.17)** becomes**: -**

$$\frac{1}{q_e - q_t} = \frac{1}{q_e} + K_2 t \quad \dots\dots\dots\dots\dots\dots\dots\dots\dots\dots\dots\dots\dots\dots.\dots\dots\dots\dots\dots\dots\dots\dots\dots (1.17)$$

In the order of the last **Equation (1.18)** becomes**:**

$$\frac{t}{q_t} = \frac{1}{K_2\, q_e{}^2} + \frac{1}{q_e} t \quad \ldots\ldots\ldots\ldots\ldots\ldots\ldots\ldots\ldots\ldots\ldots\ldots\ldots\ldots\ldots\ldots\ldots\ldots\ldots\ldots\ldots\ldots (1.18)$$

If the initial adsorption rate (**h**) is: -

$$h = K_2 q_e{}^2 \quad \ldots\ldots\ldots\ldots\ldots\ldots\ldots\ldots\ldots\ldots\ldots\ldots\ldots\ldots\ldots\ldots\ldots\ldots\ldots\ldots\ldots\ldots\ldots\ldots\ldots\ldots\ldots (1.19)$$

The **Equation (1.20)** becomes [93]:-

$$\frac{t}{q_t} = \frac{1}{h} + \frac{1}{q_e} t \quad \ldots\ldots\ldots\ldots\ldots\ldots\ldots\ldots\ldots\ldots\ldots\ldots\ldots\ldots\ldots\ldots\ldots\ldots\ldots\ldots\ldots\ldots\ldots\ldots\ldots\ldots (1.20)$$

K2 is the rate constant of pseudo-second-order (g.mg^{-1}min^{-1}).

$$K_2 = \frac{slope^2}{intercept} \quad \ldots\ldots\ldots\ldots\ldots\ldots\ldots\ldots\ldots\ldots\ldots\ldots\ldots\ldots\ldots\ldots\ldots\ldots\ldots . \ldots\ldots\ldots\ldots\ldots\ldots (1.21)$$

$$q_e = \frac{1}{slope} \quad \ldots\ldots\ldots\ldots\ldots\ldots\ldots\ldots\ldots\ldots\ldots\ldots\ldots\ldots\ldots\ldots\ldots\ldots\ldots\ldots\ldots\ldots\ldots\ldots\ldots\ldots . (1.22)$$

1.11. Thermodynamic Adsorption

Through thermodynamic functions deal with the process of adsorption “exothermic or endothermic" and knowledge of “automatic or non-automatic reaction”. Are molecules regular or irregular, the enthalpy change (ΔH) can be calculated from the Van’t Hoff Equation [94] the following **Equations (1.23), (1.25):-**

$$K_C = Ae^{-\Delta H/RT} \quad \ldots\ldots\ldots\ldots\ldots\ldots\ldots\ldots\ldots\ldots\ldots\ldots\ldots\ldots\ldots\ldots\ldots\ldots\ldots\ldots\ldots\ldots\ldots\ldots (1.23)$$

$$\ln X_m = -\frac{\Delta H}{RT} + K \quad \ldots\ldots\ldots\ldots\ldots\ldots\ldots\ldots\ldots\ldots\ldots\ldots\ldots\ldots\ldots\ldots\ldots\ldots . \ldots\ldots\ldots (1.24)$$

Where

$\ln X_m$: Natural logarithm for greatest amount adsorbed (mg/g).

K: Constant of Van’t Hoff equation.

R: Universal gas constant (8.314.10^{-3} Jmol^{-1}.K^{-1}).

T: Temperature in Kelvin.

The value of (ΔH) was calculated from the slope by drawing the relationship between **ln X_m** and the reciprocal of temperature **1/T**. The free energy change (ΔG), through which automatic or non-automatic reaction can be identified, from the following [95] **Equation (1.25):-**

$$\Delta G^{\circ} = -RTlnK \quad \ldots\ldots\ldots\ldots\ldots\ldots\ldots\ldots\ldots\ldots\ldots\ldots\ldots\ldots\ldots\ldots (1.25)$$

Where

K: Constant of Van’t Hoff equation.

ΔG: Free energy change.

R: Universal gas constant ($8.314.10^{-3}$ J $mol^{-1}.K^{-1}$).

T: Temperature in Kelvin.

Show that adsorption is spontaneously and through Gibbs relationship can identify the entropy change (ΔS) from the **Equation (1.1)** [96]**.**

1.12. Dyes

Dyes have been used since ancient times in the dyeing of fur and other materials and were extracted from natural materials, which were considered the main source of the production of dyes at the time, but at the present time is not natural materials are the only source for the production of dyes. Currently there are industrial dyes used to earn some of the colors for textiles and it used as well as in the industries the papers to earn the colors and in the leather industry [97]. Dyes are defined as colored materials that the tissue can hold firmly and cannot be removed even when the use of solvents or oxygen or acids or bases. Continued scientists are trying to find out the relationship between the material color and composition, [98] the presence an unsaturated group in the molecule is a key factor in the appearance of color, the world (Witt) has proved that appear in the organic compound when it contains unsaturated aggregates these groups which be double bonds called “chromospheres” , meaning the groups bearing color and include on totals (-N=N- ,$-NO_2$,-N=O- ,-C=O-, C=C- , -C=S-).There are groups working to deepen the color by increasing the intensity called “auxochromes” which are batch groups ,also work to improve the affinity and correlation between molecules of dyes and materials and include on totals (COOH- ,-OH, $-SO_3H$,$-NH_2$, ,-NHR ,$-NR_2$) the dye will be explained under study in detail. Classification dyes according to the chemical structure (Anthraquinone Dyes, Azine Dyes, Xanthenes Dyes, Alcidine Dyes, Oxazine Dyes and Phthalocyanine Dyes [99]). A according to the method (Acid Dyes, Basic Dyes, Disperse Dyes, vat Dyes, Reactive Dyes and sulfur Dyes). These terms have been used to distinguish dyes such as (Azo disperse dye) the used for polyester dyeing and (phthalocyanine reactive dye) to dyeing cotton [100].

1.12.1. Acid dye

Acid dyes are dyes that contain one group or more acidic and most of sulfuric, Carboxylic acid. It is used for dyeing textiles containing basic groups such as wool, silk, polyamides, nylon and modified acrylic fibers. These dyes are dissolved in water or alcohol or both, the dye molecule may be of azo type [101] and the Congo red is of a types azo [102] and Xanthene's. The dyeing process takes place in an acidic medium because the proton is given to the basic group in the tissue where it can be explained as follows [103].

$$\mathbf{Dye^{-} + H^{+} + Fibre \rightarrow Dye^{-}H^{+} - Fibre}$$

One of the dyes types is eosin; it is dye xanthenes with cyclic system heterogeneous. And from the fluorescein family and its composition tetrabromo fluorescein and his formula (**$C_{20}H_6Br_4Na_2O_5$**) and it label the systemic (**2,4,5,7- tetrabromo fluorescein, di sodium salt**) and it attended from the addition of bromine and bromine water to fluorescein and its molecular weight (691.88 g/mol) and dissolve in water and alcohol. Which depend on the compensator group other and on the color-bearing chromospheres for compounds of this group bright colors so it used in the dyeing of paper, acrylonitrile, poly ester, axis nylon and in ink [104], as well as in dyeing silk and wool as a laser dye [105], and also it used as a tracking dye with water to determine the ratio and the direction of flow and transport were used by the technological applications vital [106]. And dye eosin used generally for dyeing cytoplasm the animal cells as well as plant tissues are pigmentation semi-crystalline objects the plant and tissues containing bacteria and membrane of blood cells and connective tissue and protoplasm [107]. The properties will be mentioned in the **Table (1.3)**.

Table (1.3): *Properties of Eosin dye.*

Specification Sheet	**Formula**	**Structure dye**
Empirical formula	$C_{20}H_6O_5Br_4Na_2$	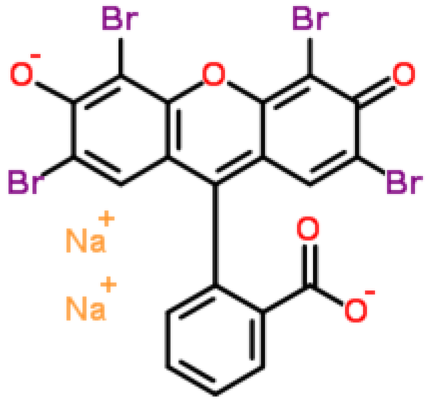 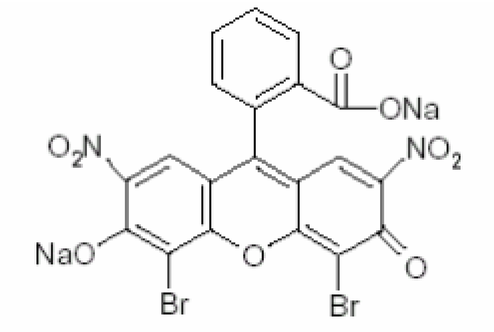
Molar mass	691.88	
Source	B.D.H	
Class	Acid dye	
Solubility	Water and Alcohol	
Melting point	300 °C	**2, 4, 5, 7- tetrabromo fluorescein, di sodium salt.**

1.13. Literature Survey

(Jing, et. al, 2002), prepared ZnO ultrafine particles through the thermal decomposition method of the precursor, zinc carbonate hydroxide. The structure and properties of the prepared ZnO were studied using TEM, XRD, Raman, XPS and UV–Vis absorption spectroscopy. It was found that the prepared ZnO exhibited obvious quantum size effect and surface effect. In addition, there were many active species on the surface of ZnO such as oxygen deficiencies and hydroxyls, both of which can improve its photo catalytic activity of ZnO [**108**].

(Wang, et. al, 2002), prepared CuO nanoparticles by using microwave irradiation. CuO nanoparticles with an average size of 4 nm have been successfully prepared by microwave irradiation, using copper (II) acetate and sodium hydroxide as the starting materials and ethanol as the solvent. The CuO nanoparticles are characterized by using techniques such as X-ray powder diffraction, transmission electron microscopy. The prepared CuO nanoparticles have regular shape, narrow size distribution and high purity. The band gap is estimated to be 2.43 eV according to the results of the optical measurements of the CuO nanoparticles [**109**].

(Zhu, et. al, 2004), used Precipitation method to prepare CuO nanoparticle by a novel quick-precipitation method where highly dispersed copper oxide (CuO) nanoparticles with an average size of 6 nm. The prepared CuO nanoparticles were characterized by X-ray diffraction (XRD), transmission electron microscopy (TEM), UV–Visible absorption spectroscopy. The results show that the prepared CuO nanoparticles have high dispersion and narrow size distribution. The influence of reaction conditions on morphology of CuO nanocrystals was discussed. Spherical, ellipsoidal and needle-shaped CuO nanocrystals could be obtained simply by varying the reaction temperature and controlling the addition of sodium hydroxide [**110**].

(Purkait, et. al, 2005), studied the adsorption of eosin dye dissolved in water by activated carbon and the factors affecting adsorption (concentration, contact time, pH and temperature). The Freundlich model was found to be most appropriate for the description of the adsorption and the kinetic results followed a second-order equation [**111**].

(porkodi, et. al, 2007), studied the sorption of eosin yellow, malachite green and crystal violet onto jute fiber carbon (JFC). Langmuir isotherm was found to be the optimum isotherm for eosin yellow/JFC system and Freundlich isotherm was found to be the optimum isotherm for malachite green/JFC and crystal violet/JFC system at equilibrium conditions. The sorption capacities of eosin yellow, malachite green and crystal violet onto JFC according to Langmuir isotherm were found to 31.49 mg/g, 136.58 mg/g, 27.99 mg/g, respectively, and the kinetic results followed a second-order equation [**112**].

(Guo, et. al, 2007), prepared CuO nanoparticle both unmodified cupric oxide (CuO) nanoparticles and those functionalized with a bifunctional coupling agent methacryloxy propyltrimethoxy silane (MPS) were used to fabricate vinyl-ester resin polymeric nanocomposites. The nanoparticle fictionalization was observed to have a significant effect on the physical properties of the cupric oxide filled vinyl-ester resin nanocomposite. Thermal degradation study by thermo-gravimetric analysis (TGA) showed increased thermo-stability in the functionalized-nanoparticle-filled vinyl-ester resin nanocomposites as compared with the unmodified-nanoparticle-filled counterparts. The more uniform particle dispersion and the chemical bond between nanoparticle and vinyl-ester resin were found to contribute to the increased thermal stability and enhanced tensile strength [**113**].

(Martinson, et. al, 2009), studied the adsorption of arsenic (III) and arsenic (V) by cupric oxide nanoparticles. We synthesized CuO nanoparticles and evaluated them as an adsorbent to remove As (III) and As (V) from groundwater. The CuO nanoparticles had a surface area of 85 m^2/g and were 12–18 nm in diameter. Adsorption occurred within minutes and CuO nanoparticles effectively removed As (III) and As (V) between pH 6 and 10. The maximum adsorption capacity was 26.9 mg/g for As (III) and 22.6 mg/g for As (V). The presence of sulfate and silicate in water did not inhibit adsorption of As (V) but only slightly inhibited adsorption of As (III). High concentrations of phosphate (>0.2 mM) reduced the adsorption of arsenic onto CuO nanoparticles. X-ray photoelectron spectroscopy (XPS) indicated that As (III) was oxidized and adsorbed in the form of As (V) on the surface of CuO. The CuO nanoparticles were also able to remove arsenic to less than (3 μg/L) from groundwater samples. These results suggest that CuO nanoparticles are an effective material for arsenic adsorption and may be used to develop a simple and efficient arsenic removal method [**114**].

(Yiamsawas, et. al, 2009), prepared ZnO nanostructures by solvothermal method. This technique is based on thermal decomposition of organometallic compound in organic solvent and has been successfully applied for the synthesis of various types of nanosized metal oxide with large surface area, high crystallinity and high thermal stability. An interesting correlation between aspect ratio of the ZnO products and physical properties of the solvent was observed and presented in this work. The size and morphology for different environmental conditions were investigated. The different environments during ZnO preparation led to the different morphology with width and length in the range of 8.9-69 nm and 68-108 nm respectively. The TEM image clearly reveals that the lattice spacing is about 0.52 Å corresponding to the (001) plane of hexagonal structured ZnO [**115**].

(Goswami, et. al, 2012), studied the adsorption arsenic by copper (II) oxide nanoparticles. The surface characteristics of copper oxide nanoparticles were investigated using TEM, BET, XRD and FTIR. Results showed that the adsorption process followed pseudo second order kinetic and endothermic behavior. Adsorption equilibrium was studied with Langmuir and Freundlich isotherm models. The adsorption process followed Langmuir isotherm with an adsorption capacity of 1086.2 μg/g [**116**].

(Sheela, et. al, 2012), studied the adsorption of Zn(II), Cd(II) and Hg(II) ions from aqueous solution by the zinc oxide nanoparticles. The Langmuir model was found to be most appropriate for the description of the adsorption and the maximum adsorption capacity was determined at 303 K and was found to be 357, 387 and 714 mg/g for Zn (II), Cd (II) and Hg (II) ions respectively. The adsorption kinetics data were well fitted by the pseudo-second-order rate model and the adsorption capacity was decreased with the increase of temperatures. Is means an exothermic process [**117**].

(Mubarak, 2012), prepared some nonmaterial's such as zinc oxide (ZnO), copper oxide (CuO) by Precipitation method and iron oxide (Fe_2O_3) by a modified sol-gel method have special physicochemical properties. The average particle size has been estimated using Debye-Scherer formula with the average particle sizes being increased as the calcining temperature increased, the average particle sizes of the ZnO calcined at 350 and 450 °C are about 41.86 and 66.19 nm respectively, and particle size values for CuO is 26.83 nm for the sample calcined at 350 °C and of 29.44 nm for the sample calcined at 450 °C. SEM was used to characterize the microstructure of samples. The study of SEM micrographs for ZnO reveals less number of pores with smaller lump size. It can also be observed that the CuO powders are composed of non-agglomerated spherical particles and flower shape nanoparticle. Density measurements are performed using Archimedes principle. There is an increase in the density and shrinkage of the sintered pellets with an increase of times and temperatures. Hardness which is a measure of a material resistance to localized plastic deformation (a small dent or a scratch),and Vickers hardness (V.H) is used to measure the hardness of ferrite samples, shows the dependence of ferrite hardness on the temperature of the heat treatment, it seems that the amount hardness increases when increases temperatures [**118**].

(Kumar, et. al, 2013), prepared ZnO nanostructures by micro emulsion route in W/S ratio of 5 at room temperature. X-ray diffraction (XRD) pattern reveals wurtzite structure of ZnO nanoparticles. Rod shape of ZnO nanoparticles of average particle size 10.0 to 12.0 nm were observed by transmission electron microscopy. FT-IR spectra confirmed the adsorption of surfactant molecules at the surface of ZnO nanoparticles and presence of Zn-O bonding. Thermal studies were carried out by the differential scanning calorimeter (DSC) techniques. In addition, UV-Visible spectra were employed to estimate the band gap energy of ZnO nanoparticles [**119**].

(Farghali, et. al, 2013), in their research showed the removal of Pb ions from aqueous solutions by using copper oxide nanostructures , Various morphologies of CuO nanostructures (oval, cluster, leaves, small rod, pours nanosheets) have been synthesized by novel simple method using microwave radiation. The produced were characterized by XRD analysis technique, (TEM), surface area analyzer (BET), and energy dispersive spectroscopy (EDS). The ability of CuO nanostructures as adsorbent was leading for adsorptive uptake of lead ions from the aqueous solutions. Different physicochemical factors such as initial concentration of ion, pH, and the equilibrium contact time were investigated. The best pH value for removal of Pb (II) from aqueous solutions was 6.5 and 4 hours was optimum contact time. The adsorption isotherms were obtained using concentrations of the lead ions ranging from 100 to 300 mg/L. It was seen that the process of adsorption was described by pseudo-second-order reaction kinetics, as well as Langmuir and Freundlich adsorption isotherms. The largest capacity of oval, cluster, leaves, small rod and pours nanosheets CuO nanostructures for Pb_2 are 125, 116, 117, 120 and 115 mg/g. Finally it is revealed that CuO nano structures were an active adsorbent for uptake of lead ions from aqueous solutions [**120**].

(Srivastava, et. al, 2013), studied the synthesis zinc oxide (n-ZnO) nanoparticles by simple solution based approaches and synthesized n-ZnO particles were characterized by XRD, TEM, SEM and FTIR. XRD and TEM confirmed the formation of man-sized zinc oxide particles in the size range of 18–31 nm [**121**].

(Phiwdang, et. al, 2013), prepared CuO nanostructures by precipitation method using different precursors as copper nitrate ($Cu(NO_3)_2$) and copper chloride ($CuCl_2$) with post-heating comparing between as-synthesized and after calcinations. Relevant properties of as-synthesized nanoparticles were investigated by X-ray diffraction (XRD), scanning electron microscope (SEM) and Fourier Transform Infrared (FTIR) Spectroscopy. Overall results suggest that the formation of CuO nanostructures with different shape, size and morphology can be achieved using different precursors via this process. The improvement in their crystallinity and purification can be further attained by post calcinations process [**122**].

(Zhang, et. al, 2013), studied the adsorption behavior and mechanism of methyl blue on zinc oxide nanoparticles. The adsorption capacity of methyl blue on the zinc oxide nanoparticles reached 10.70 ± 0.80 mmol/g and the factors affecting adsorption (concentration, contact time, pH and temperature). The adsorption kinetics was elucidated by the pseudo-second-order model and exhibited 2-stage intra-particle diffusion model. The adsorption isotherm fitted well with the Temkin model [**123**].

(Mustafa, et. al, 2013), studied the preparation of cupric oxide (CuO) nanoparticles by adopting aqueous precipitation method using copper sulphate 5-hydrate as a precursor and NaOH as a stabilizing agent. The effect of optimization parameters such as time, concentration and temperature .The CuO NPs were characterized for the studying of their structure and composition from XRD which reveals the single phase monoclinic structure. The surface morphology of these NPs was carried out by using scanning electron microscopy (SEM). The adsorption isotherm equations like Langmuir, Freundlich and Dubinin-Radushkevich were applied and the values of their respective constants were evaluated by adopting graphical method. Thermodynamic and kinetic studies were also performed to determine the feasibility of the process. The maximum MB removal was observed to be 88.93% [**124**].

(Nithya, et. al, 2014), studied the preparation and characterization of copper oxide nanoparticles by modified sol-gel method using sodium dodecyl sulphate as a surfactant. Calcinations temperature effect on particle size, band-gap, crystalline and morphology of the nanoparticles were studied with the help of particle size analysis, UV-Spectroscopy, (XRD) and (SEM) studies. Also the prepared nanoparticles were tested for their activity towards gas sensing [**125**].

(Ghaedi, M., et. al, 2014), in their research showed of Removal malachite green from aqueous solution by zinc oxide nanoparticle loaded on activated carbon ,this material was characterizated by Brunauer, Emmett and Teller (BET), scanning electron microscopy (SEM), X-ray diffraction (XRD), and Fourier transform infrared spectroscopy (FT-IR) analysis. In batch experimental set-up, optimum conditions for quantitative removal of MG by ZnO-NP-AC was attained following searching effect of variables such as adsorbent dosage, initial dye concentration and pH. Optimum values were set as pH of 7.0, 0.015 g of ZnO-NP-AC at removal time of 15 min. Kinetic studies at various adsorbent dosages and initial MG concentration show that maximum MG removal was achieved within 15 min of the start of every experiment at most conditions. The adsorption of MG follows the pseudo-second-order rate equation Equilibrium data fitted well with the Langmuir model at all amount of adsorbent, while maximum adsorption capacity was 322.58 mg g^{-1} for 0.005 g of ZnO-NP-AC [**126**].

(Fakhri, 2014), studied the adsorption of Ethidium bromide and Ethidium monoazide bromide from aqueous by cupric oxide nanoparticles. The characteristics of CuO nanoparticles were determined and found to have a surface area 89.59 m^2/g and the factors affecting adsorption (concentration, contact time, pH and temperature) the amount of removal increases with the increase in pH from one to seven and reaches the maximum when the pH is nine. Adsorption data fitted well with the Langmuir, Freundlich and Florry–Huggins models. The results show that the best fit was achieved with the Langmuir isotherm equation with maximum adsorption capacities of 0.868 and 0.662 mg/g. The adsorption process was found to follow pseudo-second-order kinetics. The calculated thermodynamic parameters, namely ΔG, ΔH and ΔS showed that adsorption of Ethidium bromide and Ethidium monoazide bromide was spontaneous and endothermic under examined conditions [**127**].

(Nekouei, et. al, 2015), studied removal acid blue 129 from liquids by copper oxide nanoparticle loaded on activated carbon .This novel adsorbent was characterized and identified using different techniques such as scanning electron microscopy (SEM), X-ray diffraction (XRD), and laser light scattering (LLS). The effects of some variables including pH, adsorbent dosage, initial dye concentration, contact time and temperature, can better describe the adsorption kinetics. Furthermore, Langmuir, Freundlich, Tempkin and Dubinin–Radushkevich models were applied for adsorption equilibrium. The adsorption kinetic results indicated that the pseudo-second-order and that the Langmuir model provides a better correlation of the experimental [**128**].

(Naghizade, et. al, 2016), studied the adsorption of two cationic dyes, basic violet 16 (BV 16) and basic red 14 (BR 14), from textile effluent by copper oxide nanoparticles. The surface characteristics of copper oxide nanoparticles were investigated using scanning electron microscope (SEM) and X-ray diffraction spectroscopy. The effect of different variables such as adsorbent dosage, initial dye concentration, pH, and mineral salts. The results indicated that the data for adsorption of BV 16 and BR 14 onto copper oxide nanoparticles fitted well with the Langmuir isotherm. The rates of sorption were best fitted by the pseudo-second order-kinetic [**129**].

(Dashamiri, S., et. al, 2016), studied the adsorption of brilliant green (BG), aura mine O (AO), ethylene blue (MB) and eosin yellow (EY) dyes by copper (II) oxide nanoparticles loaded on activated carbon. Copper oxide nanoparticles loaded on activated carbon (CuO-NPs-AC) were prepared and fully analyzed and characterized with FE-SEM, XRD and FT-IR. Subsequently. The adsorption rate well fitted by pseudo second-order while adsorption capacity according to the Langmuir model as best equilibrium isotherm model for BG, MB, AO and EY was 20.48, 21.26, 22.34 and 21.29 mg g^{-1}, respectively [**130**].

(Karim, et. al, 2017), prepared copper oxide nanoparticles (CuO) by simple precipitation method and then it characterize by XRD, SEM, and AFM techniques. XRD spectrum revealed that particle size obtained was around (7.43 nm) for it, which agreed fairly well with XRD data. Surface morphology as a main nanoparticles phenomenon was studied in terms of SEM and AFM. The prepared oxide nanoparticles was used to remove nickel ions from aqueous solution and determining the best removal percentage at different contact time (30, 60, 90, and 120 min) and different initial concentration of aqueous solutions (100, 200, and 300 mg/L) with other constant condition such as pH of 3.5, adsorbent dosage (0.1g), and room temperature .The result showed the percentage removal of nickel ions increase with increase in the contact time, and the maximum adsorption was recorded with 100 mg/L for the prepared oxide nanoparticles, Also the percentage removal seem to decrease with increase in the initial concentration of adsorbate. The correlation coefficient for the linear Freundlich isotherm regression fits are larger than that for the Langmuir one for (CuO), nanoparticles, so the Freundlich model could describe the adsorption isotherm for the uptake of nickel ions from aqueous solution on (CuO), nanoparticles surfaces [**131**].

(**Amir, et. al, 2017),** studied removed the Eosin dye from aqueous solutions by the surface Plant (waste of molasses dates production). It was determined to equilibrium time the process of adsorption and found that (90 min.) Spectroscopy using ultraviolet - visible rays and the results showed that the best weight for the surface of the adsorbent is (0.2 g). Moreover, the study was conducted in a range of acidic state (pH = 1-10). Isotherm been used (for Langmuir, Freundlich, Dubinin, Temkin) as it was found that the best Isotherm is Isotherm Dubinin. And the amount of adsorption was calculated in the range of temperatures (20-40 ºC) and found that the amount of adsorption decreased with increasing temperature and this shows that the interaction exothermic was calculated valuable thermodynamic functions and was conducted kinetic study of the adsorption and found that the adsorption follows the equation second false constants were calculated velocities and thermodynamic functions activation of front and reverse reaction [**132**].

1.14. The Aim of the Present Study

1. Preparation of (ZnO) nanoparticles and (CuO) nanoparticles by the precipitation method, and Characterization them by using XRD, SEM, AFM, FTIR, and BET.
2. Determining the best adsorption of the Eosin dye ions by using the two oxide nanoparticles (adsorbent) with a batch method at different contact time and initial concentration of aqueous solutions (adsorbate) with other constant condition such as pH value, adsorbent weight, and the temperature is the same.

3. Langmuir, Freundlich, Temkin and Dubinin-Kaganer-Radushkevich isotherms are used to describe the adsorption process.

4. Thermodynamic studies of adsorption process were investigated and the adsorption heat was calculated.

5. Kinetic studies of adsorption process were investigated by using two kinetics models: pseudo-first order model and pseudo-second-order model.

6. Comparative study of adsorption of Eosin dye using CuO and ZnO as Nanosurfaces.

CHAPTER TWO

Experimental study

2. Experimental study

2.1. Instruments

Table (2.1) illustrates the list of instruments used in this project work, their manufacturers, model, and the place of the instruments.

Table (2.1): *List of instruments.*

Instrument	Model	Place of Instrument
Water bath shaker	BS-11, Korea	Chemistry department in College of education for pure sciences /Diyala University.
Centrifuge	EBA20, Germany.	
PH-meter	7110(wtw), Germany	
Balance Electric	Sartorius median. Germany	
Drying Oven	BINDER, Germany	
Hot Plate and magnetic Stirrer	LMS-100, Korea	
UV-Visible	Shimadzu U.V-visible ,Japan.1700	
FTIR	SHIMADZU (IR PRESTIGE 21)	
AFM	SPM-AA 3000, Advanced Angstrom Inc.	College of science. Baghdad University.
BET	Q-surf 9600 (USA)	Petroleum Research and Development Center in Iraq.
XRD	Shimadzu company (Japan) (XRD-6000)	University of Technology /Center of Nano Technology and Advanced Materials.
SEM	Type TESCAN	University of Technology/Center of Nano Technology and Advanced Materials.

2.2. The Chemical Material

Chemicals used in the present study are given in **Table (2.2)** together with their purity and suppliers.

Table (2.2): *Chemicals, purity, and suppliers.*

Name	Chemical Formula	Supplier	Purity %
Zinc nitrate hex hydrate	$Zn(NO_3)_2.6H_2O$	India	98 %
Sodium bicarbonate	$NaHCO_3$	India	99 %
Cupric nitrate	$Cu(NO_3)_2.3H_2O$	England	99 %
Hydrochloric acid	HCl	Sigma-Aldrich	36.5 %
Sodium hydroxide	NaOH	Sigma-Aldrich	98.0 %

2.3. The Adsorbate

The adsorbate used in this study is Eosin dye, and Table (2.3) explains its Physical and chemical properties of it.

Table (2-3): *Chemical and physical properties of the Eosin dye.*

Specification Sheet	Formula	Structure dye
Emprical formula	$C_{20}H_6O_5Br_4Na_2$	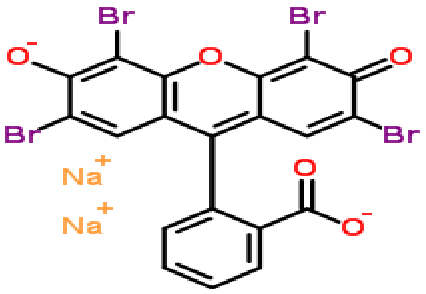
Molar mass	**691.88**	
Solubility	**Water and Alcohol**	
Melting point	**300 °C**	**2,4,5,7- tetrabromo fluorescein,di sodium salt**

2.4. The Adsorbent

The adsorbents used in this study are zinc oxide (ZnO) and copper oxide (CuO) nanoparticles and were prepared by precipitation method. This method is easy if compared to other methods and the chemicals required for these methods are available and cheap to the removal of Eosin dye from aqueous solutions.

2.5. Preparation zinc oxide nanoparticles

2.5.1 Preparation of solution

The aqueous solution (0.2 M) Zinc nitrate ($Zn(NO_3)_2.6H_2O$) and the solution (0.4 M) of sodium bicarbonate ($NaHCO_3$) are prepared in distilled water separately by dissolution (59.4 g) Zinc nitrate hexhydrate and (33.6 g) sodium bicarbonate in (1000 ml).

2.5.2. Precipitation procedure

The Zinc nitrate solution (0.2 M) was placed in (2000 ml) beaker placed on a hot plate magnetic stirrer. A magnetic bar is used in order to obtain homogeneous mixing of the material. The electrode of pH meter was inserted into the solution. Measure and monitor the pH value of the solution during the slow addition of the sodium bicarbonate solution (0.4 M) from a burette. The temperature of the solution was fixed at 80°C. The addition continued until the pH of the solution reaches (6.8) where the precipitation was completed. After the completion of the reaction, the precipitate is allowed to settle overnight. It is then filtered off and the precipitate is washed several times with distilled water, until free from excess bicarbonate which may be present then dried the precipitates at 70-80 °C for 2 hours and then calcined at 400 °C for 3 hours in an oven to obtain the ZnO nanoparticles [118].

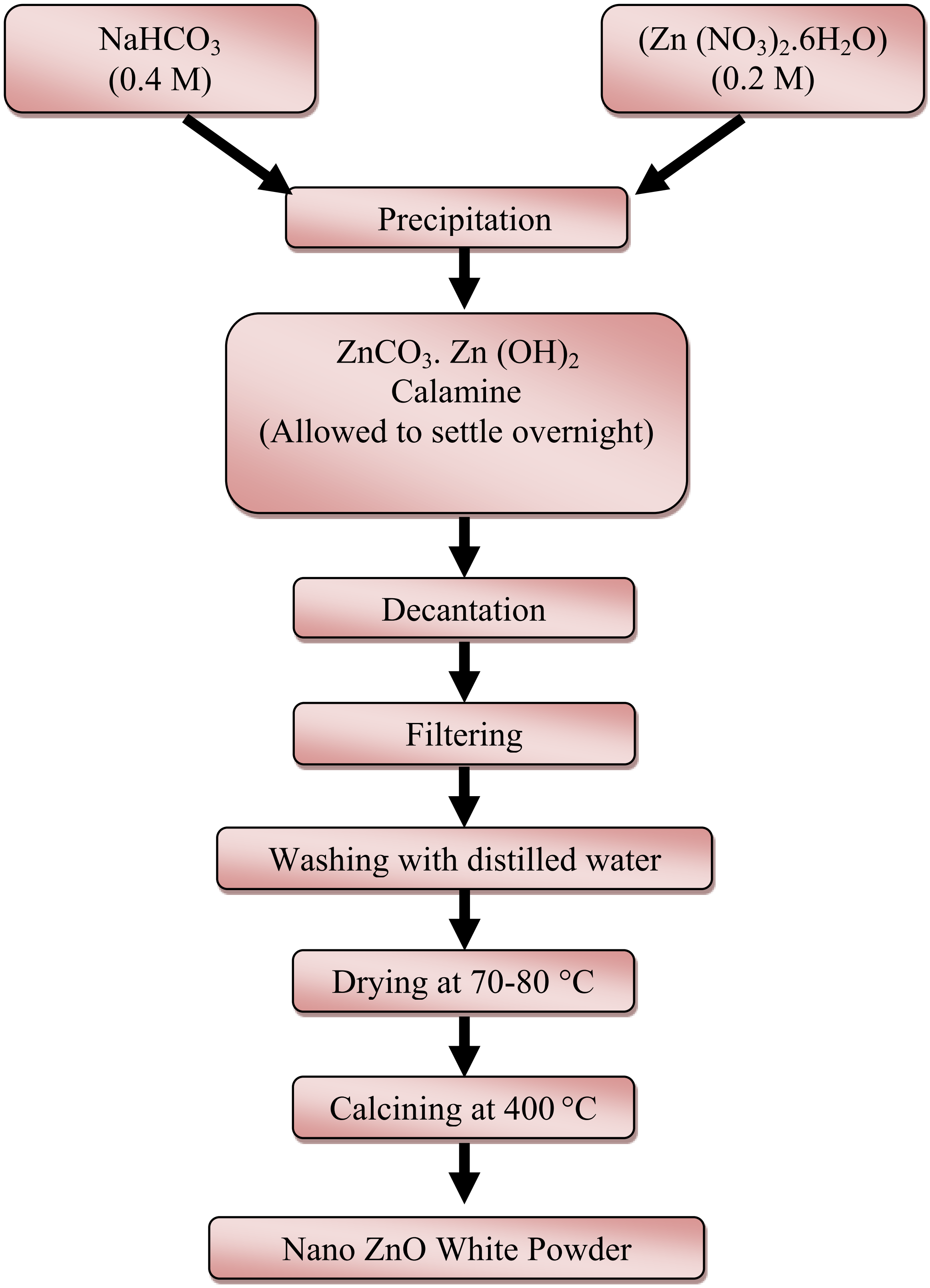

Figure (2.1): *Steps of process ZnO preparation.*

2.6. Preparation copper oxide nanoparticles

2.6.1. Preparation of solution

The aqueous solution (0.2M) Copper nitrate (Cu $(NO_3)_2.3H_2O$) and the solution (0.4 M) of sodium bicarbonate ($NaHCO_3$) are prepared in distilled water separately by dissolution (48.2 g) Copper nitrate trihydrate and (33.6 g) sodium bicarbonate in (1000 ml).

2.6.2. Precipitation procedure

The Copper nitrate solution (0.2 M) was placed in (2000 ml) beaker placed on a hot plate magnetic stirrer. A magnetic bar is used in order to obtain homogeneous mixing of the material. The electrode of pH meter was inserted into the solution. Measure and monitor the pH value of the solution during the slow addition of the sodium bicarbonate solution (0.4 M) from a burette. The temperature of the solution was fixed at 80°C. The addition continued until the pH of the solution reaches (6.8) where the precipitation was completed. After the completion of the reaction, the precipitate is allowed to settle overnight. It is then filtered off and the precipitate is washed several times with distilled water, until free from excess bicarbonate. A pale blue color precipitate is observed and the supernatant solution is then discarded carefully. The precipitate is dried at 70-80 °C for 2 hours and then calcined at 400 °C for 3 hours in an oven to obtain the CuO nanoparticles [118].

2.7. Characterization of (ZnO, CuO) nanoparticles

2.7.1. Fourier Transform Infrared Spectrophotometer (FT-IR)

Fourier transformed infrared spectroscopy (FT-IR) is used to study functional groups on the surface of materials using the discrete energy levels for vibrations of atoms in these groups. By scanning over a range of wavelengths (4000-400 cm^{-1}) and recording the amount of transmitted light for each wavelength it is possible to determine which functional groups are present on the surface.

***Figure (2.2):** Fourier transforms infrared spectrophotometer (FT-IR).*

2.7.2. X-ray diffraction (XRD)

X-ray diffraction patterns are recorded from (2Θ =20°–80°) scanning range**,** using Cu Kα (**λ** = 1.5406Å) with an accelerating voltage of 40kV, current 30 am, of the Shimadzu company (Japan) (XRD-6000). Data are collected with a counting rate of (5 deg/min). From XRD the crystallite size can be found out by using the Scherer's **Equation (2.1)** [118]**:-**

$D = 0.9\lambda / \beta \cos \Theta$ ……………..………………………………………………… (2.1)

D: Crystallite size, **λ:** Wavelength (1.54 Å), **β:** Full width at half maximum (FWHM) and **Θ:** Diffraction angle.

Figure (2.3): *X-ray diffraction (XRD).*

2.7.3. The Surface area (BET)

The specific surface area of (ZnO, CuO) nanoparticles was measured using instrument model Q-surf 9600 (USA), based on Brunauer, Emmett, and Teller (BET). The instrument in Petroleum Research and Development Centre in Baghdad is shown in **Figure (2.4)**.

.

Figure (2.4): Surface area (BET).

.

2.7.4. The Scanning Electron Microscope (SEM)

SEM is an analytical tool measuring surface topography using energetic electron beams. The electron beam can be focused by a magnetic field from micro to nanometer level, thus enabling measurement of surface topography. SEM provides images of secondary electron (SE) or backscattered electron (BSE) models. In general, the SEM mode mainly supplies images based on the topographical information.

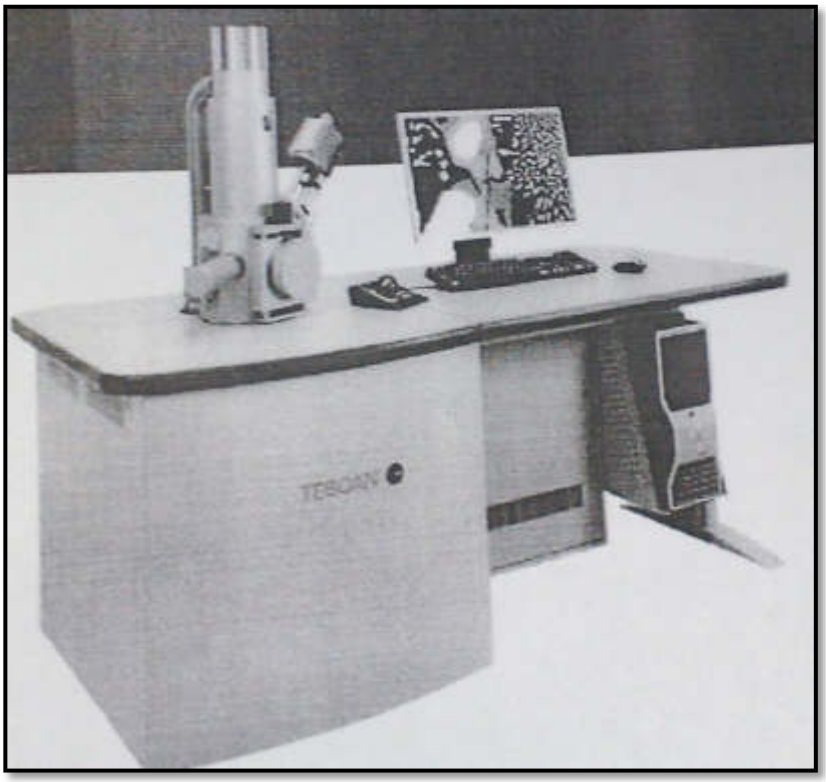

Figure (2.5): *Scanning electron microscope (SEM).*

2.7.5. Atomic Force Microscopy (AFM)

The AFM is one of the foremost tools for imaging, measuring, and manipulating matter at the nanoscale. The information is gathered by "feeling" the surface with a mechanical probe. Piezoelectric elements that facilitate tiny but accurate and precise movements on (electronic) command enable the very precise scanning.

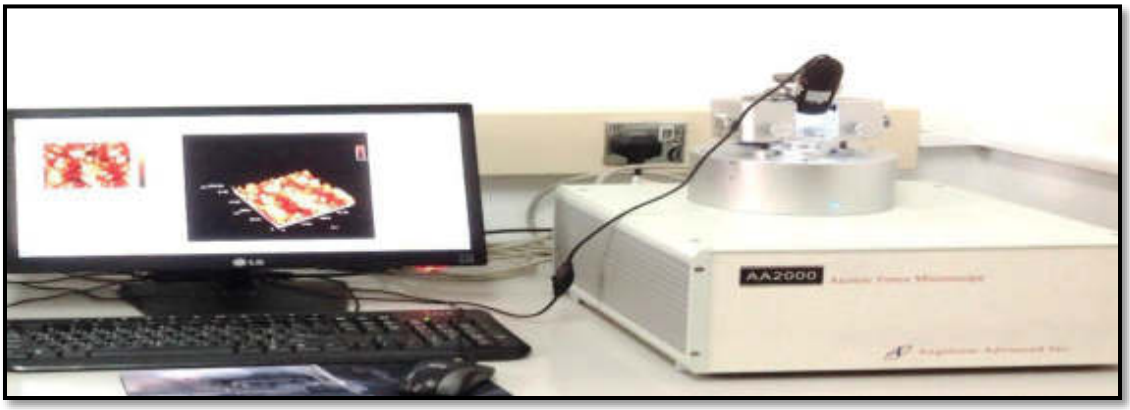

Figure (2.6): *Atomic force microscopy (AFM).*

2.8. Preparation of Standard Solutions for Eosin dye

A standard solution of Eosin dye, which was (25) ppm, was prepared by dissolving (0.025g) in the volumetric flask (1000 ml) of distilled water. Solutions of different concentrations (2-20) ppm were prepared by dilutions from the standard solution and the solutions are left for 24 hours in order to homogenize. Dilute (0.1 M) HCl and (0.1 M) NaOH was used for pH adjustment in order not to increase the volume of samples too much and keep the error created by pH adjustment in a reasonable range.

2.9. Determination of λ_{max} and Calibration curve for Eosin dye

The adsorbate was analyzed spectrophotometrically by the appropriate method. To determine the wavelength at maximum absorption (λ max), absorption values for Eosin dye by using UV- visible spectrophotometer at the (λ_{max} 516 nm) has been recorded in the range (200-800 nm) by using quartz cell of (1cm) thickness (path length) as in Figure (2.7). The calibration curve was determined by fixing the λ_{max} that obeys the (Lambert beer's law) at specific concentrations prepared (2-20) ppm for Eosin dye. After that, the absorption has been recorded and a calibration curve plotted between absorption and concentration, the line between points have been drawn using the least square method as in Figure (2.8) which shows Calibration curve of Eosin dye at different pH and temperature 25 °C (298 K). Table (2.4) the values of the calibration curve.

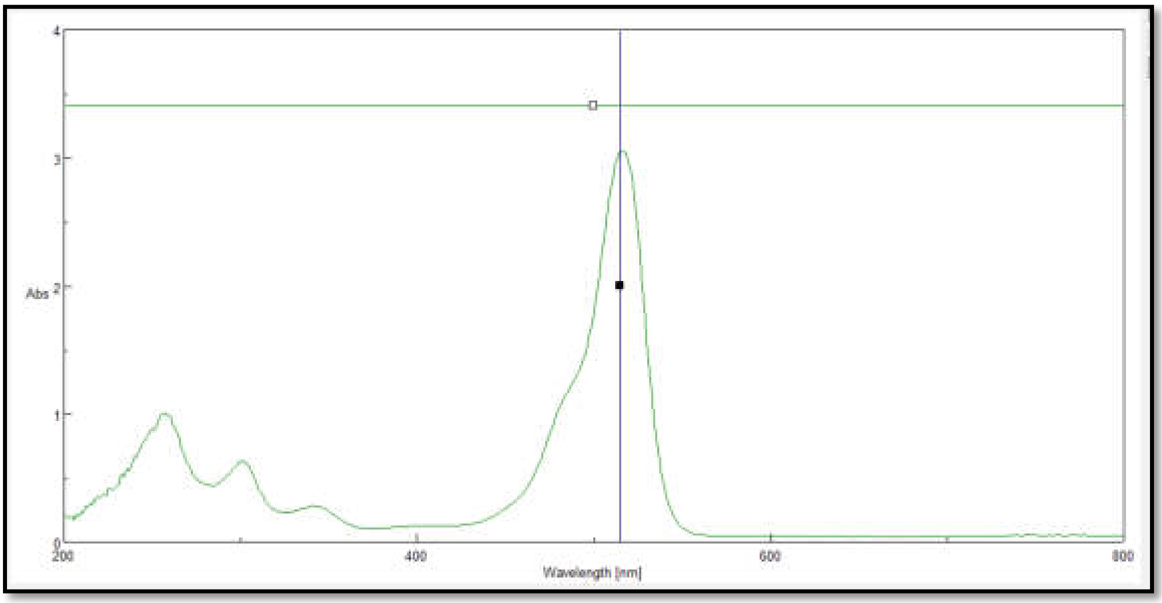

Figure (2.7): *The scan spectrum curve of Eosin dye.*

Table (2.4): *Values of concentrations and absorbance for calibration curve at different pH; and temperature = 25 °C.*

Conc. (ppm)	**Eosin**		
	Absorbance		
	pH=4	**pH=7**	**pH=10**
2	**0.150**	**0.255**	**0.280**
4	**0.400**	**0.440**	**0.479**
6	**0.610**	**0.622**	**0.746**
8	**0.822**	**0.868**	**0.990**
10	**1.032**	**1.059**	**1.229**
12	**1.241**	**1.330**	**1.460**
14	**1.476**	**1.487**	**1.793**
16	**1.769**	**1.811**	**1.919**
18	**1.879**	**1.966**	**2.187**
20	**2.140**	**2.211**	**2.263**

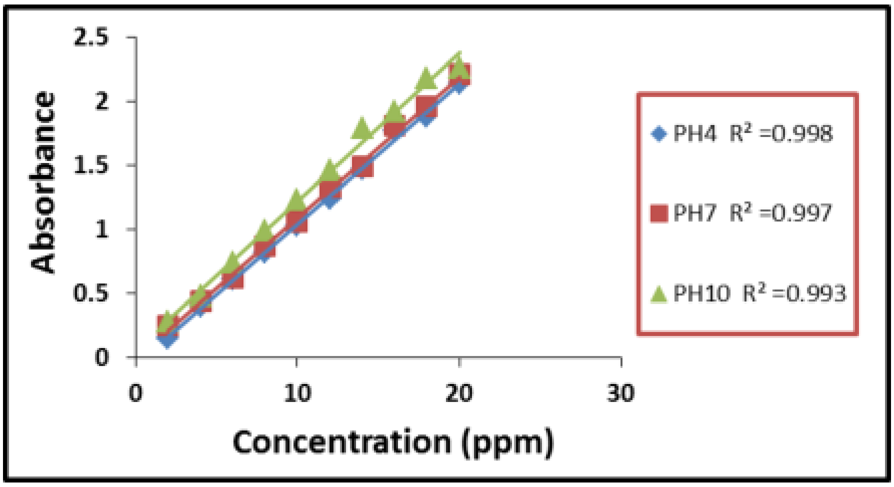

Figure (2.8): *The calibration curve for Eosin dye at different pH; and temperature = 25 °C.*

2.10. Optimum conditions for adsorption

2.10.1 Determination of Equilibrium Time

To determination of the equilibrium time between adsorbate and adsorbent surface of through the preparation the volumetric flasks (50 ml) containing equal volumes (30 ml) from Eosin dye of initial concentration (10) ppm and weight (0.04 g) for (CuO, ZnO) nanoparticles and placed it in water path shaker (at 185 rpm) and a specified temperature 25 ºC after continuous shaking, the samples was withdrawn from the shaker for regular time intervals of (10, 20, 30….) min and was filtered by filter papers to separate the adsorbent and placed in a centrifuge for 15 min(at 3500 rpm) and then filtered again. UV-Vis spectrophotometer has been used to measure the absorbance of the solutions at **(λ $_{\mathbf{max}}$** 516 nm) for Eosin dye. The results showed that equilibrium time (50) min for CuO and (120) min for ZnO.

2.10.2. Determination of Adsorbent Weight

To determination of the adsorbent weight the optimal for adsorption through the preparation ten volumetric flasks (50 ml) containing equal volumes (30 ml) from Eosin dye of initial concentration (10) ppm and different weights (0.01-0.09g) for (CuO,ZnO) nanoparticles and placed it in water path shaker (at 185 rpm) and a specified temperature 25 ºC and leaves for (50) min of CuO and (120) min for ZnO after continuous shaking, the samples was withdrawn from the shaker and was filtered by filter papers to separate the adsorbent and placed in a centrifuge for 15 min (at 3500 rpm) and then filtered again. UV-Vis spectrophotometer has been used to measure the absorbance of the solutions at **(λ_{max}** 516 nm**)** for Eosin dye. The results showed that the optimal weight for an adsorbent surface that gave less absorption is (0.04 g).

2.10.3. Study Effect of concentration adsorption

The study effect of concentration adsorption of dye was studied on the two surfaces through the preparation of ten volumetric flasks (50ml) containing equal volumes (30 ml) from Eosin dye of different initial concentration (2-20) ppm with weight (0.04 g) for (CuO, ZnO) nanoparticles and placed it in water bath shaker (at 185 rpm) and a specified temperature 25 ºC for (50) min of CuO and (120) min for ZnO after continuous shaking, the samples was withdrawn from the shaker and was filtered by filter papers to separate the adsorbent and placed in a centrifuge for 15 min (at 3500 rpm) and then filtered again, and then estimate the percentage for adsorption by using spectroscopic methods by calibration curve.

2.10.4. Adsorption Kinetics

The adsorption kinetics for Eosin dye was studied on the surface of the CuO through the preparation of five volumetric flasks (50 ml) containing equal volumes (30ml) of Eosin dye of different initial concentration (10) ppm and weight (0.04 g) of CuO nanoparticles and placed it in water path shaker (at 185 rpm) and a specified temperature 25 ºC after continuous shaking, the samples was withdrawn from the shaker for regular time intervals of (10, 20, 30….) min for (50) min of CuO and was filtered by filter papers to separate the adsorbent and placed in a centrifuge for 15 min (at 3500 rpm) and then filtered again. UV-Vis spectrophotometer has been used to measure the absorbance of the solutions at (**λ_{max}** 516 nm) of Eosin dye. To study adsorption kinetics for Eosin dye on the surface of the ZnO the previous steps are repeated the same except the preparation of twelve volumetric flasks and the time continues for (120) min. The previous operation on the two surfaces at the following thermal degrees is repeated 20, 25, 30, 35, 40 °C.

2.10.5. Effect of temperature

The study effect of temperature on adsorption of Eosin dye on the two surfaces through the preparation of ten volumetric flasks (50 ml) containing equal volumes (30 ml) from Eosin dye of different initial concentration (2-20) ppm with weight (0.04g) for (CuO, ZnO) nanoparticles and placed it in water bath shaker (at 185 rpm) and a specified temperature 25 ºC until reaching equilibrium time for (50) min of CuO and (120) min for ZnO after continuous shaking, the samples was withdrawn from the shaker and was filtered by filter papers to separate the adsorbent and placed in a centrifuge for 15 min (at 3500 rpm) and then filtered again. UV-Vis spectrophotometer has been used to measure the absorbance of the solutions at (**λ_{max}** 516 nm) for Eosin dye. **Q_e** (mg/g) was calculated from the following **Equation (2.3)**. The previous operation at the following thermal degrees is repeated 20, 25, 30, 35, 40 °C.

$$\mathbf{Q_e = \frac{C_o - C_e}{m} . V_{sol.}} \ldots\ldots\ldots\ldots\ldots\ldots\ldots\ldots\ldots\ldots\ldots\ldots\ldots\ldots\ldots\ldots\ldots\ldots\ldots\ldots\ldots\ldots\ldots\ldots\ldots\ldots\ldots\ldots\ldots\ldots \mathbf{(2.2)}$$

Q_e: Amount of solute adsorbed per unit weight of adsorbent (mg/g).

C_e: Equilibrium concentration of solute (mg/L).

$V_{sol.}$: Volume of solution (L).

m: Mass of adsorbent (g).

C_o: Initial concentration of solute (mg/L).

2.10.6. Calculation of Thermodynamic function

Thermodynamic functions were calculated (ΔS, ΔG, ΔH) and using the **Equations (1.1), (1.24) and (1.25)** and calculate the equilibrium constant at a different temperature (20, 25, 30, 35, and 40) °C.

2.10.7. Determination of Adsorption Isotherm

To determination of adsorption isotherm for the Eosin dye of through the preparation of ten volumetric flasks (50 ml) containing equal volumes (30 ml) of different initial concentration (2-20) ppm with weight (0.04 g) for (CuO, ZnO) nanoparticles and placed it in water bath shaker (at 185 rpm) and a specified temperature 25 ºC until reaching equilibrium time for (50) min of CuO and (120) min for ZnO after continuous shaking, the samples was withdrawn from the shaker and was filtered by filter papers to separate the adsorbent and placed in a centrifuge for 15 min (at 3500 rpm) and then filtered again. UV-Vis spectrophotometer has been used to measure the absorbance of the solutions at (λ_{max} 516 nm) for Eosin dye. **Q_e** (mg/g) was calculated and the previous operation at the following thermal degrees is repeated 20, 25, 30, 35, 40 °C.

2.10.8. Effect of pH

The study effect of pH on adsorption of Eosin dye on the two surfaces through the preparation of ten volumetric flasks (50 ml) containing equal volumes (30 ml) of different initial concentration (2-20 ppm) and put drops of hydrochloric acid (0.1 M) until it became (pH=4) and this process is followed by a pH meter. UV-Vis spectrophotometer has been used to measure the absorbance of the solutions at (**λ** $_{\textbf{max}}$ 516 nm) for Eosin dye before adding the weight of the adsorbent surface and then adding the weight of the adsorbent surface is (0.04 g) for (CuO, ZnO) nanoparticles and placed it in water bath shaker (at 185 rpm) and a specified temperature 25 ºC until reaching equilibrium time for (50 min) of CuO and (120 min) for ZnO after continuous shaking, the samples were withdrawn from the shaker and was filtered by filter papers to separate the adsorbent and placed in a centrifuge for 15 min (at 3500 rpm) and then filtered again. UV-Vis spectrophotometer has been used to measure the absorbance for the solutions for calculated $\mathbf{Q_e}$ (mg/g), the same process is repeated but with changes a pH to (7 and 10).To the study of better pH for the adsorption of Eosin dye through the preparation of ten volumetric flasks (50 ml) containing equal volumes (30 ml) of initial concentration (18) ppm with weight (0.04 g) for (CuO, ZnO) nanoparticles and with change the pH (1-10) for each flask and placed it in water bath shaker (at 185 rpm) and a specified temperature 25 ºC until reaching equilibrium time for (50) min of CuO and (120) min for ZnO after continuous shaking, the samples was withdrawn from the shaker and was filtered by filter papers to separate the adsorbent and placed in a centrifuge for 15 min (at 3500 rpm) and then filtered again. UV-Vis spectrophotometer has been used to measure the absorbance of the solutions at (**λ** $_{\textbf{max}}$ 516 nm) for Eosin dye.

CHAPTER Three

Results
&
Discussions

3.1. Characterization of ZnO and CuO Nanoparticles

3.1.1. Fourier transforms infrared spectrum analysis (FTIR)

FTIR spectra of ZnO nanoparticles are shown in **Figure (3.1)**. Metal oxides generally give absorption bands in fingerprint region i.e. below 1000 cm^{-1} arising from inter-atomic vibrations .The peak observed at 3446.79 cm^{-1} may be due to O-H stretching assigned to the water adsorption on the metal surface. The peak at 1651.07 cm^{-1} corresponds to Zn-O stretching, the peaks at 669.68 and 545.85 cm^{-1} correspond to deformation vibration. The metal –oxygen frequencies observed for the respective metal oxides are in accordance with literature values [119].

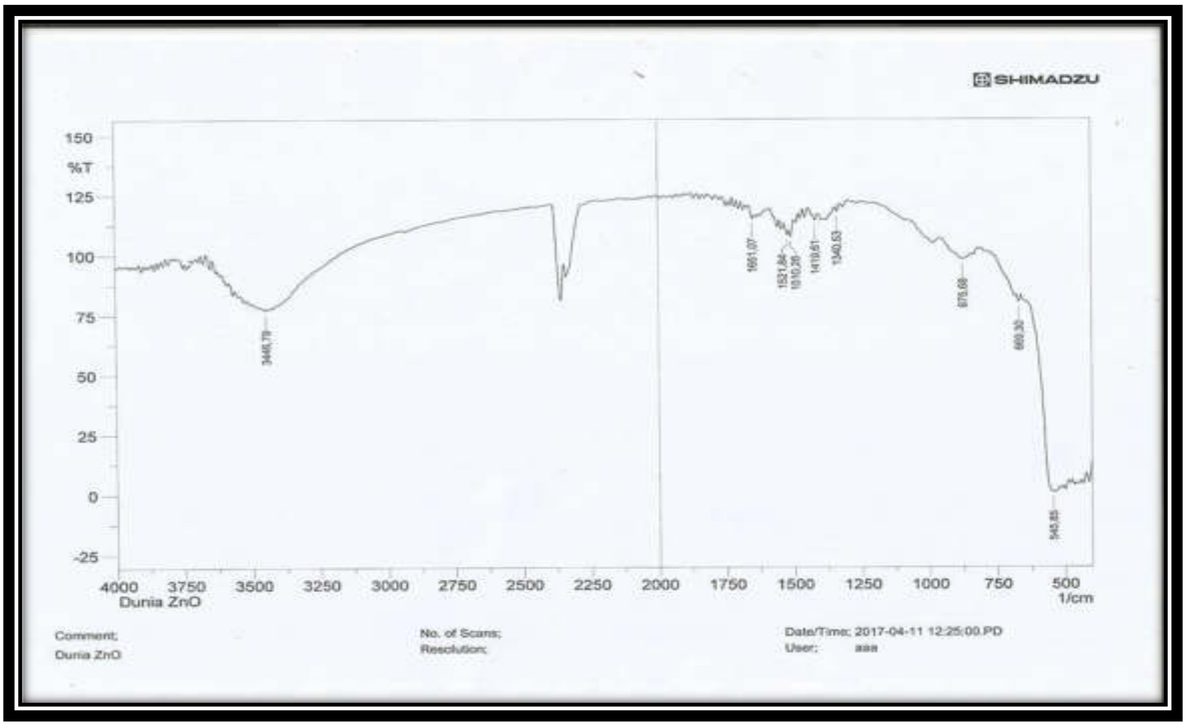

Figure (3.1): *FTIR spectrum of ZnO nanoparticles.*

Figure (3.2) show the FTIR spectra of CuO nanoparticles has a noticeable peak at 540 and 560 cm^{-1} which are attributable to Cu-O stretching modes, confirming the formation of highly pure CuO nanoparticles a band at 669 cm^{-1} was attributed to Cu_2O.The sample has the absorption peaks in the range of 1637-1445 cm^{-1}that may be assigned to O-H bending vibrations combined with copper atoms [122].

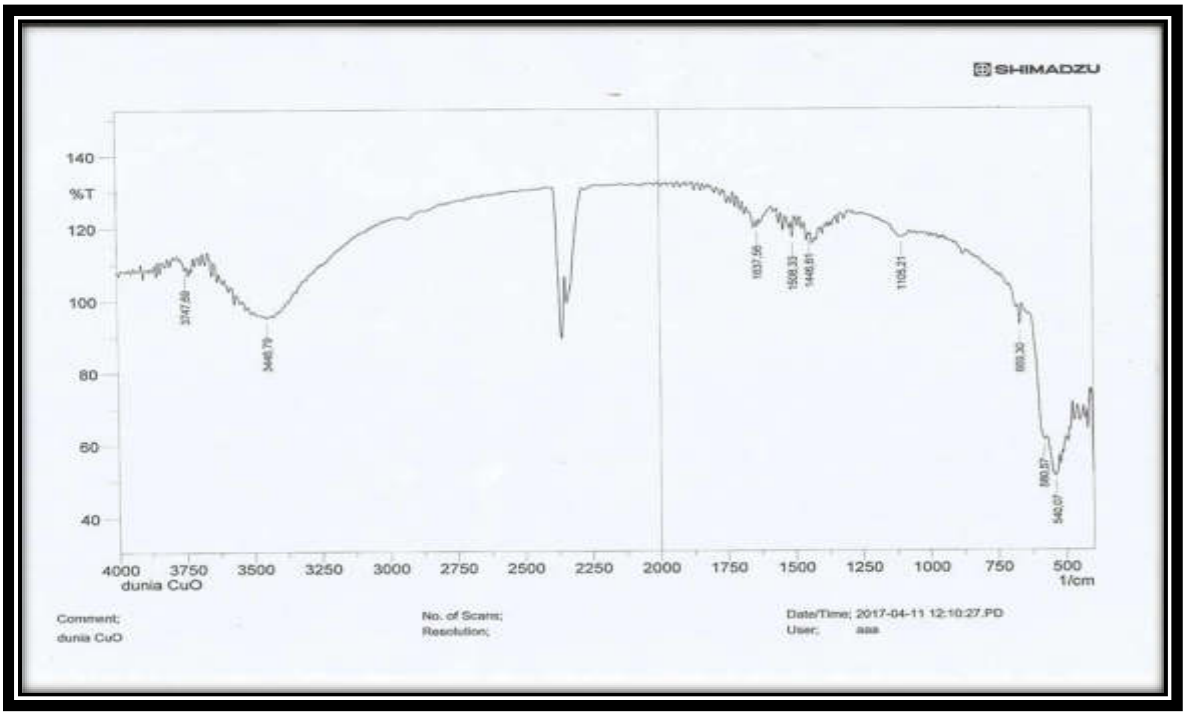

Figure (3.2): FTIR spectrum of CuO nanoparticles.

3.1.2. X-ray diffraction (XRD)

3.1.2.1. Structural XRD pattern of CuO nanoparticles

In **Figure (3.3)** the crystal planes of (110), (002) and (111) belong to the monoclinic system. All data in good agreement with JCPDS file **NO. 45-0937**, cell parameter (a = 4,685, b= 3.425, c = 5.130 Å) and no other phases are detected, and the diffraction peaks are sharp with the crystal growing completely with high purity.

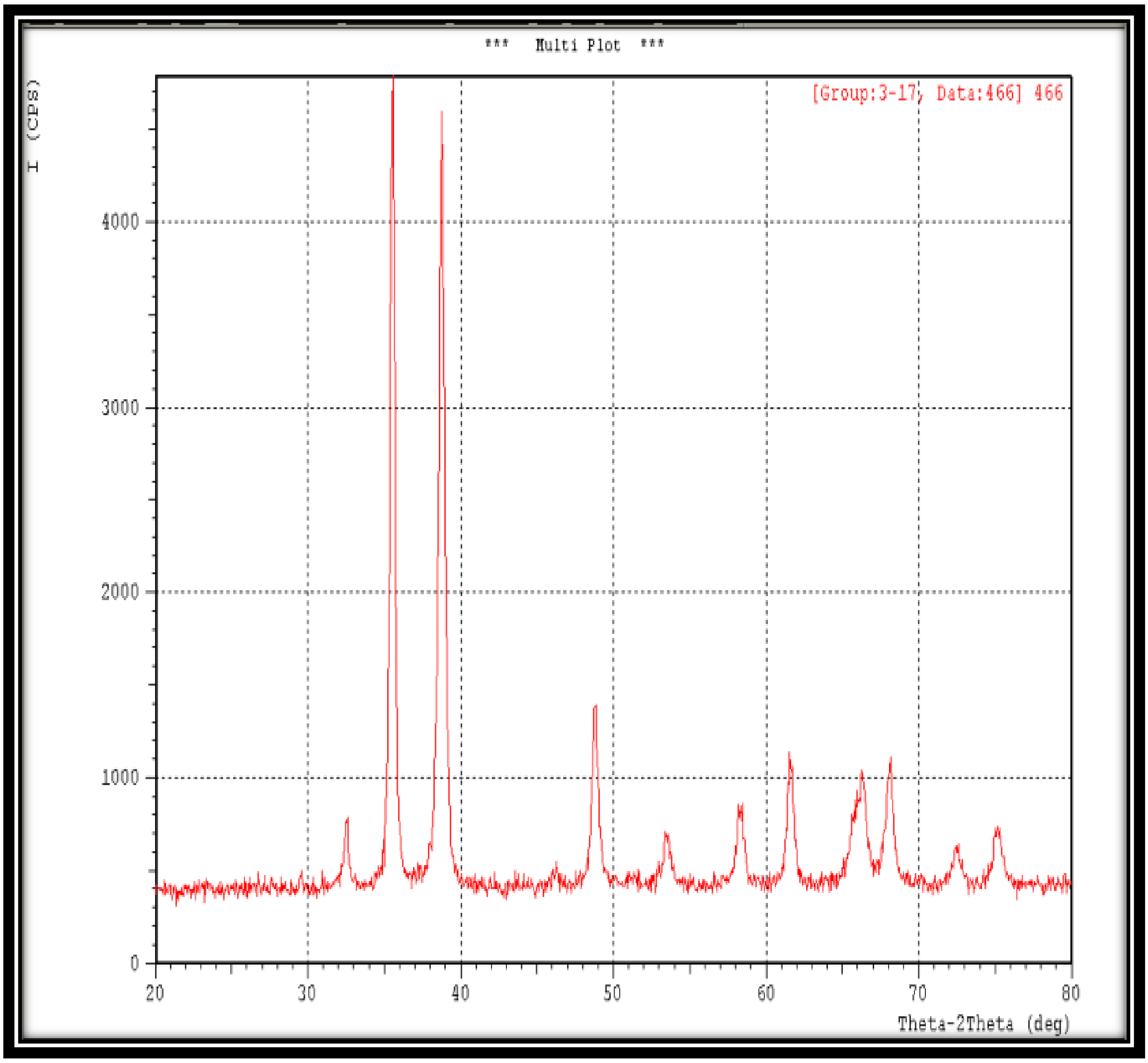

Figure (3.3): *XRD pattern of CuO nanoparticles.*

Figure (3.3) show the XRD pattern of CuO nanoparticles sample. It is very clear that the major reflections between (2Θ =30°–40°) indicate more crystalline regions in the CuO sample. The detailed analysis of the XRD and the assignments of various reflections are given in the **Table (3.1)** [138].

Table (3.1): *Strongest three peaks in XRD of CuO nanoparticles.*

No.	Peak No.	2θ (deg)	d(Å)	FWHM (deg)	Intensity (counts)
1	2	35.5496	2.52329	0.35890	1748
2	4	38.7735	2.32058	0.43660	1595
3	5	48.7942	1.86487	0.41920	410

Particle size calculation from x-ray diffraction of CuO;

Particle size has been estimated by using Debye-Scherer's **Equation (2.1):-**

D =23.4 nm calcined at 400 °C.

3.1.2.2. Structural XRD pattern of ZnO nanoparticles

In **Figure (3.4)** the crystal planes of (100), (002) and (101) belong to hexagonal wurtzite system. The crystal parameters are (a= 3.249Å and c= 5.206 Å). All diffraction data are in good agreement with JCPDS files **No. 36-1451**, no other phases are detected, and the diffraction peaks are sharp and the crystal grows completely with high purity.

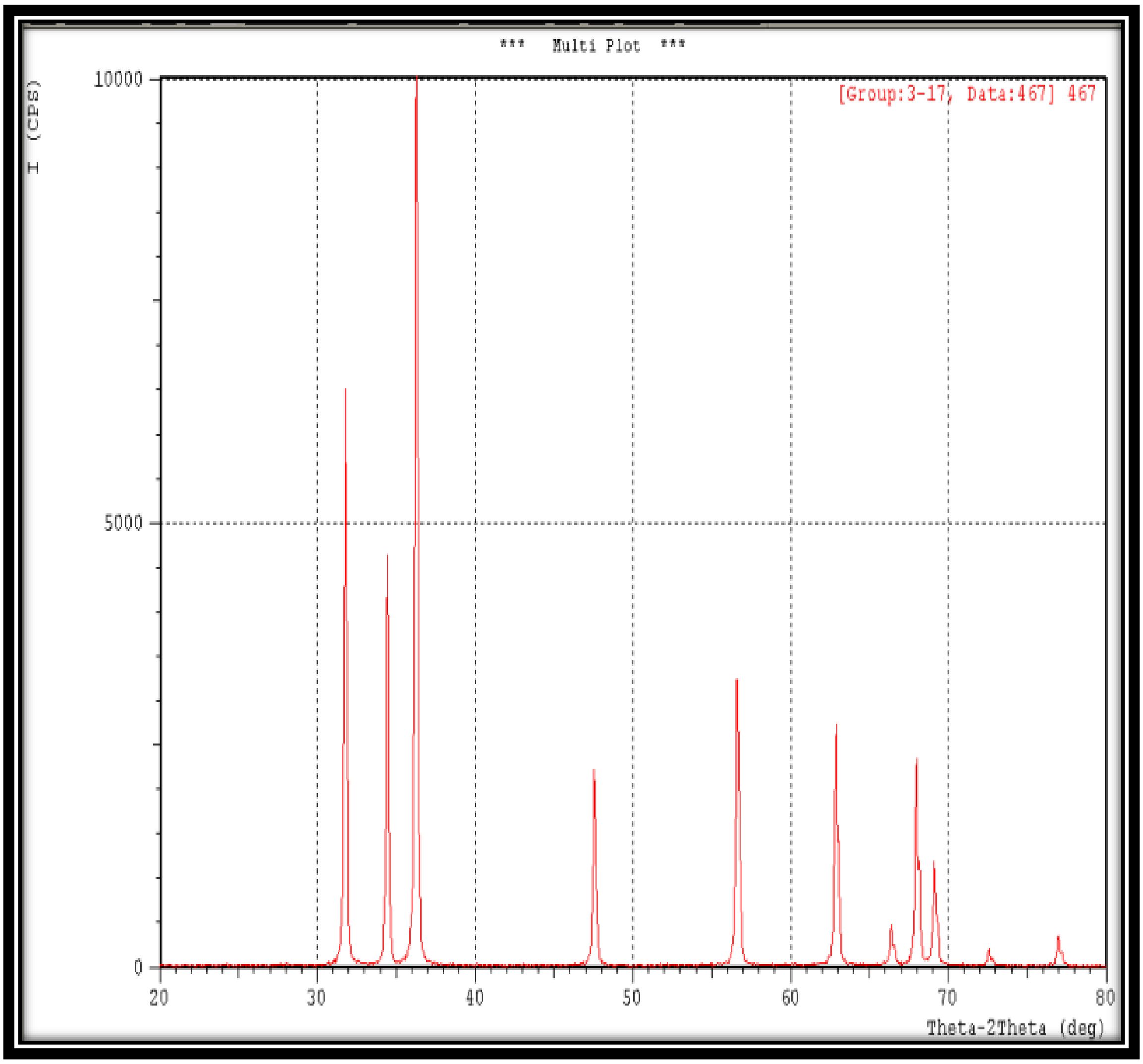

Figure (3.4): XRD pattern of ZnO nanoparticles.

Figure (3.4) show the XRD pattern of ZnO Nanoparticles. It is very clear that the major reflections between (2Ө =30°–40°) indicate more crystalline regions in the CuO sample, also the less intense peaks at 48°, 57°, 63° and 67° (2Ө values).The detailed analysis of the XRA and the assignments of various reflections are given in the **Table (3.2)** [139].

Table (3.2): *Strongest three peaks in XRD of ZnO nanoparticles.*

No.	Peak No.	2θ (deg)	d(Å)	FWHM (deg)	Intensity (counts)
1	3	36.2942	2.47321	0.18160	4543
2	1	31.8134	2.81058	0.19020	2635
3	2	34.4619	2.60040	0.17650	1899

Particle size calculation from x-ray diffraction of ZnO;

Particle size has been estimated by using Debye-Scherer's **Equation (2.1):-**

D =47.8 nm calcined at 400 °C.

3.1.3. The surface area (BET)

The specific surface area of adsorbents surfaces should be determined if any physical-chemical interpretation of its behavior as an adsorbent is to be possible. The properties of surface area were provided through the adsorption of nitrogen at 77 K which is the temperature equilibrium between the vapor and liquid phase.

The results of surface area for the (CuO, ZnO) nanoparticles are 35.6351 and 6.706 m^2/g respectively [108].

3.1.4. Scanning electron microscopy analysis (SEM)

3.1.4.1. SEM of CuO nanoparticles

The SEM images of the CuO nanoparticles sample that prepare by precipitation method are shown in **Figure (3.5)**.

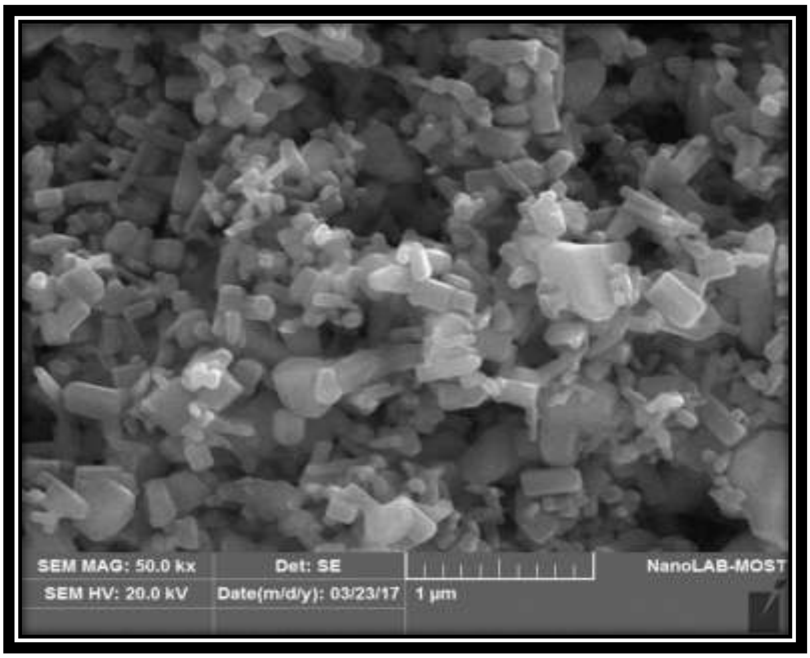

Figure (3.5): *SEM image of CuO nanoparticles.*

In **Figure (3.5)** shown a homogeneous distribution of non-spherical shape and with irregular distribution. From SEM images it is confirmed that the particles having size (39-41) nm [118].

3.1.4.2. SEM of ZnO nanoparticles

The SEM images of the ZnO nanoparticles sample that prepare by precipitation method are shown in **Figure (3.6)**.

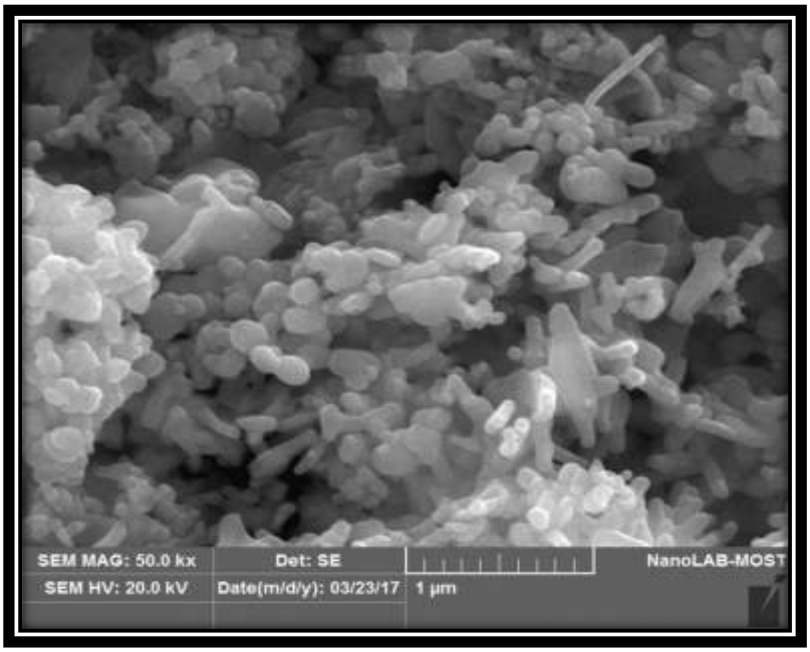

Figure (3.6): *SEM image of ZnO nanoparticles.*

In **Figure (3.6)** shown a homogeneous distribution with bigger agglomerates results in lack of coagulation of particles and existence of some voids along the deposited layer. From SEM images it is confirmed that the particles having size (100-150) nm [118].

3.1.5. Atomic Force Microscopy (AFM)

Atomic force microscopy (AFM) is a powerful characterization tool for determining the particle size and surface organization of the synthesized materials. The wet ability of a surface is dependent on its chemical composition, and also on the topography of the surfaces.

(CuO, ZnO) nanoparticles are characterized by AFM image in two and three-dimensional and particles sizes distributions for each adsorbents surface were represented in Figures (3.7, 3.8) and (3.9, 3.10) respectively. They show that the average diameters of the particles were (39.4 and 139 nm) for CuO and ZnO respectively [118].

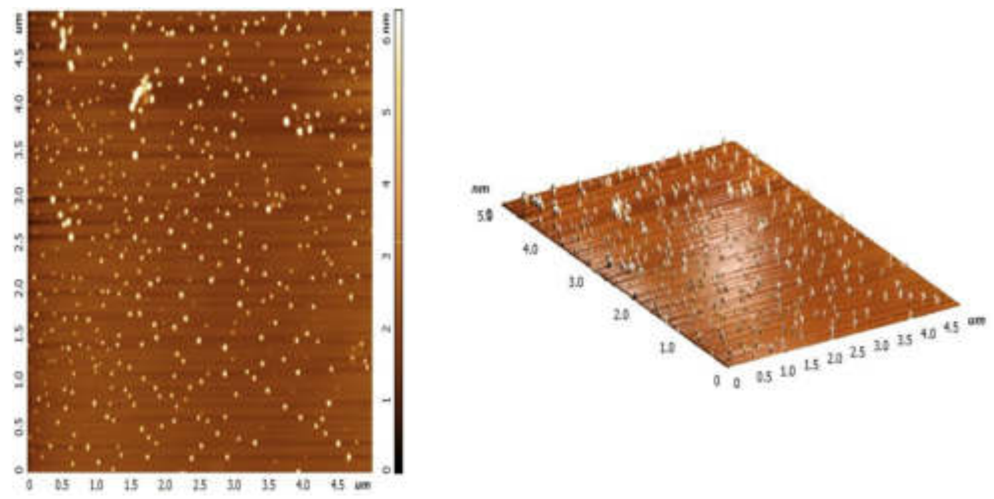

Figure (3. 7): *AFM images of CuO nanoparticles.*

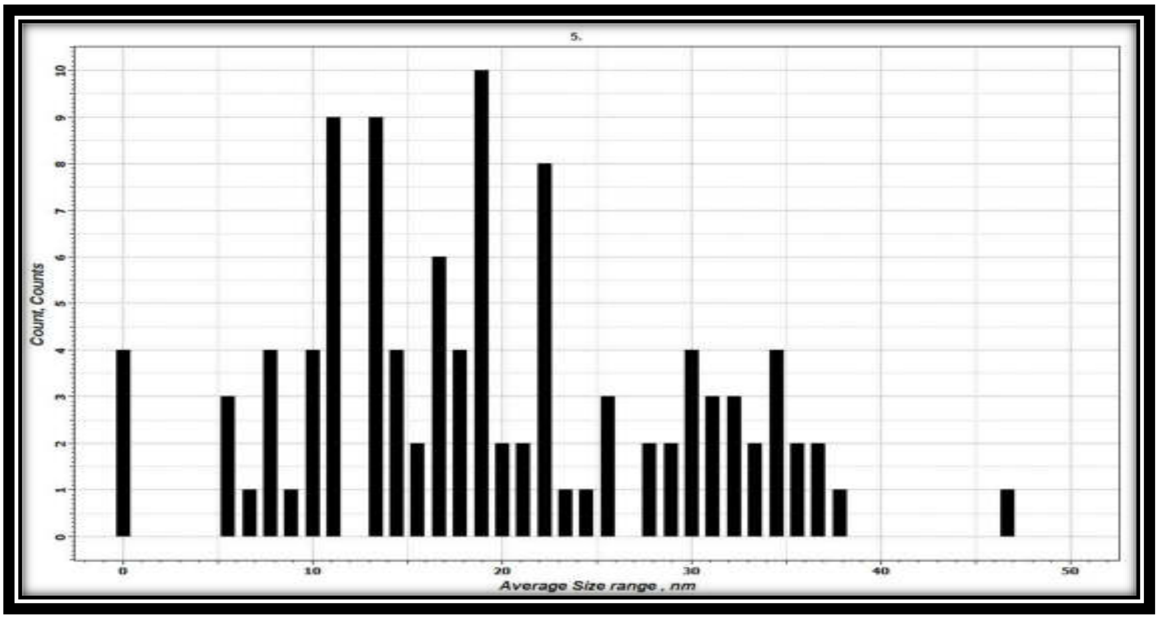

Figure (3. 8): *Particle size distribution of CuO nanoparticles.*

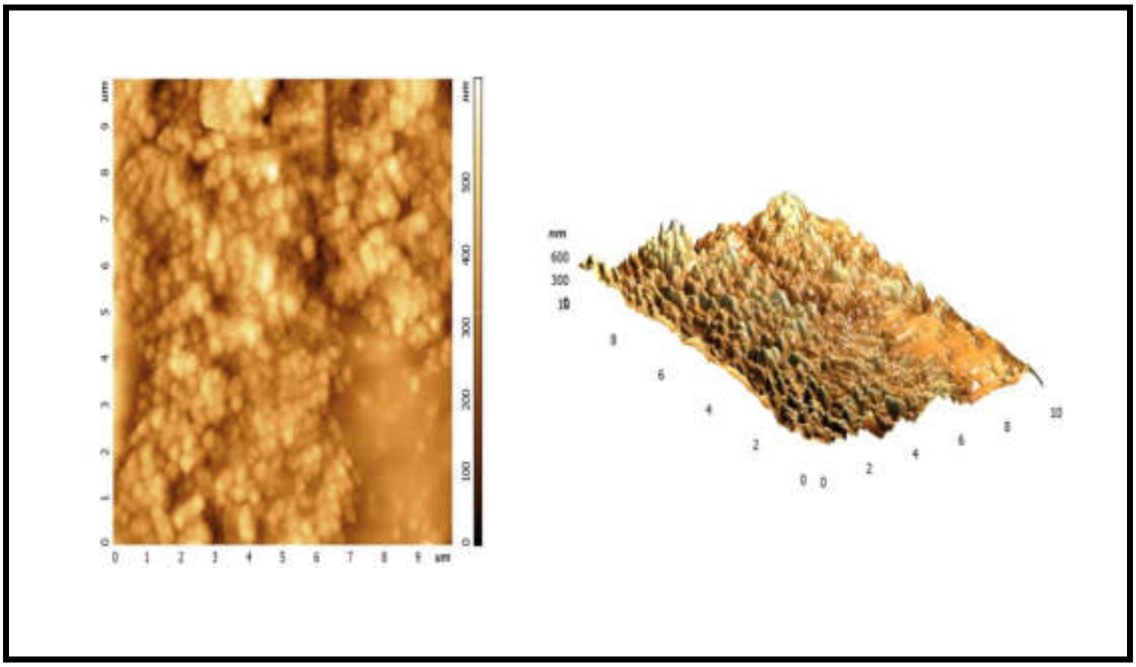

Figure (3. 9): *AFM images of ZnO nanoparticles.*

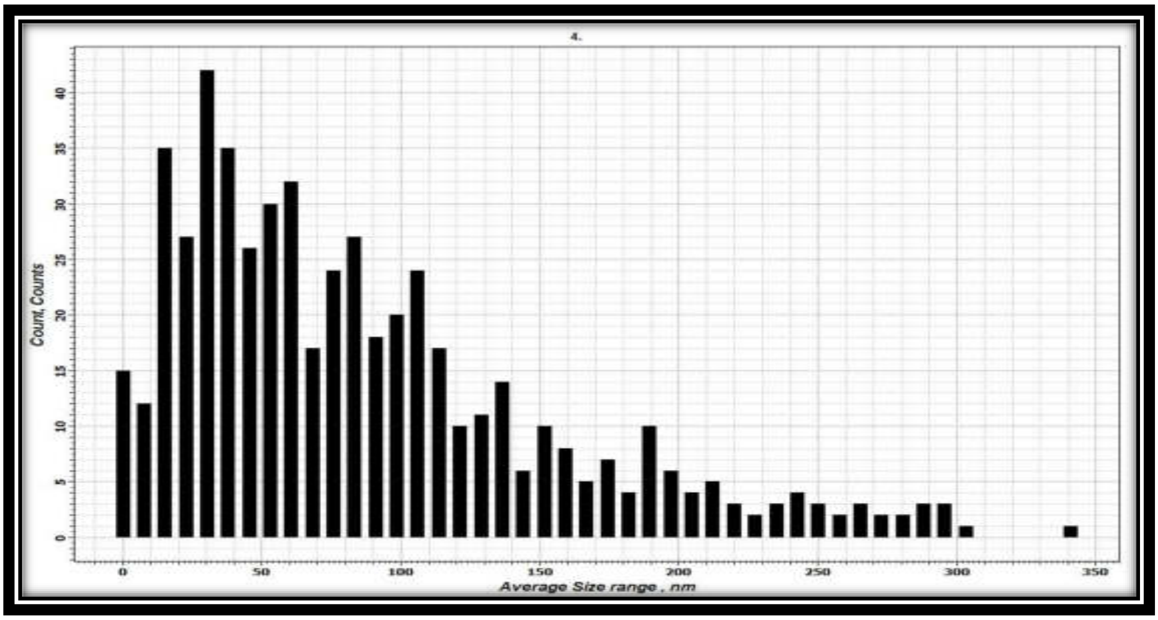

Figure (3. 10): *Particle size distribution of ZnO nanoparticles.*

3.2. Optimum conditions for adsorption

3.2.1. Determination of Equilibrium Time of adsorption

To determination of equilibrium time for adsorption of the Eosin dye solution on adsorbents surfaces (CuO, ZnO) nanoparticles at 25 ^{o}C using a fixed concentration (C_o=10) ppm, pH=7 and fixed weight of the adsorbent surfaces (0.04 g) were studied at different periods (10-140) min. The results showed in **Table (3.3)** presented in **Figure (3.11)** that equilibrium time (50) min for adsorption of Eosin dye on CuO and (120) min for ZnO. It was observed that the amount adsorbate increased with the increase in equilibrium time until it reaches a constant value [133]. This can be explained by the fact that initially, the number of surface sites is very large which allows adsorption to take place very easily. But as the time passes, active sites become saturated and thus slowing down the removal of dye [134].These results are in agreement with surface area results were obtained by BET method. CuO has a higher affinity for adsorption than ZnO.

Table (3.3): *Effect of equilibrium time for adsorption of Eosin dye at temperature =25 ^{o}C; and C_o=10 ppm on (CuO, ZnO) nanoparticles.*

Time (min)	**Cu**			**ZnO**		
	C_e (mg/L)	**q_t (mg/g)**	**% adsorption**	**C_e (mg/L)**	**q_t (mg/g)**	**% adsorption**
10	0.909	6.8182	90.10	5.944	3.0420	40.56
20	0.907	6.8197	90.93	5.942	3.0435	40.58
30	0.900	6.8250	91	5.940	3.0450	40.60
40	0.899	6.8257	91.01	5.939	3.0457	40.61
50	0.895	6.8287	91.05	5.936	3.0480	40.64
60	0.895	6.8287	91.05	5.930	3.0525	40.70
70	0.895	6.8287	91.05	5.928	3.0540	40.72
80	0.895	6.8287	91.05	5.923	3.0577	40.77
90	0.895	6.8287	91.05	5.921	3.0592	40.79
100	0.895	6.8287	91.05	5.920	3.0600	40.80
110	0.895	6.8287	91.05	5.919	3.0607	40.81
120	0.895	6.8287	91.05	5.918	3.0615	40.82
130	0.895	6.8287	91.05	5.918	3.0615	40.82
140	0.895	6.8287	91.05	5.918	3.0615	40.82

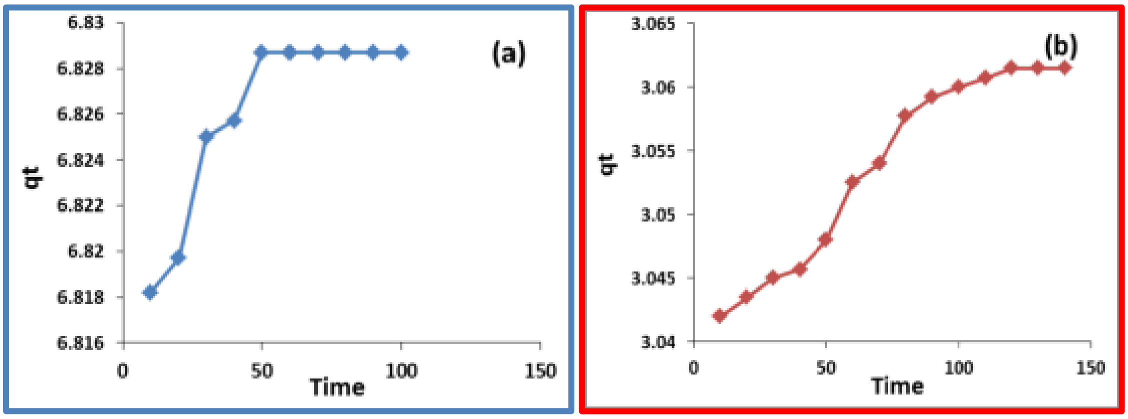

Figure (3.11): *Effect of equilibrium time for adsorption of Eosin dye at temperature =25 ^{o}C and C_o=10 ppm on **(a)** CuO nanoparticles. **(b)** ZnO nanoparticles.*

3.2.2. Adsorbent Weight

The effect of adsorbent weight on the adsorption process of (CuO, ZnO) nanoparticles was studied at 25 °C using a fixed concentration (C_o=10) ppm and different weight of adsorbents (0.01-0.09 g). The contact time is fixed at (50) min for CuO and (120) min for ZnO. The **Table (3.4)** presented in **Figure (3.12)** shows the percentage adsorption of Eosin dye increased with the increase in the weight of adsorbents. The percentage adsorption reach maximum value with 0.04 g of weight is **92**% for CuO and **52%** for ZnO, and then the percentage starts to decrease. These results can be explained the number of a site available for adsorption site increases by increasing the adsorbent weight, but as the time passes, active sites become saturated and thus slowing down the removal of dye. CuO has a higher affinity for adsorption than ZnO.

The percentage adsorption can be calculated from the following **Equation (3.1)** [135].

$$\% \mathbf{Adsorption} = \frac{C_o - C_e}{C_o} \times \mathbf{100} \quad \ldots\ldots\ldots\ldots\ldots\ldots\ldots\ldots\ldots\ldots\ldots\ldots\ldots\ldots\ldots\ldots\ldots\ldots\ldots (\mathbf{3.1})$$

Table (3.4): *Effect of adsorbents weight on the adsorption of Eosin dye at temperature =25 °C and C_o=10 ppm on (CuO, ZnO) nanoparticles.*

W (gm)	**Cu**		**ZnO**	
	C_e (mg/L)	**% adsorption**	**C_e (mg/L)**	**% adsorption**
0.01	0.95	90.5	4.97	50.3
0.02	0.81	91.82	4.83	51.7
0.03	0.808	91.92	4.819	51.81
0.04	0.80	92	4.80	52
0.05	0.89	91.1	4.84	51.51
0.06	0.92	90.8	4.96	50.4
0.07	0.96	90.4	5.15	48.5
0.08	0.98	90.2	5.60	44.6
0.09	1.08	89.2	5.94	40.6

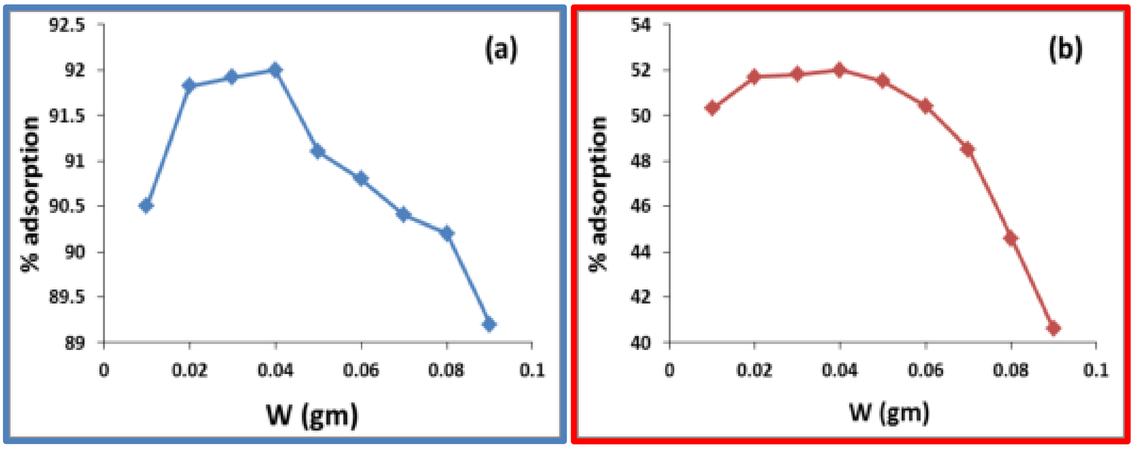

Figure (3.12): *Effect of adsorbents weight on the adsorption of Eosin dye at temperature =25 °C and C_o=10 ppm on **(a)** CuO nanoparticles. **(b)** ZnO nanoparticles.*

3.2.3. Study Effect of concentration on adsorption

The effect of adsorbate concentration on the adsorption process was studied at 25 ^{o}C using a fixed weight of adsorbents (0. 04 g) and different concentration of adsorbate (C_o=2-20) ppm. **Table (3.5)** presented in **Figure (3.13)** shows the effect of initial Eosin dye concentrations on (CuO, ZnO) nanoparticles. As we find that the highest the percentage adsorption of Eosin dye at (C_o=10) ppm and in general, the percentage adsorption of CuO is higher than ZnO.

Table (3.5): *Effect of adsorbates concentration on adsorption of Eosin dye at temperature =25 ^{o}C; and C_o=10 ppm on (CuO, ZnO) nanoparticles.*

C_o (mg/L)	**Cu**		**ZnO**	
	C_e (mg/L)	**% adsorption**	**C_e (mg/L)**	**% adsorption**
2	0.480	76	1.488	25.6
4	0.577	85.57	2.711	32.22
6	0.668	88.86	3.899	35.01
8	0.763	90.46	5.106	36.17
10	0.595	94.05	3.918	60.82
12	1.375	88.54	6.991	41.74
14	1.487	89.37	7.989	42.93
16	2.508	84.32	8.879	44.50
18	3.128	82.62	9.873	45.15
20	3.695	81.52	10.659	46.70

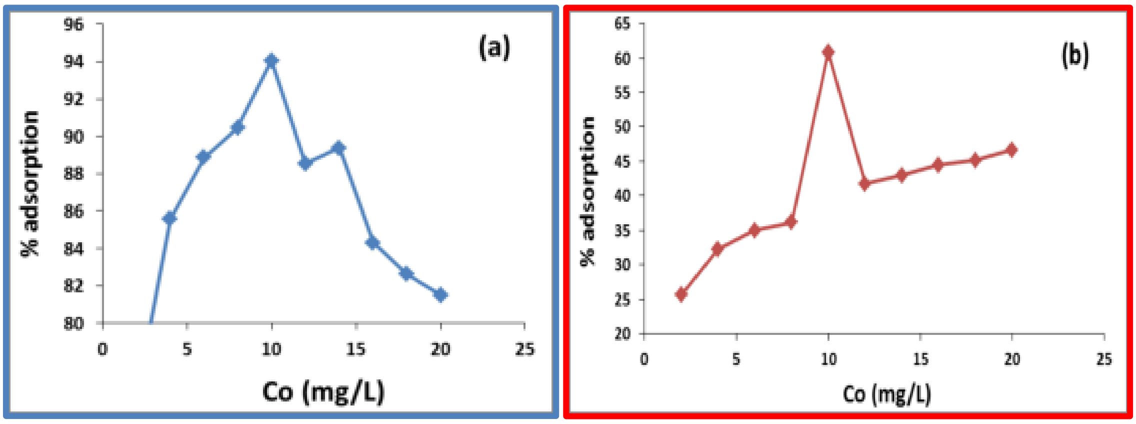

Figure (3.13): *Effect of adsorbates concentration on adsorption of Eosin dye at temperature =25 ^{o}C and C_o=10 ppm on* ***(a)*** *CuO nanoparticles.* ***(b)*** *ZnO nanoparticles.*

3.2.4. Effect of pH

The effect of pH on the adsorption of the Eosin dye on the (CuO, ZnO) nanoparticles was studied by changing pH (4,7and 10) and a fixed weight of adsorbents (0. 04 g) with different concentrations of the Eosin dye within the range (2-20) ppm while maintaining on the constant temperature at 25 ^{O}C and the equilibrium time (50) min for CuO and (120) min for ZnO. The results are shown in **Table (3.6)** and **Figure (3.14)** for the surface of the CuO and **Table (3.7)** and **Figure (3.15)** for the surface of the ZnO.

Table (3.6): *Effect of pH on the adsorption of Eosin dye on CuO nanoparticles at 25 ^oC.*

C_o (mg/L)	pH=4		pH=7		pH=10	
	C_e (mg/L)	Q_e (mg/g)	C_e (mg/L)	Q_e (mg/g)	C_e (mg/L)	Q_e (mg/g)
2	0.303	1.272	0.480	1.140	0.730	0.952
4	0.489	2.633	0.577	2.567	1.588	1.809
6	0.501	4.124	0.668	3.999	2.318	2.761
8	0.620	5.535	0.763	5.427	2.891	3.831
10	0.769	6.923	0.895	6.828	2.955	5.283
12	0.920	8.310	1.054	8.209	3.012	6.741
14	1.066	9.700	1.122	9.658	3.394	7.954
16	1.191	11.106	1.244	11.067	3.699	9.225
18	1.276	12.543	1.370	12.472	3.712	10.716
20	1.359	13.980	1.490	13.882	3.876	12.093

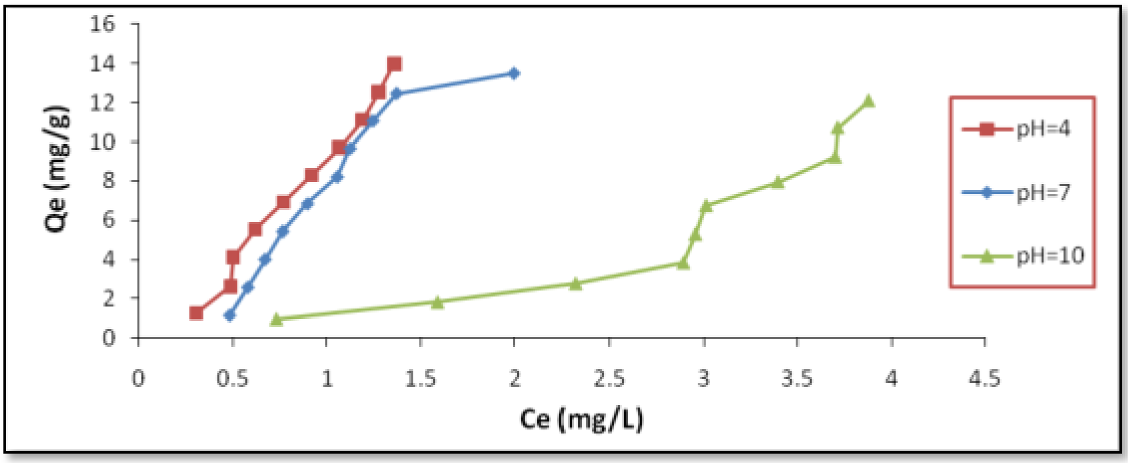

Figure (3.14): *Effect of pH on the adsorption of Eosin dye on CuO nanoparticles at 25 ^oC.*

Table (3.7): *Effect of pH on the adsorption of Eosin dye on ZnO nanoparticles at 25 ᵒC.*

C_o (mg/L)	pH=4		pH=7		pH=10	
	C_e (mg/L)	Q_e (mg/g)	C_e (mg/L)	Q_e (mg/g)	C_e (mg/L)	Q_e (mg/g)
2	1.289	0.533	1.488	0.384	1.887	0.084
4	1.465	1.172	2.711	0.966	3.022	0.733
6	2.421	2.684	3.899	1.575	4.970	0.772
8	4.232	2.826	5.106	2.170	6.245	1.316
10	5.693	3.230	5.918	3.061	6.987	2.259
12	6.468	4.149	6.991	3.756	7.879	3.090
14	7.075	5.193	7.989	4.508	8.340	4.245
16	8.583	5.562	8.879	5.340	9.845	4.616
18	9.264	6.552	9.873	6.095	10.932	5.301
20	10.383	7.212	10.659	7.005	11.688	6.234

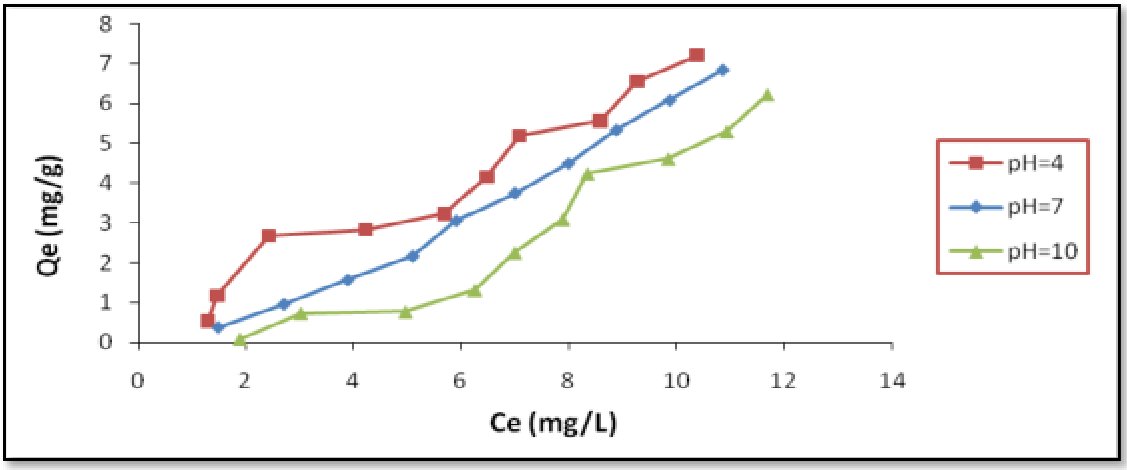

Figure (3.15): *Effect of pH on the adsorption of Eosin dye on ZnO nanoparticles at 25 ᵒC.*

The effect the amount adsorbate of Eosin dye on (CuO, ZnO) decreases with the increase of pH and according to the following**:**

pH = 4 > 7 > 10

Two surfaces contain groups (**OH^-**) and in the acidic solution (**pH=4**), the positive charge was increasing on two surfaces as a result of the abundance of protons. On the other hand, increasing the concentration of hydrogen ions works on displace (**Na^+**) from (**$-CO_2$ and -ONa**) groups in the Eosin dye and replace them without changing in the color or λ_{max} so that the interference ratio increases between the dye and two surfaces through the association between the oxygen atoms for Eosin dye and two surfaces. So increases the tendency of the dye for association with two surfaces more than its tendency to the association to the solvent molecules, so the amount adsorbate is increased in the acidic media. But in the basic media (**pH=10**), the amount adsorbate was decreasing attributable to turns this formula to the salt where (**OH^-**) group turns into phenoxide ion generating a negative charge on the oxygen atom so that increases its solubility because of its ability to the molecular interventions in the adsorption media, so weaken the percentage adsorption. The two a surfaces will gain a negative charge through the solution. The hydroxyl groups work on the pull (**Na^+**) from the Eosin dye from (**$-CO_2$ and -ONa**) the group and make this group carry a negative charge but without color change or λ_{max}. Therefore, there will be a strong repulsion for the similar charges of dye and two surfaces so reducing the amount adsorbate on the surface to occur the electrostatic repulsion between them. The study better pH for the two surfaces is found (**pH=1**). The percentage adsorption is increasedin the acidic media on two surfaces and these results shown in **Table (3.8)** and **Figure (3.16)** [132].

Table (3.8): *Effect of changing the pH on the amount adsorbate of Eosin dye on (CuO, ZnO) nanoparticles at 25 ^oC.*

pH	**CuO**			**ZnO**		
	C_e (mg/L)	**C_o-C_e**	**% adsorption**	**C_e (mg/L)**	**C_o-C_e**	**% adsorption**
1	0.260	17.74	98.55	2.865	15.13	84.08
2	0.711	17.28	96.05	7.711	10.28	57.16
3	0.823	17.17	95.42	8.898	9.10	50.56
4	1.276	16.72	92.91	9.264	8.73	48.53
5	1.355	16.64	92.47	9.321	8.67	48.21
6	1.391	16.60	92.27	9.545	8.45	46.97
7	1.370	16.63	92.38	9.873	8.12	45.15
8	1.676	14.32	90.68	9.899	8.10	45
9	3.701	14.29	79.43	9.912	8.08	44.93
10	3.712	14.28	79.37	10.932	7.06	39.26

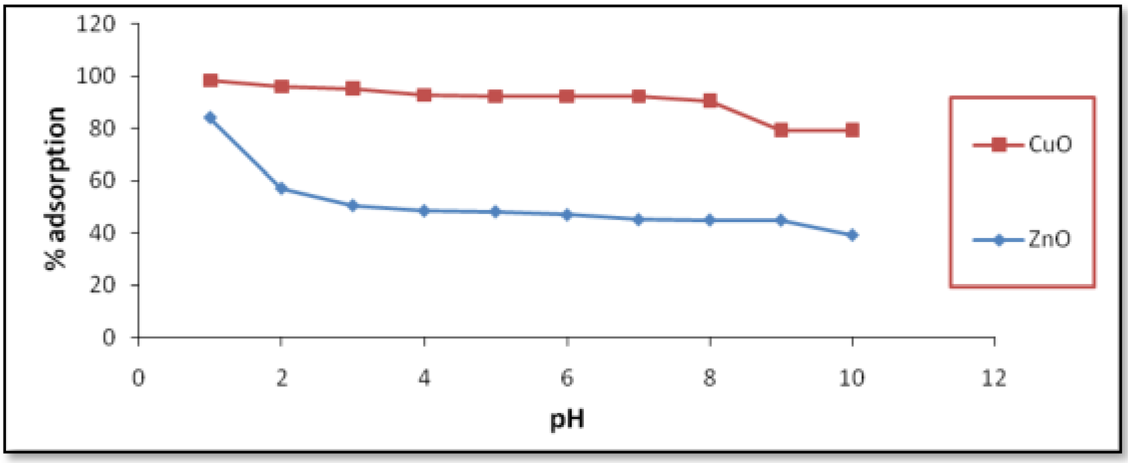

Figure (3.16): *Effect of change the pH on the amount adsorbate of Eosin dye on (CuO, ZnO) nanoparticles at 25 ^oC.*

3.2.5. Effect of temperature on adsorption and calculation of thermodynamic functions

The temperature effect on the adsorption of Eosin dye on (CuO, ZnO) nanoparticles has been studied at different temperatures (20-40) ^{o}C and at different initial concentrations (2-20) ppm. The graphical representation of the effect of temperature change on adsorption obtained by plotting the amount of solute adsorbed per unit weight of adsorbent (Q_e) against the equilibrium concentration of the solute in the solution (C_e).

The results of this study are shown in **Tables (3.9 and 3.10)** and **Figures (3.17 and 3.18)**, respectively, the amount of adsorbent decreases with increasing temperatures, so the adsorption process is an exothermic process because of desorption caused by an increase in the available thermal energy. Higher temperature induces higher mobility of the adsorbate causing desorption [117, 132].

Table (3.9): *Effect of temperature change on the adsorption of the Eosin dye on CuO nanoparticles.*

C_o (mg/L)	20 °C		25 °C		30 °C		35 °C		40 °C	
	C_e (mg/L)	Q_e (mg/g)	C_e (mg/L)	Q_e (mg/g)	C_e (mg/L)	Q_e (mg/g)	C_e (mg/L)	Q_e (mg/g)	C_e (mg/L)	Q_e (mg/g)
2	0.466	1.150	0.480	1.140	0.489	1.133	0.499	1.125	0.503	1.122
4	0.560	2.580	0.577	2.567	0.580	2.565	0.588	2.559	0.594	2.554
6	0.656	4.008	0.668	3.999	0.673	3.995	0.687	3.984	0.697	3.977
8	0.753	5.435	0.763	5.427	0.789	5.408	0.812	5.391	0.831	5.376
10	0.881	6.839	0.895	6.828	0.899	6.825	0.911	6.816	0.957	6.782
12	0.998	8.258	1.054	8.209	1.062	8.203	1.077	8.192	1.112	8.166
14	1.099	9.675	1.122	9.658	1.129	9.653	1.157	9.632	1.176	9.618
16	1.235	11.073	1.244	11.067	1.249	11.063	1.265	11.051	1.272	11.046
18	1.366	12.475	1.370	12.472	1.382	12.463	1.398	12.451	1.401	12.449
20	1.435	13.923	1.490	13.882	1.499	13.875	1.509	13.868	1.529	13.853

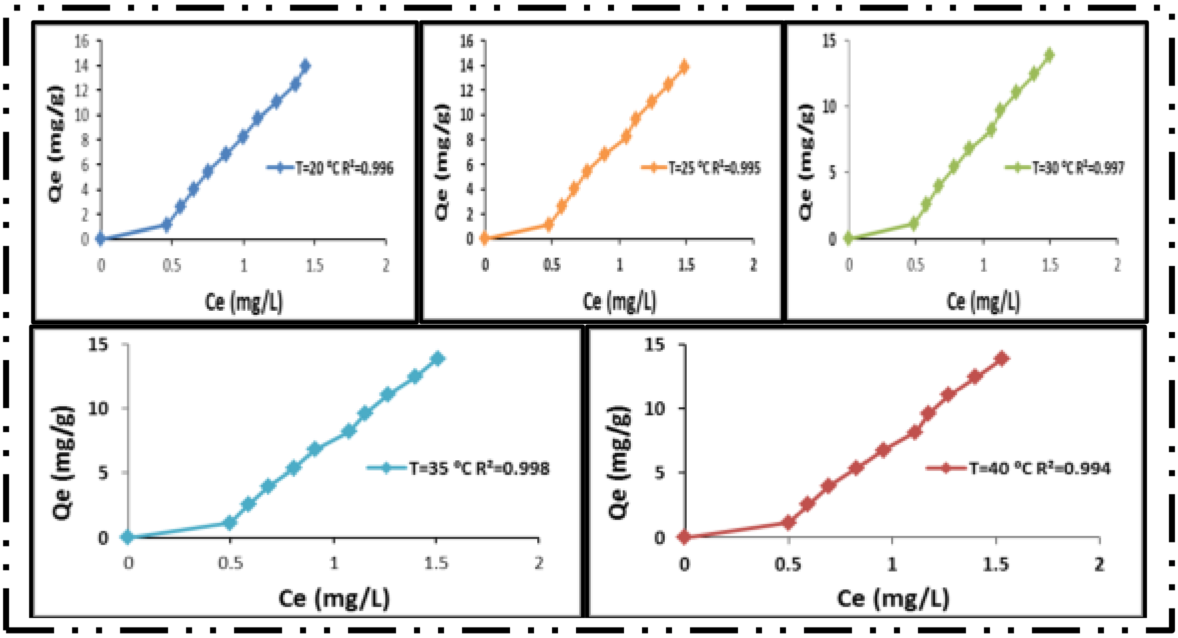

Figure (3.17): *Effect of temperature change on the adsorption of the Eosin dye on CuO nanoparticles.*

Table (3.10): *Effect of temperature change on the adsorption of the Eosin dye on ZnO nanoparticles.*

C_o (mg/L)	20 °C		25 °C		30 °C		35 °C		40 °C	
	C_e (mg/L)	Q_e (mg/g)	C_e (mg/L)	Q_e (mg/g)	C_e (mg/L)	Q_e (mg/g)	C_e (mg/L)	Q_e (mg/g)	C_e (mg/L)	Q_e (mg/g)
2	1.480	0.390	1.488	0.3840	1.490	0.382	1.498	0.376	1.505	0.371
4	2.690	0.982	2.711	0.966	2.723	0.957	2.727	0.954	2.735	0.948
6	3.891	1.581	3.899	1.575	3.901	1.574	3.905	1.571	3.909	1.568
8	4.999	2.250	5.106	2.170	5.117	2.162	5.124	2.157	5.129	2.153
10	5.901	3.074	5.918	3.061	5.927	3.054	5.933	3.050	5.947	3.039
12	6.898	3.826	6.991	3.756	7.011	3.741	7.021	3.734	7.028	3.729
14	7.977	4.517	7.989	4.508	7.993	4.505	7.995	4.503	7.998	4.501
16	8.876	5.343	8.879	5.340	8.885	5.336	8.887	5.334	8.890	5.332
18	9.869	6.098	9.873	6.095	9.879	6.090	9.881	6.089	9.889	6.083
20	10.654	7.009	10.659	7.005	10.668	6.999	10.671	6.996	10.678	6.991

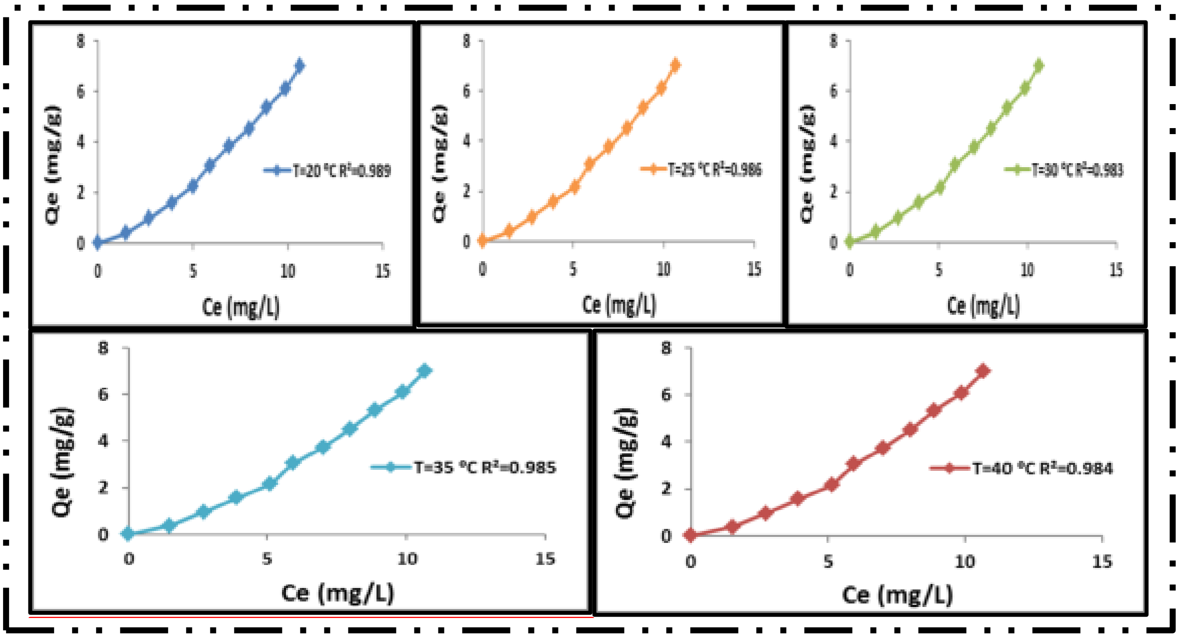

Figure (3.18): *The effect of temperature change on the adsorption of the Eosin dye on ZnO nanoparticles.*

The enthalpy change (ΔH) can be calculated from the Van't Hoff **Equations (1.24, 1.25)** and through drawing the relationship between **$\ln X_m$** and the reciprocal of temperature **1/T** can be obtained on (ΔH) from the slope as shown in **Table (3.11)** and **Figure (3.19)**.

Table (3.11): *Values of greatest amounts adsorbed ($\ln X_m$) for Eosin dye on CuO and ZnO nanoparticles at different temperature (20-40) °C and K.*

Oxide nanoparticles	C_o	T (°C)	T (K)	1/T	X_m	$\ln X_m$
CuO	**20ppm**	20	293	0.00341	13.923	2.633
		25	298	0.00337	13.882	2.631
		30	303	0.00331	13.875	2.630
		35	308	0.00324	13.868	3.629
		40	318	0.00319	13.853	3.628
ZnO	**20ppm**	20	293	0.00341	7.009	1.947
		25	298	0.00337	7.005	1.946
		30	303	0.00331	6.999	1.945
		35	308	0.00324	6.996	1.944
		40	318	0.00319	6.991	1.943

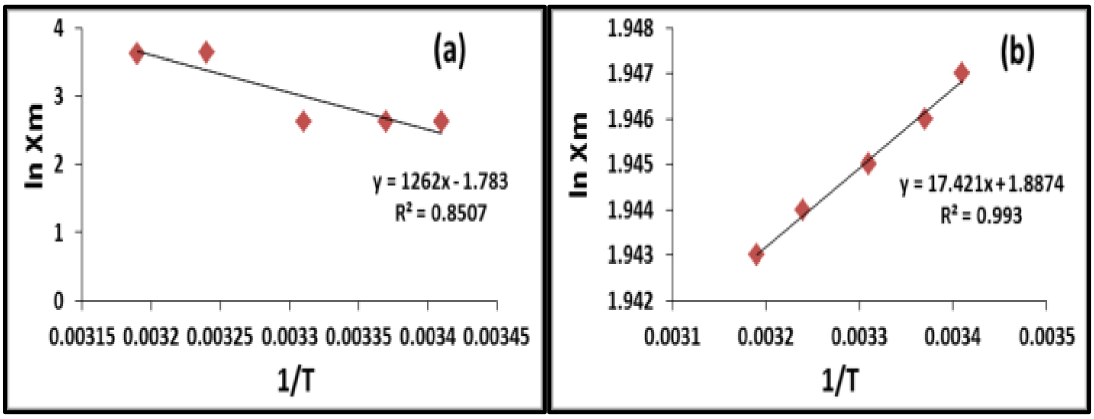

Figure (3.19): *Values of greatest amounts adsorbed ($\ln X_m$) for Eosin dye on **a** and **b** of CuO, and ZnO nanoparticles respectively at different temperature (20-40) °C and K.*

The change in free energy (ΔG) and the change in entropy (ΔS) were calculated from the **Equation (1.26, 1.27, and 1.28)**. The results of the thermodynamic functions are shown in **Table (3.12)** for the Eosin dye on (CuO, ZnO) nanoparticles.

Table (3.12): *Values of thermodynamic functions for adsorption Eosin dye on (CuO, ZnO) nanoparticles.*

Oxide nanoparticles	C_e (mg/L)	Thermodynamic function	20 ^{o}C	25 ^{o}C	30 ^{o}C	35 ^{o}C	40 ^{o}C
CuO	**20ppm**	**ΔH kJ.mol^{-1}**	**-10.492**				
		ΔG kJ.mol^{-1}	**-5.534**	**-5.529**	**-5.605**	**-5.680**	**-5.826**
		ΔS J.mol^{-1} K^{-1}	**-0.0169**	**-0.0164**	**-0.0161**	**-0.0156**	**-0.0146**
ZnO	**20ppm**	**ΔH kJ.mol^{-1}**	**-0.144**				
		ΔG kJ.mol^{-1}	**-5.033**	**-5.116**	**-5.197**	**-5.281**	**-5.447**
		ΔS J.mol^{-1} K^{-1}	**0.016686**	**0.016684**	**0.016676**	**0.016678**	**0.016676**

Gibb's free energy values of the adsorption process were negative at all temperatures under study and changed with the rise in temperature for CuO and ZnO **Table (3.12)**. This behavior indicates that the adsorption process was spontaneous [127,132,136]. The values of ΔH were negative, indicating that the adsorption process was exothermic in nature. The negative values of ΔS indicate that the molecules adsorbed for Eosin dye are arranged on the surface more than a solution, any decrease of disorder [117,132]. Either the positive values of ΔS indicates that that the molecules adsorbed for Eosin dye are still in continuous movement on the surface more than it is in the solution (liquid phase) [138].

3.2.6. Adsorption Kinetics

The kinetic study was carried out on adsorption of Eosin dye on (CuO, ZnO) nanoparticles by using a batch method at initial concentration (10) ppm and different temperatures (20-40) °C. Pseudo first order and pseudo second-order models were applied on the experimental data to examine the adsorption kinetics of Eosin dye on (CuO, ZnO) nanoparticles.

Table (3.13): *Values of the Pseudo-Second Order Model for adsorption of Eosin dye on CuO nanoparticles.*

T (°C)	Time (min)	C_e (mg/L)	q_t (mg/g)	ln(q_e-q_t)	t/q_t
20 °C	**10**	0.901	6.8242	-4.199	1.465
	20	0.898	6.8265	-4.366	2.929
	30	0.892	6.8310	-4.803	4.391
	40	0.890	6.8325	-5.005	5.854
	50	0.881	6.8392		7.310
25 °C	**10**	0.909	6.8182	-4.556	1.466
	20	0.907	6.8197	-4.710	2.932
	30	0.900	6.8250	-5.599	4.395
	40	0.899	6.8257	-5.809	5.860
	50	0.895	6.8287		7.322
30 °C	**10**	0.915	6.8137	-4.422	1.467
	20	0.910	6.8175	-4.803	2.933
	30	0.906	6.8205	-5.259	4.398
	40	0.902	6.8235	-6.119	5.862
	50	0.899	6.8257		7.325
35 °C	**10**	0.921	6.8092	-4.892	1.468
	20	0.918	6.8115	-5.259	2.936
	30	0.916	6.8130	-5.599	4.403
	40	0.913	6.8152	-6.502	5.869
	50	0.911	6.8167		7.334
40 °C	**10**	0.970	6.7725	-4.635	1.476
	20	0.967	6.7747	-4.892	2.952
	30	0.965	6.7762	-5.115	4.427
	40	0.960	6.7800	-6.119	5.899
	50	0.957	6.7822		7.372

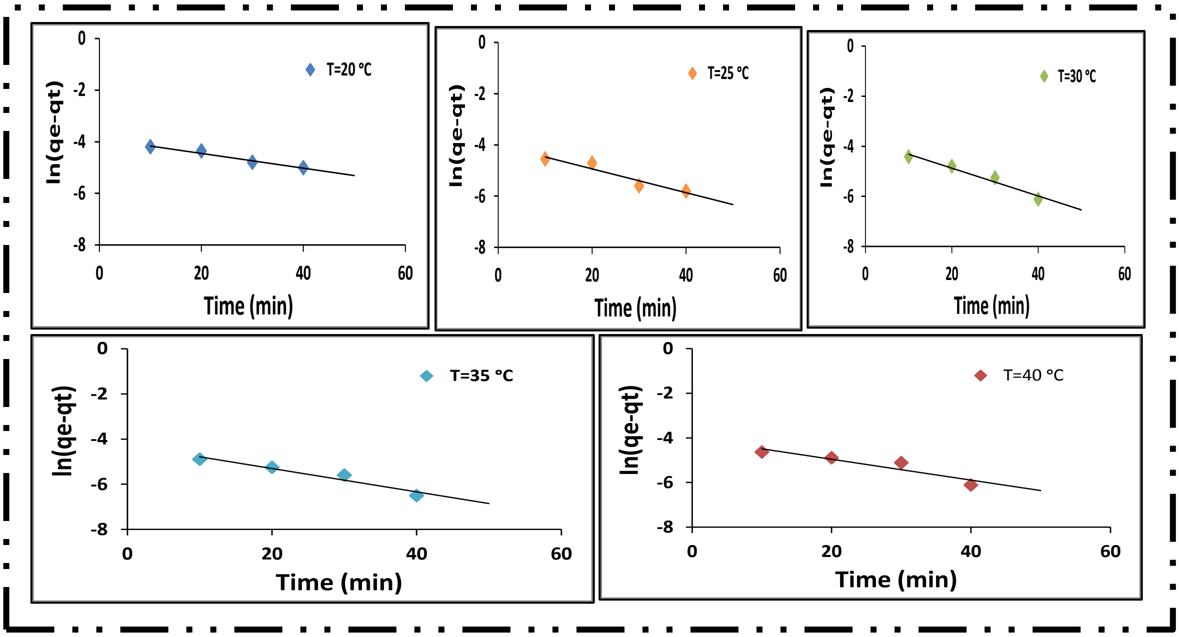

***Figure* (3.20):** *The Pseudo-First Order Model of Eosin dye on CuO nanoparticles.*

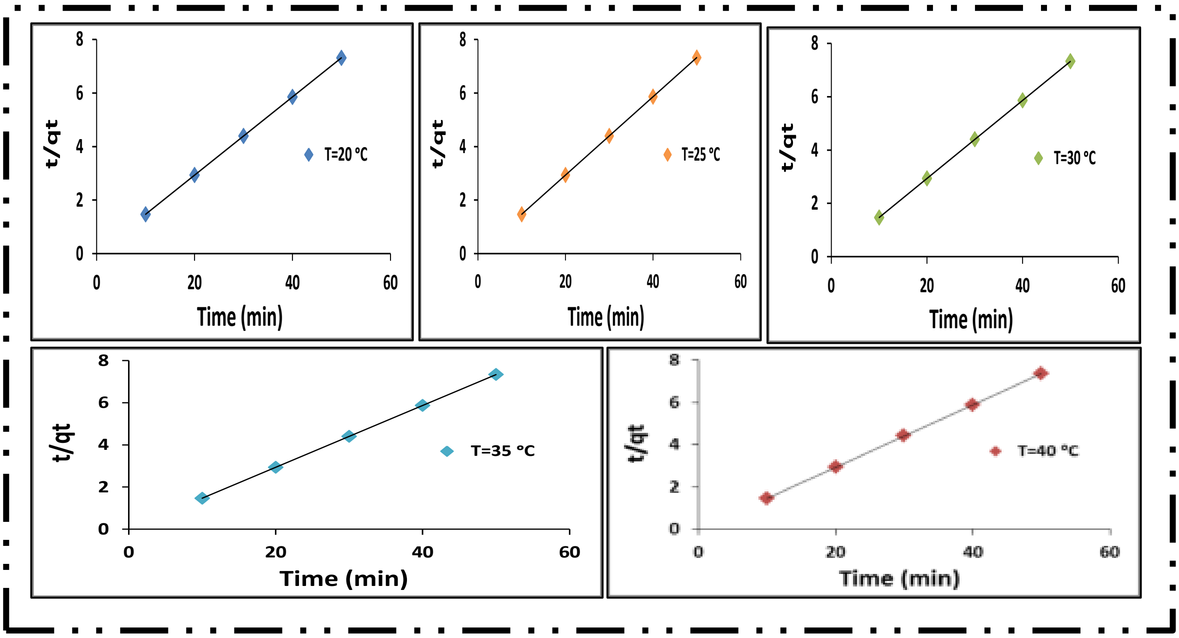

***Figure* (3.21):** *The Pseudo –Second Order Model of Eosin dye on CuO nanoparticles.*

Table (3.14): *Adsorption Kinetics Constants of Eosin dye on CuO nanoparticles*

	T (c^0)	q_e (exp.)	pseudo-first -order			pseudo-second –order			
			q_e (calc.)	K_1 min^{-1}	R^2	q_e (calc.)	K_2 $g.mg^{-1}.min^{-1}$	H	R^2
C_o 10 ppm	**20**	6.839	0.020	0.028	0.969	6.839	4.048	189.33	1
	25	6.828	0.018	0.046	0.914	6.830	7.194	335.59	1
	30	6.825	0.023	0.055	0.960	6.825	6.134	285.72	1
	35	6.816	0.013	0.051	0.937	6.816	6.211	288.54	1
	40	6.782	0.017	0.046	0.863	6.784	6.211	285.84	1

Table (3.15): *Values of the Pseudo-Second Order Model for adsorption of Eosin dye on ZnO nanoparticles.*

T (°C)	Time (min)	C_e (mg/L)	q_t (mg/g)	$\ln(q_e-q_t)$	t/q_t
20 °C	**10**	5.930	3.0525	-3.830	3.276
	20	5.929	3.0532	-3.863	6.550
	30	5.926	3.0555	-3.979	9.818
	40	5.924	3.0570	-4.062	13.084
	50	5.920	3.0600	-4.254	16.339
	60	5.916	3.0630	-4.491	19.588
	70	5.910	3.0675	-5.005	22.819
	80	5.908	3.0690	-5.259	26.067
	90	5.904	3.0720	-6.119	29.296
	100	5.903	3.0727	-6.502	32.544
	110	5.902	3.0735	-7.264	35.789
	120	5.901	3.0742		39.034

25 °C	**10**	5.944	3.0420	-3.937	3.287
	20	5.942	3.0435	-4.017	6.571
	30	5.940	3.0450	-4.104	9.852
	40	5.939	3.0457	-4.147	13.133
	50	5.936	3.0480	-4.305	16.404
	60	5.930	3.0525	-4.710	19.656
	70	5.928	3.0540	-4.892	22.920
	80	5.923	3.0577	-5.572	26.163
	90	5.921	3.0592	-6.074	29.419
	100	5.920	3.0600	-6.502	32.679
	110	5.919	3.0607	-7.130	35.939
	120	5.918	3.0615		39.196
30 °C	**10**	5.955	3.0337	-3.863	3.296
	20	5.953	3.0352	-3.937	6.589
	30	5.951	3.0367	-4.017	9.879
	40	5.949	3.0382	-4.104	13.165
	50	5.946	3.0405	-4.254	16.444
	60	5.942	3.0435	-4.491	19.714
	70	5.940	3.0450	-4.635	22.988
	80	5.935	3.0487	-5.115	26.240
	90	5.931	3.0517	-5.809	29.491
	100	5.929	3.0532	-6.502	32.752
	110	5.928	3.0540	-7.264	36.018
	120	5.927	3.0547		39.283
35 °C	**10**	5.962	3.0285	-3.830	3.301
	20	5.960	3.0300	-3.902	6.600
	30	5.959	3.0307	-3.937	9.898
	40	5.957	3.0322	-4.017	13.191
	50	5.955	3.0337	-4.104	16.481
	60	5.949	3.0382	-4.422	19.748
	70	5.944	3.0420	-4.803	23.011
	80	5.941	3.0442	-5.115	26.279
	90	5.937	3.0472	-5.809	29.535
	100	5.935	3.0487	-6.502	32.800
	110	5.934	3.0495	-7.264	36.071
	120	5.933	3.0502		39.341

40 ^{o}C	**10**	5.976	3.0180	-3.830	3.313
	20	5.974	3.0195	-3.902	6.623
	30	5.973	3.0202	-3.937	9.933
	40	5.968	3.0240	-4.154	13.227
	50	5.963	3.0277	-4.422	16.514
	60	5.959	3.0307	-4.710	19.797
	70	5.955	3.0337	-5.115	23.0741
	80	5.954	3.0345	-5.449	26.363
	90	5.950	3.0375	-6.119	29.629
	100	5.949	3.0382	-6.502	32.914
	110	5.948	3.0390	-7.264	36.196
	120	5.947	3.0397		39.477

Table (3.16): *Adsorption Kinetics Constants of Eosin dye on ZnO nanoparticles*

	T (c^0)	**q_e (exp.)**	**pseudo-first -order**			**pseudo-second –order**			
			q_e (calc.)	**K_1 min^{-1}**	**R^2**	**q_e (calc.)**	**K_2 $g.mg^{-1}$ min^{-1}**	**H**	**R^2**
C_o 10 ppm	**20**	3.074	0.053	0.033	0.897	3.078	1.529	14.411	1
	25	3.061	0.044	0.032	0.906	3.065	1.715	16.113	1
	30	3.054	0.049	0.031	0.852	3.058	1.555	14.543	1
	35	3.050	0.054	0.032	0.861	3.054	1.459	13.615	1
	40	3.039	0.049	0.034	0.930	3.043	1.644	15.230	1

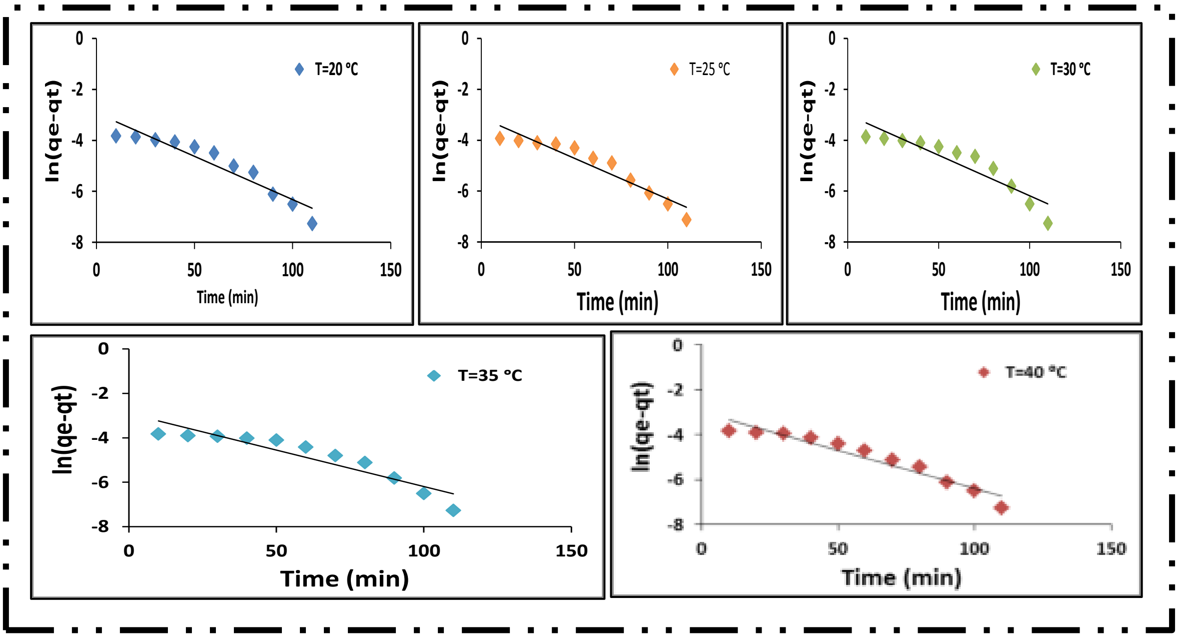

Figure (3.22): The Pseudo-First Order Model of Eosin dye on ZnO nanoparticles.

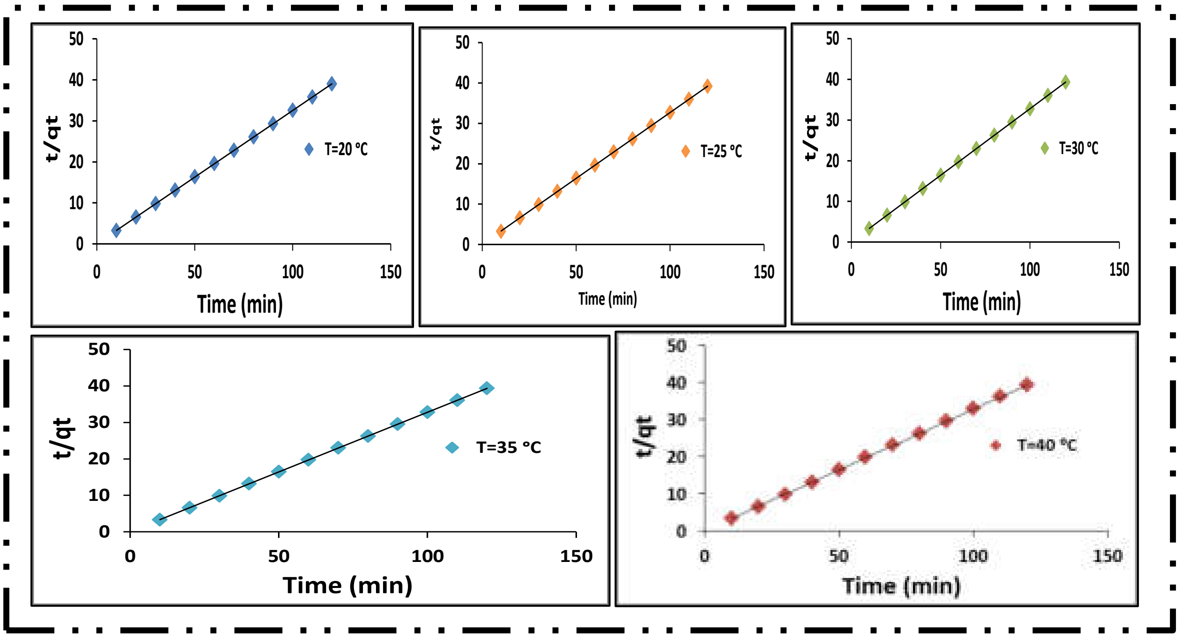

Figure (3.23): The Pseudo –Second-Order Model of Eosin dye on ZnO nanoparticles.

Figures (3.20, 3.22) (3.21, 3.23) for (CuO, ZnO) nanoparticles, respectively were used to determine the pseudo first-order, pseudo-second-order rate constants and **(q_e)** value, respectively. The adsorption constant with correlation for the **pseudo- first order** and **pseudo second-order models** are shown in **Tables (3.14 and 3.16)** for (CuO, ZnO) nanoparticles, respectively. The results showed in **Tables (3.14 and 3.16)** show the correlation coefficient of pseudo-second order as higher in comparison with the pseudo-second-order and the kinetic data fits well with a pseudo-second-order for adsorption Eosin dye on (CuO, ZnO) nanoparticles surface[111,112,116,130,131,132].

.

3.2.7. Adsorption Isotherm

The information given by adsorption isotherms is important. It gives an idea of how molecules are distributed between the liquid phase and the solid phase when adsorption reaches to equilibrium. Adsorption isotherm was studied for Eosin dye with concentrations (2-20) ppm and different temperatures (20, 25, 30, 35, 40) ^{o}C. The results shown in the **Tables (3.17) (3.18)** and **Figures (3.24) (3.25)** for CuO and ZnO, respectively.

Table (3.17): *Effect of temperature change on the adsorption of the Eosin dye on CuO nanoparticles.*

C_o (mg/L)	20 °C		25 °C		30 °C		35 °C		40 °C	
	C_e (mg/L)	Q_e (mg/g)	C_e (mg/L)	Q_e (mg/g)	C_e (mg/L)	Q_e (mg/g)	C_e (mg/L)	Q_e (mg/g)	C_e (mg/L)	Q_e (mg/g)
2	0.466	1.150	0.480	1.140	0.489	1.133	0.499	1.125	0.503	1.122
4	0.560	2.580	0.577	2.567	0.580	2.565	0.588	2.559	0.594	2.554
6	0.656	4.008	0.668	3.999	0.673	3.995	0.687	3.984	0.697	3.977
8	0.753	5.435	0.763	5.427	0.789	5.408	0.812	5.391	0.831	5.376
10	0.881	6.839	0.895	6.828	0.899	6.825	0.911	6.816	0.957	6.782
12	0.998	8.258	1.054	8.209	1.062	8.203	1.077	8.192	1.112	8.166
14	1.099	9.675	1.122	9.658	1.129	9.653	1.157	9.632	1.176	9.618
16	1.235	11.073	1.244	11.067	1.249	11.063	1.265	11.051	1.272	11.046
18	1.366	12.475	1.370	12.472	1.382	12.463	1.398	12.451	1.401	12.449
20	1.435	13.923	1.490	13.882	1.499	13.875	1.509	13.868	1.529	13.853

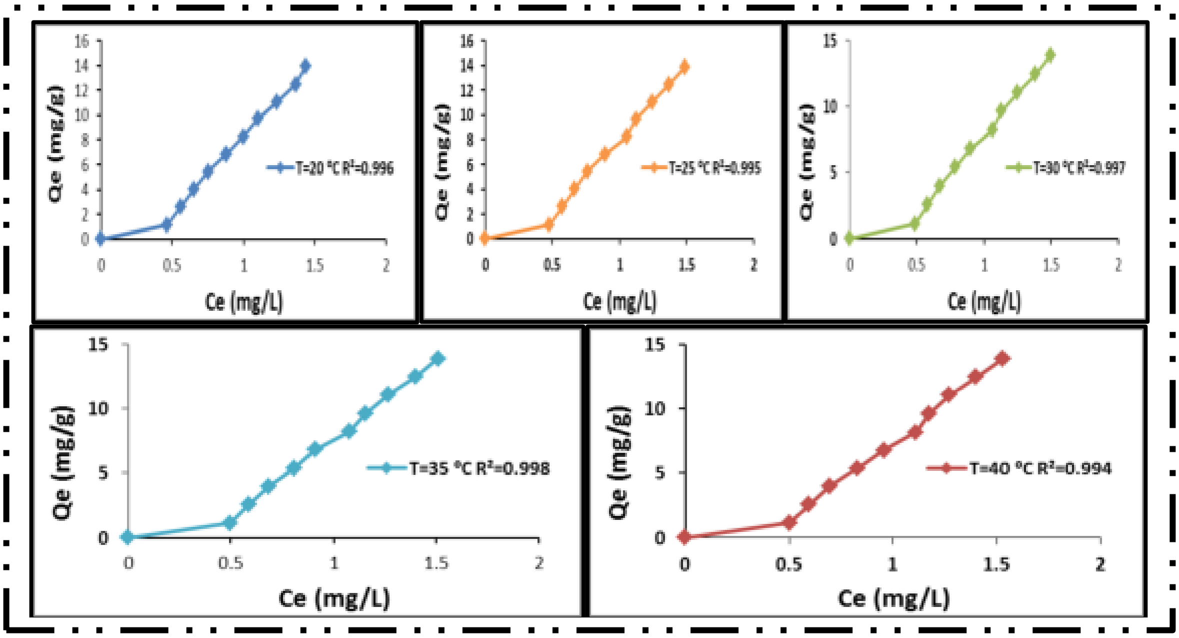

Figure (3.24): *Effect of temperature change on the adsorption of the Eosin dye on CuO nanoparticles.*

Table (3.18): *Effect of temperature change on the adsorption of the Eosin dye on ZnO nanoparticles.*

C_o (mg/L)	20 °C		25 °C		30 °C		35 °C		40 °C	
	C_e (mg/L)	Q_e (mg/g)	C_e (mg/L)	Q_e (mg/g)	C_e (mg/L)	Q_e (mg/g)	C_e (mg/L)	Q_e (mg/g)	C_e (mg/L)	Q_e (mg/g)
2	1.480	0.390	1.488	0.384	1.490	0.382	1.498	0.376	1.505	0.371
4	2.690	0.982	2.711	0.966	2.723	0.957	2.727	0.954	2.735	0.948
6	3.891	1.581	3.899	1.575	3.901	1.574	3.905	1.571	3.909	1.568
8	4.999	2.250	5.106	2.170	5.117	2.162	5.124	2.157	5.129	2.153
10	5.901	3.074	5.918	3.061	5.927	3.054	5.933	3.050	5.947	3.039
12	6.898	3.826	6.991	3.756	7.011	3.741	7.021	3.734	7.028	3.729
14	7.977	4.517	7.989	4.508	7.993	4.505	7.995	4.503	7.998	4.501
16	8.876	5.343	8.879	5.340	8.885	5.336	8.887	5.334	8.890	5.332
18	9.869	6.098	9.873	6.095	9.879	6.090	9.881	6.089	9.889	6.083
20	10.654	7.009	10.659	7.005	10.668	6.999	10.671	6.996	10.678	6.991

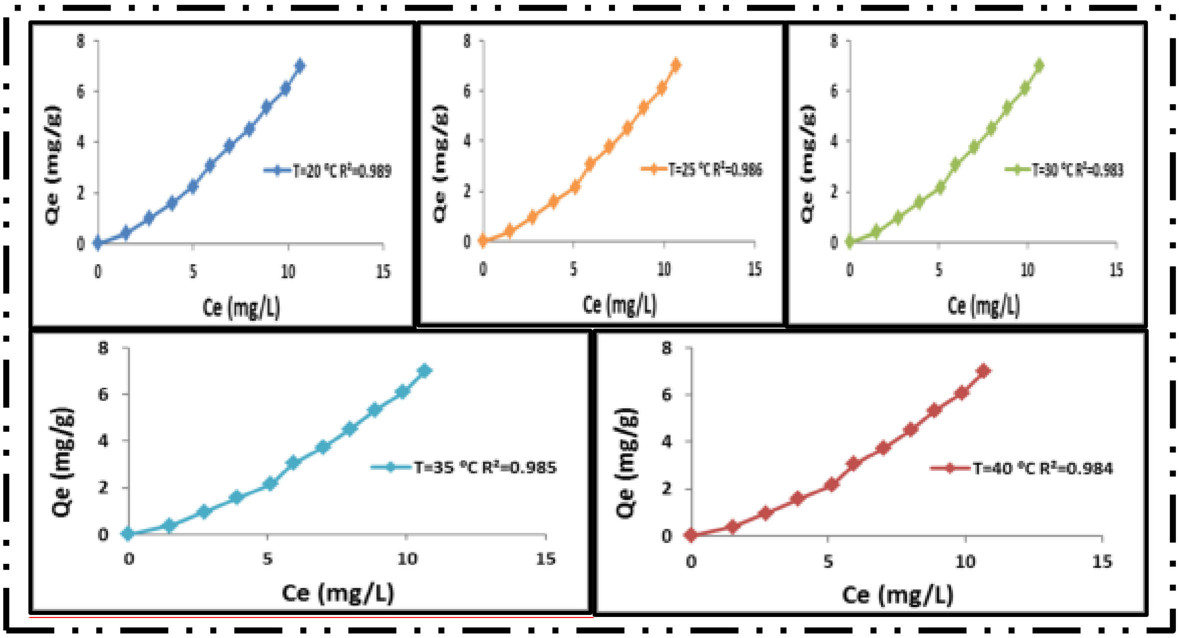

Figure (3.25): *Effect of temperature change on the adsorption of Eosin dye on ZnO nanoparticles.*

The results showed the general shape of the adsorption isotherms of Eosin dye removal on the (CuO, ZnO) nanoparticles are consistent with L-Type of Giles classification shown in **Figure (1.5)** .The isotherm of the mentioned system obeyed to the assumption of high adsorption of Eosin dye on adsorbent surfaces at the beginning. This strongly adsorbed on the adsorbent because there is no competition from solvent for adsorbent sites [131].

Table (3.19): *Isotherm Langmuir for Eosin dye at different concentrations (2-20) ppm; and temperature (20, 25, 30, 35, 40)* ^{o}*C on CuO nanoparticles.*

C_o (mg/L)	**20 ^{o}C**		**25 ^{o}C**		**30 ^{o}C**		**35 ^{o}C**		**40 ^{o}C**	
	C_e (mg/L)	**C_e/ Q_e (g/L)**	**C_e (mg/L)**	**C_e/ Q_e (g/L)**	**C_e (mg/L)**	**C_e/ Q_e (g/L)**	**C_e (mg/L)**	**C_e/ Q_e (g/L)**	**C_e (mg/L)**	**C_e/ Q_e (g/L)**
2	0.466	0.405	0.480	0.421	0.489	0.431	0.499	0.443	0.503	0.448
4	0.560	0.217	0.577	0.224	0.580	0.226	0.588	0.229	0.594	0.232
6	0.656	0.163	0.668	0.167	0.673	0.168	0.687	0.172	0.697	0.175
8	0.753	0.138	0.763	0.140	0.789	0.145	0.812	0.150	0.831	0.154
10	0.881	0.128	0.895	0.131	0.899	0.131	0.911	0.133	0.957	0.141
12	0.998	0.120	1.054	0.128	1.062	0.129	1.077	0.131	1.112	0.136
14	1.099	0.113	1.122	0.116	1.129	0.117	1.157	0.120	1.176	0.122
16	1.235	0.111	1.244	0.112	1.249	0.113	1.265	0.114	1.272	0.115
18	1.366	0.109	1.370	0.110	1.382	0.111	1.398	0.112	1.401	0.113
20	1.435	0.107	1.490	0.107	1.499	0.108	1.509	0.108	1.529	0.110

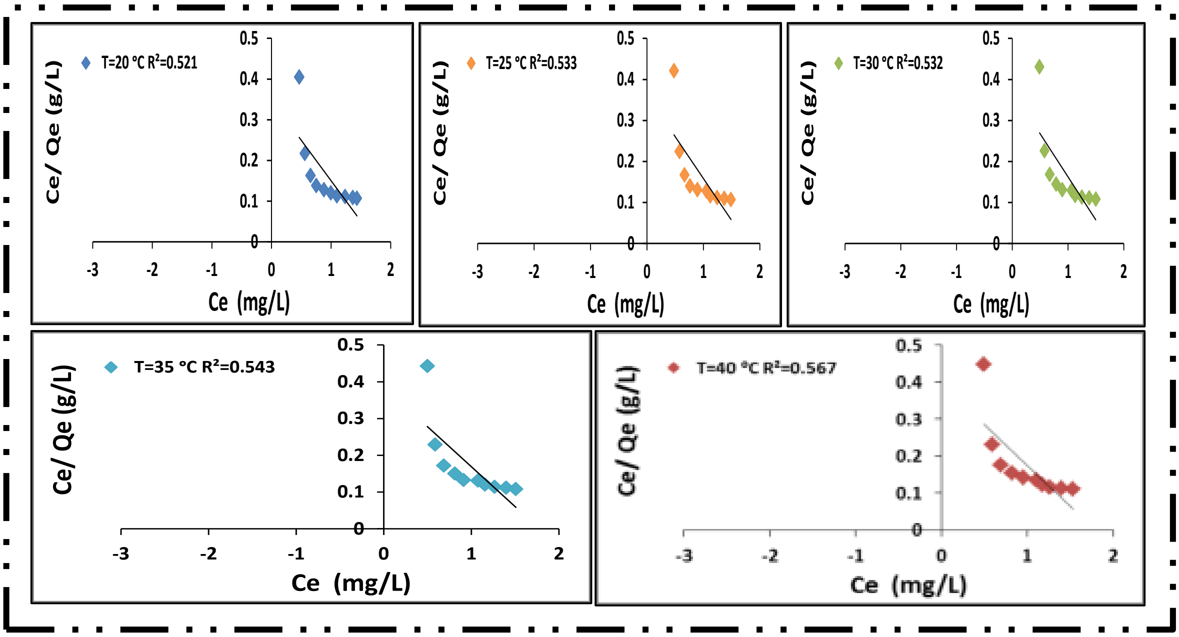

Figure (3.26): *Isotherm Langmuir for Eosin dye at different concentrations (2-20) ppm; and temperature (20, 25, 30, 35, 40) ^{o}C on CuO nanoparticles.*

Table (3.20): *Isotherm Freundlich for Eosin dyes at different concentrations and temperature on CuO nanoparticles.*

C_o (mg/L)	20 ^{o}C		25 ^{o}C		30 ^{o}C		35 ^{o}C		40 ^{o}C	
	ln C_e (mg/L)	ln Q_e (mg/g)	ln C_e (mg/L)	ln Q_e (mg/g)	ln C_e (mg/L)	ln Q_e (mg/g)	ln C_e (mg/L)	ln Q_e (mg/g)	ln C_e (mg/L)	ln Q_e (mg/g)
2	-0.763	0.139	-0.733	0.131	-0.715	0.124	-0.715	0.117	-0.687	0.115
4	-0.579	0.947	-0.549	0.942	-0.544	0.941	-0.544	0.939	-0.520	0.937
6	-0.421	1.388	-0.403	1.386	-0.396	1.385	-0.396	1.382	-0.360	1.380
8	-0.283	1.692	-0.270	1.691	-0.236	1.687	-0.236	1.684	-0.185	1.681
10	-0.126	1.922	-0.110	1.921	-0.106	1.920	-0.106	1.919	-0.043	1.914
12	-2.002	2.111	0.052	2.105	0.060	2.104	0.060	2.103	0.106	2.099
14	0.094	2.269	0.115	2.267	1.129	2.267	1.129	2.265	0.162	2.263
16	0.211	2.404	0.218	2.403	0.222	2.403	0.222	2.402	0.240	2.402
18	0.311	2.523	0.314	2.523	0.323	2.522	0.323	2.521	0.337	2.521
20	0.396	2.630	0.398	2.630	0.404	2.630	0.404	2.629	0.424	2.628

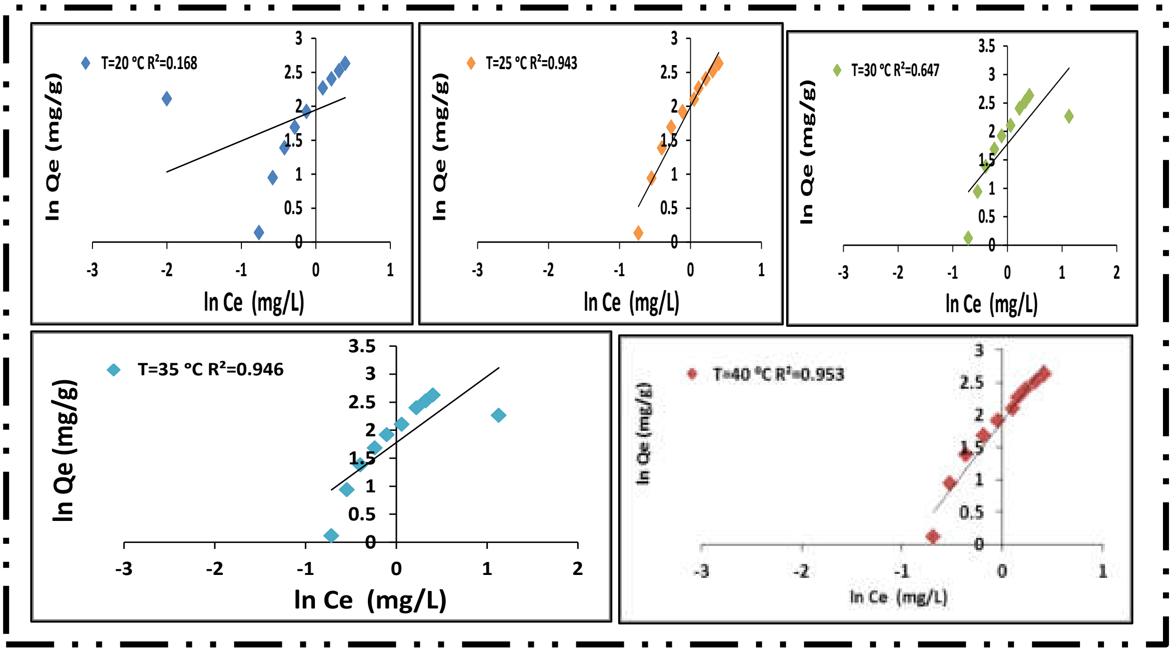

Figure (3.27): Isotherm Freundlich for Eosin dyes at different concentrations and temperature on CuO nanoparticles.

Table (3.21): Isotherm Dubinin (DKR) for Eosin dyes at different concentrations and temperature on CuO nanoparticles.

C_o (mg/L)	20 °C		25 °C		30 °C		35 °C		40 °C	
	$(\varepsilon)^2$	ln Q_e	$(\varepsilon)^2$	ln Q_e	$(\varepsilon)^2$	ln Q_e	$(\varepsilon)^2$	ln Q_e	$(\varepsilon)^2$	ln Q_e
2	7.779	0.139	7.768	0.131	7.861	0.124	7.919	0.117	8.365	0.115
4	6.222	0.947	6.199	0.942	6.371	0.941	6.465	0.939	6.795	0.937
6	5.077	1.388	5.139	1.386	5.255	1.385	5.287	1.382	5.524	1.380
8	4.237	1.692	4.300	1.691	4.246	1.687	4.217	1.684	4.351	1.681
10	3.409	1.922	3.443	1.921	3.541	1.920	3.590	1.919	3.563	1.914
12	2.858	2.111	2.722	2.105	2.789	2.104	2.821	2.103	2.872	2.099
14	2.476	2.269	2.490	2.267	2.542	2.267	2.536	2.265	2.643	2.263
16	2.079	2.404	2.129	2.403	2.186	2.403	2.221	2.402	2.343	2.402
18	1.788	2.523	1.836	2.523	1.878	2.522	1.905	2.521	2.023	2.521
20	1.567	2.630	1.615	2.630	1.657	2.630	1.692	2.629	1.768	2.628

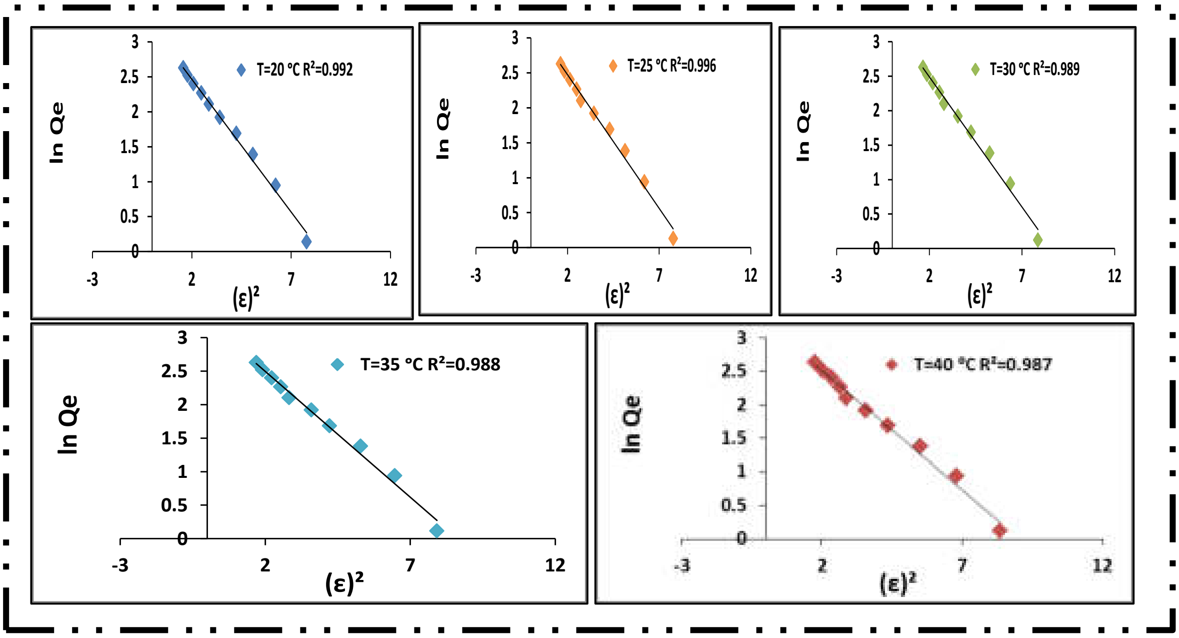

Figure (3.28): *Isotherm Dubinin (DKR) for Eosin dyes at different concentrations and temperature on CuO nanoparticles.*

Table (3.22): *Isotherm Temkin for Eosin dyes at different concentrations and temperature on CuO nanoparticles.*

C_o (mg/L)	20 °C		25 °C		30 °C		35 °C		40 °C	
	ln C_e	Q_e (mg/g)	ln C_e	Q_e (mg/g)	ln C_e	Q_e (mg/g)	ln C_e	Q_e (mg/g)	ln C_e	Q_e (mg/g)
2	-0.763	1.150	-0.733	1.140	-0.715	1.133	-0.715	1.125	-0.687	1.122
4	-0.579	2.580	-0.549	2.567	-0.544	2.565	-0.544	2.559	-0.520	2.554
6	-0.421	4.008	-0.403	3.999	-0.396	3.995	-0.396	3.984	-0.360	3.977
8	-0.283	5.435	-0.270	5.427	-0.236	5.408	-0.236	5.391	-0.185	5.376
10	-0.126	6.839	-0.110	6.828	-0.106	6.825	-0.106	6.816	-0.043	6.782
12	-2.002	8.258	0.052	8.209	0.060	8.203	0.060	8.192	0.106	8.166
14	0.094	9.675	0.115	9.658	1.129	9.653	1.129	9.632	0.162	9.618
16	0.211	11.073	0.218	11.067	0.222	11.063	0.222	11.051	0.240	11.046
18	0.311	12.475	0.314	12.472	0.323	12.463	0.323	12.451	0.337	12.449
20	0.396	13.923	0.398	13.882	0.404	13.875	0.404	13.868	0.424	13.853

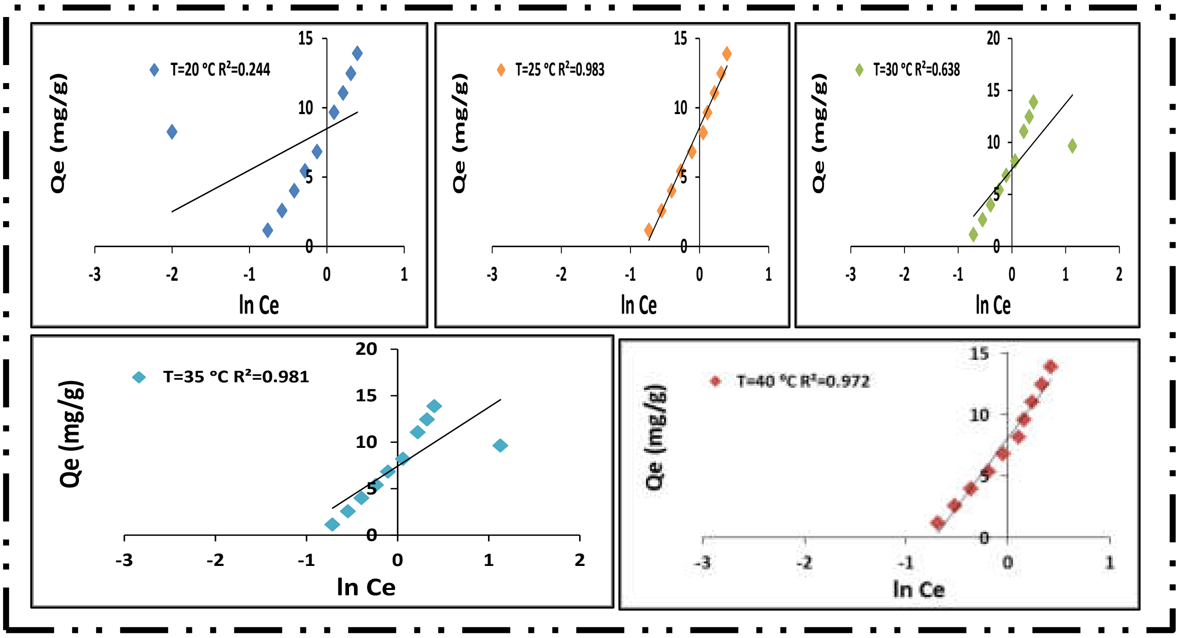

Figure (3.29): *Isotherm Temkin for Eosin dye at different concentrations and temperature on CuO nanoparticles.*

Table (3.23): *The calculated adsorption parameters of the four used isotherms for CuO nanoparticles.*

	Langmuir				Freundlich		
T(°C)	**K_L**	**R_L**	**q_{max}**	**R^2**	**K_F**	**1/n**	**R^2**
20	0.558	6.580	5.235	0.521	7.008	1.019	0.168
25	0.563	0.150	4.889	0.533	7.346	2.007	0.943
30	0.570	0.149	4.766	0.532	5.939	1.178	0.647
35	0.577	0.147	4.595	0.543	6.959	2.051	0.946
40	0.581	0.146	4.492	0.567	6.702	2.062	0.953
	Dubinin (DKR)				Temkin		
T(°C)	**β**	**q_{max}**	**E**	**R^2**	**K_T**	**B**	**R^2**
20	-0.3802	26.789	0.872	0.962	17.081	2.988	0.244
25	-0.3824	14.195	0.748	0.990	3.373	11.123	0.983
30	-0.3781	10.525	0.669	0.989	6.221	6.337	0.638
35	-0.3760	10.024	0.652	0.988	6.110	11.290	0.981
40	-0.3556	9.263	0.622	0.987	7.463	11.246	0.972

Table (3.24): *Isotherm Langmuir for Eosin dye at different concentrations (2-20) ppm; and temperature (20-40) °C on ZnO nanoparticles.*

C_o (mg/L)	20 °C		25 °C		30 °C		35 °C		40 °C	
	C_e (mg/L)	C_e/ Q_e (g/L)	C_e (mg/L)	C_e/ Q_e (g/L)	C_e (mg/L)	C_e/ Q_e (g/L)	C_e (mg/L)	C_e/ Q_e (g/L)	C_e (mg/L)	C_e/ Q_e (g/L)
2	1.480	3.794	1.488	3.875	1.490	3.895	1.498	3.978	1.505	4.054
4	2.690	2.737	2.711	2.804	2.723	2.843	2.727	2.856	2.735	2.882
6	3.891	2.460	3.899	2.474	3.901	2.478	3.905	2.485	3.909	2.492
8	4.999	2.221	5.106	2.352	5.117	2.366	5.124	2.375	5.129	2.382
10	5.901	1.919	5.918	1.933	5.927	1.940	5.933	1.945	5.947	1.956
12	6.898	1.802	6.991	1.860	7.011	1.874	7.021	1.880	7.028	1.884
14	7.977	1.765	7.989	1.772	7.993	1.774	7.995	1.775	7.998	1.776
16	8.876	1.661	8.879	1.662	8.885	1.665	8.887	1.665	8.890	1.667
18	9.869	1.618	9.873	1.619	9.879	1.621	9.881	1.622	9.889	1.625
20	10.654	1.519	10.659	1.521	10.66	1.524	10.671	1.525	10.678	1.527

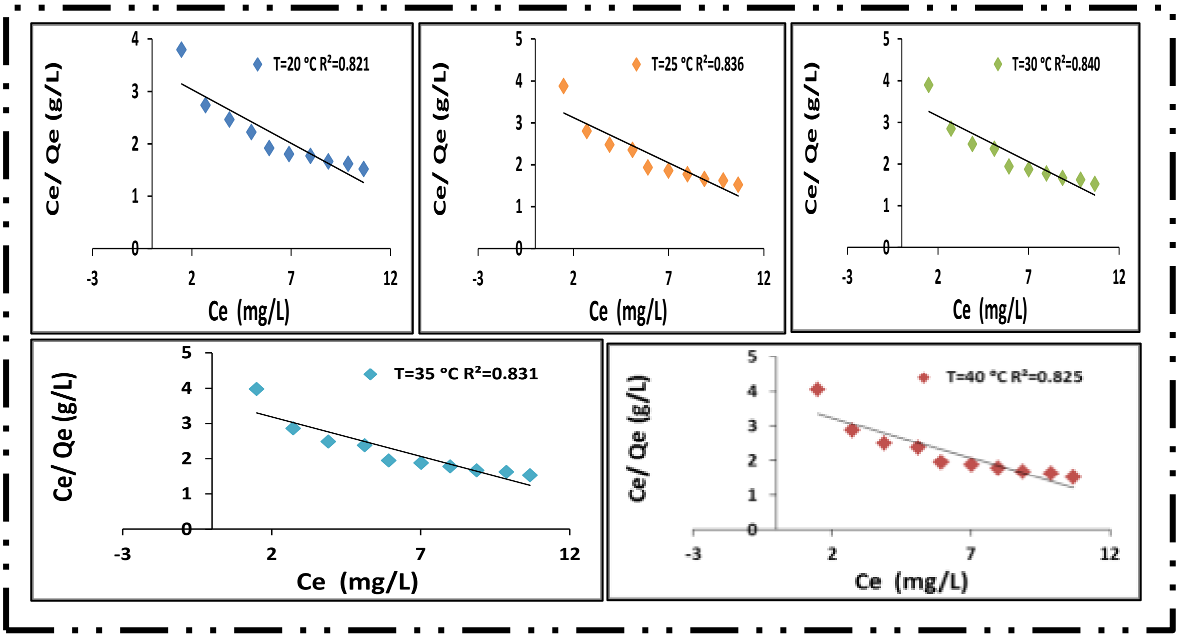

Figure (3.30): *Isotherm Langmuir for Eosin dyes on ZnO nanoparticles at different temperature (20-40) °C.*

Table (3.25): *Isotherm Freundlich for Eosin dyes at different concentrations and temperature on ZnO nanoparticles.*

C_o (mg/L)	20 ^{o}C		25 ^{o}C		30 ^{o}C		35 ^{o}C		40 ^{o}C	
	ln C_e (mg/L)	ln Q_e (mg/g)	ln C_e (mg/L)	ln Q_e (mg/g)	ln C_e (mg/L)	Ln Q_e (mg/g)	ln C_e (mg/L)	ln Q_e (mg/g)	ln C_e (mg/L)	ln Q_e (mg/g)
2	0.392	-0.941	0.397	-0.957	0.398	-0.962	0.404	-0.978	0.408	-0.991
4	0.989	-0.018	0.997	-0.034	1.001	-0.043	1.003	-0.047	1.006	-0.053
6	1.221	0.458	1.360	0.454	1.361	0.453	1.362	0.451	1.363	0.449
8	1.609	0.810	1.630	0.774	1.632	0.771	1.633	0.768	1.635	0.766
10	1.775	1.122	1.778	1.118	1.779	1.116	1.780	1.115	1.782	1.111
12	1.931	1.341	1.944	1.323	1.947	1.319	1.948	1.317	1.949	1.316
14	2.076	1.507	2.078	1.505	2.078	1.505	2.078	1.504	2.079	1.504
16	2.183	1.675	2.183	1.675	2.184	1.674	2.184	1.674	2.184	1.673
18	2.289	1.808	2.289	1.807	2.290	1.806	2.290	1.806	2.291	1.805
20	2.365	1.947	2.366	1.946	2.367	1.945	2.367	1.945	2.368	1.944

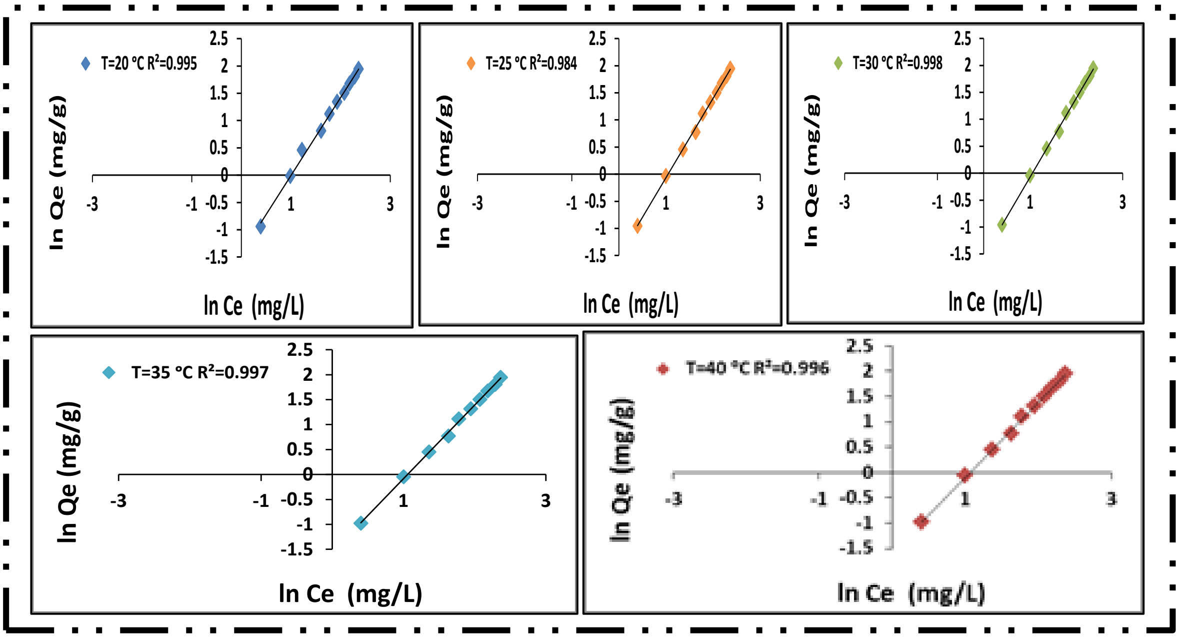

Figure (3.31): *Isotherm Freundlich for Eosin dyes at different concentrations and temperature on ZnO nanoparticles.*

Table (3.26): *Isotherm Dubinin (DKR) for Eosin dyes at different concentrations and temperature on ZnO nanoparticles.*

C_o (mg/L)	20 °C		25 °C		30 °C		35 °C		40 °C	
	$(\varepsilon)^2$	$\ln Q_e$	$(\varepsilon)^2$	$\ln Q_e$	$(\varepsilon)^2$	$\ln Q_e$	$(\varepsilon)^2$	$\ln Q_e$	$(\varepsilon)^2$	$\ln Q_e$
2	1.573	-0.941	1.621	-0.957	1.670	-0.962	1.712	-0.978	1.810	-0.991
4	0.588	-0.018	0.601	-0.034	0.617	-0.043	0.634	-0.047	0.676	-0.053
6	0.308	0.458	0.316	0.454	0.327	0.453	0.337	0.451	0.360	0.449
8	0.196	0.810	0.197	0.774	0.201	0.771	0.207	0.768	0.218	0.766
10	0.144	1.122	0.147	1.118	0.152	1.116	0.157	1.115	0.167	1.111
12	0.106	1.341	0.108	1.323	0.110	1.319	0.114	1.317	0.121	1.316
14	0.081	1.507	0.084	1.505	0.086	1.505	0.089	1.504	0.095	1.504
16	0.066	1.675	0.068	1.675	0.071	1.674	0.073	1.674	0.078	1.673
18	0.054	1.808	0.056	1.807	0.058	1.806	0.060	1.806	0.064	1.805
20	0.045	1.947	0.047	1.946	0.049	1.945	0.050	1.945	0.054	1.944

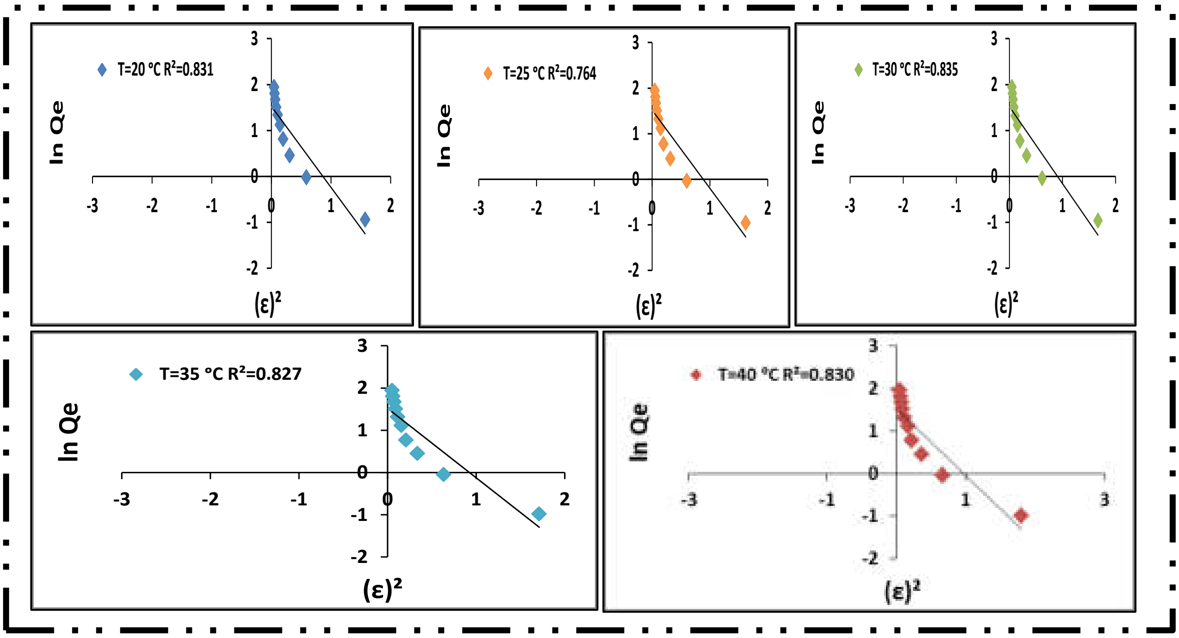

Figure (3.32): *Isotherm Dubinin (DKR) for Eosin dye at different concentrations and temperature on ZnO nanoparticles.*

Table (3.27): *Isotherm Temkin for Eosin dyes at different concentrations and temperature on ZnO nanoparticles.*

C_o (mg/L)	20 °C		25 °C		30 °C		35 °C		40 °C	
	ln C_e	Q_e (mg/g)	ln C_e	Q_e (mg/g)	ln C_e	Q_e (mg/g)	ln C_e	Q_e (mg/g)	ln C_e	Q_e (mg/g)
2	0.392	0.390	0.397	0.3840	0.398	0.382	0.404	0.376	0.408	0.371
4	0.989	0.982	0.997	0.966	1.001	0.957	1.003	0.954	1.006	0.948
6	1.221	1.581	1.360	1.575	1.361	1.574	1.362	1.571	1.363	1.568
8	1.609	2.250	1.630	2.170	1.632	2.162	1.633	2.157	1.635	2.153
10	1.775	3.074	1.778	3.061	1.779	3.054	1.780	3.050	1.782	3.039
12	1.931	3.826	1.944	3.756	1.947	3.741	1.948	3.734	1.949	3.729
14	2.076	4.517	2.078	4.508	2.078	4.505	2.078	4.503	2.079	4.501
16	2.183	5.343	2.183	5.340	2.184	5.336	2.184	5.334	2.184	5.332
18	2.289	6.098	2.289	6.095	2.290	6.090	2.290	6.089	2.291	6.083
20	2.365	7.009	2.366	7.005	2.367	6.999	2.367	6.996	2.368	6.991

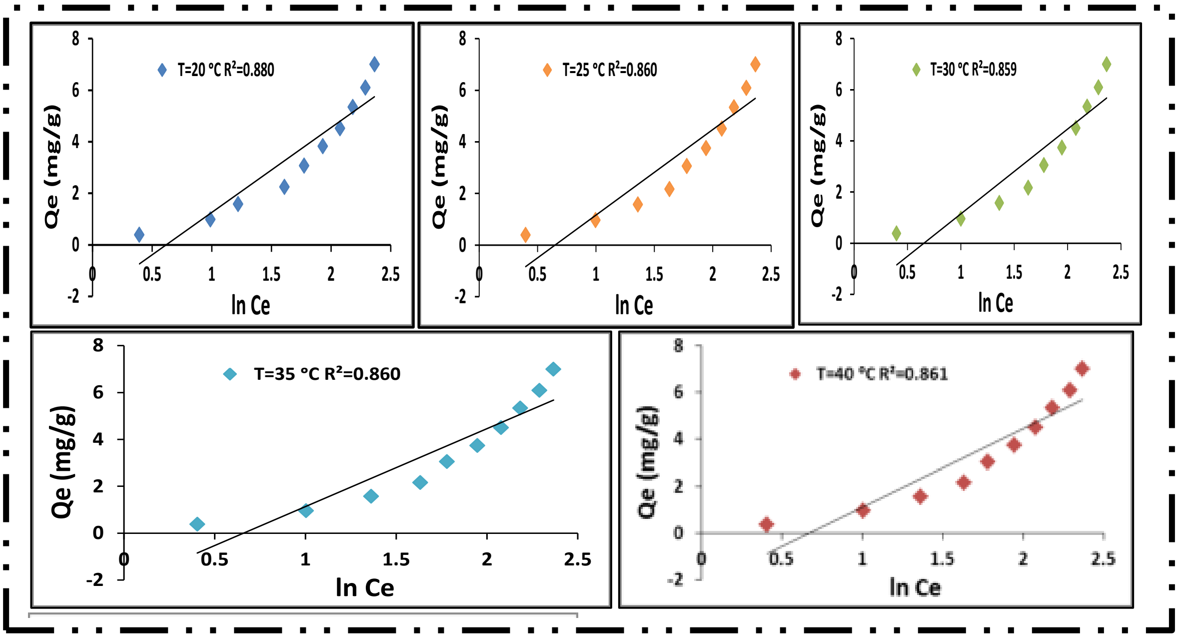

Figure (3.33): *Isotherm Temkin for Eosin dye at different concentrations and temperature on ZnO nanoparticles.*

Table (3.28): *The calculated adsorption parameters of the four used isotherms for ZnO nanoparticles.*

Langmuir					Freundlich		
T(°C)	K_L	R_L	q_{max}	R^2	K_F	1/n	R^2
20	0.0596	0.628	4.866	0.821	0.238	1.427	0.995
25	0.0606	0.625	4.640	0.836	0.216	1.464	0.984
30	0.0610	0.621	4.578	0.840	0.213	1.467	0.998
35	0.0615	0.619	4.468	0.831	0.209	1.478	0.997
40	0.0622	0.616	4.359	0.825	0.205	1.486	0.996
Dubinin (DKR)					**Temkin**		
T(°C)	β	q_{max}	E	R^2	K_T	B	R^2
20	-1.5296	4.616	0.571	0.831	0.540	3.285	0.880
25	-1.5192	4.568	0.573	0.764	0.522	3.314	0.860
30	-1.5170	4.558	0.574	0.835	0.520	3.315	0.859
35	-1.5190	4.567	0.573	0.827	0.517	3.326	0.860
40	-1.5209	4.576	0.573	0.830	0.514	3.332	0.861

As presented in **Tables (3.23 and 3.28)**, the adsorption of Eosin dye on CuO nanoparticles was fit to Dubinin-Kaganer-Radushkevich isotherm by higher correlation factor (R^2) values [131]. But for ZnO nanoparticles was fit to Freundlich isotherm. The results show what is otherwise based on the correlation coefficient data [111, 120, 124, 131].

The values of dimensionless sorption factor (K_L) were close to zero and this indication for favorable adsorption. The intensity of adsorption (n) showed low values ($n<1$); this indicates a very low affinity between adsorbents and adsorbate. The Freundlich constant (k_F) decreases with increasing the temperature and this indication for an exothermic reaction

[141]. In isotherm Dubinin (DKR), the energy equation gives us a perception of the adsorption mechanism. (E <8 KJ /mol) indicates that the physical force influence adsorption and that (E> 16) indicates the spread of molecules and when (E) is between (8-16) indicates that adsorption is directed by ion exchange The results for the energy listed in **Table (3.23 and 3.28)** for the surface of the (CuO, ZnO) nanoparticle respectively, that it was less than (8) indicating that the force is physical, that is, physical adsorption. This is the same result that we obtained from the equation Fruendlich. The Temkin constant (K_T) for CuO greater than ZnO due to increasing the surface area for CuO than ZnO [142], and the values of (B) less than (40 kJ/mol) this indication for physical adsorption [132].

3.3. Conclusions

1. The two metal oxide nanoparticles (CuO) and (ZnO) can be prepared by a simple precipitation method. XRD spectrum revealed that particle size obtained is around (23.4 nm) for (CuO), nanoparticles and (47.8 nm) for (ZnO), nanoparticles which agreed fairly well with FTIR, BET, SEM and AFM data. Surface morphology as main nanoparticles phenomenon is studied in terms of SEM and AFM spectroscopic techniques which prove XRD and BET data. The surface area of CuO is (35.635) and ZnO is (6.704) m^2 /g.

2. The (CuO) and (ZnO) nanoparticles have been successfully utilized for the removal of Eosin dye from an aqueous solution via the surface adsorption process involving the electrostatic attraction mechanism (physical adsorption).

3. The effect of pH investigated for values ranging from 1 to 10, showed maximum adsorption of Eosin dye on the CuO and ZnO were at pH=1 at a fixed weight of the sorbent surfaces (0.04 g), different concentrations (2-20) ppm at 25 ^{o}C.

4. The correlation coefficient for the Freundlich regression fits is higher for ZnO nanoparticles but for CuO was fit to Dubinin-Kaganer-Radushkevich isotherm, so the Freundlich and Dubinin-Kaganer-Radushkevich models could describe the adsorption isotherm for the removal of Eosin dye from aqueous solution on ZnO and CuO, respectively.

5. The kinetics results confirm. The best correlation of the experimental data of adsorption of Eosin dye on CuO and ZnO by pseudo-second-order equation.

6. Thermodynamic functions for adsorption of Eosin dye on CuO and ZnO, The thermodynamic values negative of ΔG for CuO and ZnO indicates that the nature of the adsorption process is thermodynamically spontaneous. Negative values of ΔH indicate an exothermic process in nature and indicating that the process occurs is physical adsorption because of its values less than 40 kJ / mol. Negative values of ΔS indicates that the molecules adsorbed for Eosin dye are arranged on the surface more than the solution, any decrease of a disorder. Either the positive values of ΔS indicates that that the molecules adsorbed for Eosin dye are still in continuous movement on the surface more than it is in the solution (liquid phase), any increase of disorder.

3.4. Recommendations

Further researches are required to cover other aspects of the project as follows**:-**

1. The study of the adsorption process in both fixed and fluidized-bed columns techniques at similar and different experimental conditions.

2. An attempt may be made to test the suitability of other metal oxides and natural raw materials as adsorbents.

3. Study adsorption of other pollutants using ZnO and CuO nanoparticles.

References

References

[1] Nassar, N. N., Marei, N. N., Vitale, G., and Arar, L. A. (2015). Adsorptive removal of dyes from synthetic and real textile wastewater using magnetic iron oxide nanoparticles: Thermodynamic and mechanistic insights. The Canadian Journal of Chemical Engineering, 93(11), 1965-1974.

[2] Tadesse, B., Teju, E., and Megersa, N. (2015). The Teff straw: a novel low-cost adsorbent for quantitative removal of Cr (VI) from contaminated aqueous samples. Desalination and Water Treatment, 56(11), 2925-2936.

[3] Wang, Y., Tang, X. W., and Wang, H. Y. (2015).Characteristics and mechanisms of Ni (II) removal from aqueous solution by Chinese loess. Journal of Central South University, 11(22), 4184-4192.

[4] Mane, S., Ponrathnam, S., and Chavan, N. (2016).Selective solid-phase extraction of metal for water decontamination. Journal of Applied Polymer Science, 133(1).

[5] Memon, F. N., and Memon, S. (2015). Sorption and desorption of basic dyes from industrial wastewater using Calix [4] arene based impregnated material. Separation Science and Technology, 50(8), 1135-1146.

[6] Foroughi-Dahr, M., Abolghasemi, H., Esmaili, M., Shojamoradi, A., and Fatoorehchi, H. (2015). Adsorption characteristics of Congo red from aqueous solution onto tea waste. Chemical Engineering Communications, 202(2), 181-193.

[7] Zhang, Z., Wang, W., and Wang, A. (2015). Highly effective removal of methylene blue using functionalized attapulgite via a hydrothermal process. Journal of Environmental Sciences, 33, 106-115.

[8] Ahmed, M. J., and Theydan, S. K. (2015). Adsorptive removal of p-nitrophenol on microporous activated carbon by FeCl3 activation: equilibrium and kinetics studies. Desalination and Water Treatment, 55(2), 522-531.

[9] Maida Hameed Saleem (2011). Removal of o-, m-, and p-Nitrophenol by Surfactant modified Attapulgite. Master Thesis, University of Baghdad.

[10] Moza, P. N., Fytianos, K., Samanidou, V., and Korte, F. (1988). Photodecomposition of chlorophenols in an aqueous medium in presence of hydrogen peroxide. Bulletin of environmental contamination and toxicology, 41(4-6), 678-682.

[11] Stem, M., Heinzle, E., Kut, G. M., and Hungerbühler, K. (1997). Removal of substituted pyridines by combined ozonation/fluidized bed biofilm treatment. Water Science and Technology, 35(4), 329-335.

[12] Kwak, S. Y., Yeom, M. O., Roh, I. J., Kim, D. Y., and Kim, J. J. (1997). Correlations of chemical structure, atomic force microscopy (AFM) morphology, and reverse osmosis (RO) characteristics in aromatic polyester high-flux RO membranes. Journal of membrane science, 132(2), 183-191.

[13] Fierro, D., Boschetti-de-Fierro, A., and Abetz, V. (2012). The solution-diffusion with imperfections model as a method to understand organic solvent nanofiltration of multicomponent systems. Journal of membrane science, 413, 91-101.

[14] Ahmad, T., Mustafa, S., Naeem, A., Anwar, F., Mehmood, T., and Shah, K. H. (2014). Ion Exchange Removal of Chromium (III) from Tannery Wastes by Using a Strong Acid Cation Exchange Resin Amber lite

IR-120 H+ and its Hybrids. Journal of the Chemical Society of Pakistan, 36(5).

[15] Basma Jafar Ahmed Al-Taai (2011). Clay-polymer Nanocomposites as an adsorbent for some organic pollutants. Master Thesis, University of Baghdad.

[16] Hofmann, H. (1991). M. Suzuki: Adsorption Engineering, Vol. 25 aus der Reihe: Chemical Engineering Monographs, Elsevier Science Publishers, Amsterdam and New York 1989. 306 Seiten. Preis: 139.-USS. Berichte der Bunsengesellschaft für physikalische Chemie, 95(3), 450-451.

[17] Waghmare, S., Arfin, T., Rayalu, S., Lataye, D., Dubey, S., and Tiwari, S. (2015). Adsorption behavior of modified zeolite as novel adsorbents for fluoride removal from drinking water: surface phenomena, kinetics and thermodynamics studies‖. International Journal of Science, Engineering and Technology Research, 4(12), 4114-24.

[18] Zuo, L., Song, W., Shi, T., Lv, C., Yao, J., Liu, J., and Weng, Y. (2014). Adsorption of aniline on template-synthesized porous carbons. Microporous and Mesoporous Materials, 200, 174-181.

[19] Franco, C. A., Cortés, F. B., and Nassar, N. N. (2014). Adsorptive removal of an oil spill from oil-in-fresh water emulsions by hydrophobic alumina nanoparticles functionalized with petroleum vacuum residue. Journal of colloid and interface science, 425, 168-177.

[20] Memon, S., Memon, S., and Memon, N. (2014). A highly efficient p-tert-butylcalix[8] arene-based modified silica for the removal of Hexachlorocyclohexane isomers from aqueous media. Desalination and Water Treatment, 52(13-15), 2572-2582.

[21] Peng, S., Zeng, Q., Guo, Y., Niu, B., Zhang, X., and Hong, S. (2013). Defluoridation from aqueous solution by chitosan modified natural zeolite. Journal of Chemical Technology and Biotechnology, 88(9), 1707-1714.

[22] Henderson, A. P., Seetohul, L. N., Dean, A. K., Russell, P., Pruneanu, S., and Ali, Z. (2008). A novel isotherm, modeling self-assembled monolayer adsorption and structural changes. Langmuir, 25(2), 931-938.

[23] Ho, Y. S. (2014). Affinity adsorption of lysozyme with Reactive Red 120-modified magnetic chitosan microspheres. Food Chemistry, 161, 323.

[24] Casper, J. M. (1977). Physical chemistry of surfaces, Arthur W. Adamson, Wiley-Interscience, New York, 1976, 698 pp. $24.95. Journal of Polymer Science Part C: Polymer Letters, 15(10), 632-633.

[25] Ertl, G. (1979). Chemisorption of Gases on Metals. Von FC Tompkins. Academic Press, London 1978. XII, 370 S., geb.£ 16.80. Angewandte Chemie, 91(12), 1032-1033..

[26] Adamson, W. (1982). Physical Chemistry of Surface 4th ed. John Wiley&Sons. New York.

[27] Xing, Y., and Li, S. (2014). Biosorption of methylene blue from aqueous solution by poly (amic acid) -modified chitosan. Environmental Progress & Sustainable Energy, 33(4), 1180-1186.

[28] Pillai, S. S., Deepa, B., Abraham, E., Girija, N., Geetha, P., Jacob, L., and Koshy, M. (2013). Biosorption of Cd (II) from aqueous solution using xanthate nano banana cellulose: equilibrium and kinetic studies. Ecotoxicology and environmental safety, 98, 352-360.

[29] Pal, P., Banat, F., and AlShoaibi, A. (2013). Adsorptive removal of heat stable salt anions from industrial lean amine solvent using anion exchange resins from gas sweetening unit. Journal of Natural Gas Science and Engineering, 15, 14-21.

[30] Sikarwar, S., and Jain, R. (2014). Kinetics and thermodynamic study of balsalazide adsorption by unsaturated polyester resin (UPR): a non-carbon adsorbent. Water, Air, & Soil Pollution, 225(2), 1842.

[31] Nettem, K., and Almusallam, A. S. (2013). Equilibrium, kinetic, and thermodynamic studies on the biosorption of selenium (IV) ions onto Ganoderma Lucidum biomass. Separation Science and Technology, 48(15), 2293-2301.

[32] Xin, Y., and Li, S. (2014). Neutral red adsorption onto modified chitosan: effect of pH and temperature. Separation Science and Technology, 49(14), 2241-2248.

[33] Tang, X., Zhang, Q., Liu, Z., Pan, K., Dong, Y., and Li, Y. (2014). Removal of Cu (II) by loofah fibers as a natural and low-cost adsorbent from aqueous solutions. Journal of Molecular Liquids, 199, 401-407.

[34] Yan, Y., Li, Q., Sun, X., Ren, Z., He, F., Wang, Y., and Wang, L. (2015). Recycling flue gas desulphurization (FGD) gypsum for removal of Pb (II) and Cd (II) from wastewater. Journal of colloid and interface science, 457, 86-95.

[35] Suess, E. (1970). Interaction of organic compounds with calcium carbonate—I. Association phenomena and geochemical implications. Geochimica et Cosmochimica Acta, 34(2), 157-168.

[36] Adamson, A. W., and Gast, A. P. (1990). Capillarity. Physical Chemistry of Surfaces, 6th ed, New York: John Wiley and Sons, Inc, 4-47.

[37] Lasheen, M. R., El-Sherif, I. Y., Sabry, D. Y., El-Wakeel, S. T., and El-Shahat, M. F. (2014). Removal and recovery of Cr (VI) by magnetite nanoparticles. Desalination and Water Treatment, 52(34-36), 6464-6473.

[38] Katsou, E., Malamis, S., and Haralambous, K. (2011). Pre-treatment of industrial wastewater polluted with lead using adsorbents and ultrafiltration or microfiltration membranes. Water Environment Research, 83(4), 298-312.

[39] Sapsford, K. E., Algar, W. R., Berti, L., Gemmill, K. B., Casey, B. J., Oh, E., ... and Medintz, I. L. (2013). Functionalizing nanoparticles with biological molecules: developing chemistries that facilitate nanotechnology. Chemical reviews, 113(3), 1904-2074.

[40] Hübler, A. W., and Osuagwu, O. (2010). Digital quantum batteries: Energy and information storage in nano vacuum tube arrays. Complexity, 15(5), 48-55.

[41] ELRIDGE, T. (2014). Achieving industry integration with nanomaterials through financial markets. Nanotechnology Now.

[42] McGovern, C. (2010). Commoditization of Nanomaterials. Nanotechnology Perceptions, 6(3), 155-178.

[43] Zeng, S., Baillargeat, D., Ho, H. P., and Yong, K. T. (2014). Nanomaterials enhanced surface plasmon resonance for biological and chemical sensing applications. Chemical Society Reviews, 43(10), 3426-3452.

[44] Stephenson, C., Lyon, D., & Hübler, A. (2017). Topological properties of a self-assembled electrical network via ab initio calculation. Scientific reports, 7, 41621.

[45] Lyon, D., and Hubler, A. (2013). Gap size dependence of the dielectric strength in nano vacuum gaps. IEEE Transactions on Dielectrics and Electrical Insulation, 20(4), 1467-1471.

[46] Kerativitayanan, P., Carrow, J. K., and Gaharwar, A. K. (2015). Nanomaterials for engineering stem cell responses. Advanced healthcare materials, 4(11), 1600-1627. [47] Ramsden, J.J. (2011). Nanotechnology: An Introduction. Elsevier, Amsterdam.

[47] Khomutov, G. B., and Koksharov, Y. A. (2009). Organized Ensembles of Magnetic Nanoparticles: Preparation, Structure, and Properties. Magnetic Nanoparticles, 117-195.

[48] Battez, A. H., González, R., Viesca, J. L., Fernández, J. E., Fernández, J. D., Machado, A., ... and Riba, J. (2008). CuO, ZrO 2 and ZnO nanoparticles as an antiwear additive in oil lubricants. Wear, 265(3), 422-428.

[49] Klingshirn, C. F., Waag, A., Hoffmann, A., and Geurts, J. (2010). Zinc oxide: from fundamental properties towards novel applications (Vol. 120). Springer Science & Business Media.

[50] Fierro, J. L. G. (Ed.). (2005). Metal oxides: chemistry and applications. CRC press.

[51] Morales-Masis, M. (2007). Fabrication and Study of ZnO Micro-and Nanostructures.

[52] Rossler, U. (1999). Landolt-Bornstein, New Series, Group III. Vol. 17B, 22,41B.

[53] Baruah, S., and Dutta, J. (2009). Hydrothermal growth of ZnO nanostructures. Science and Technology of Advanced Materials, 10(1), 013001.

[54] Klingshirn, C. (2007). ZnO: material, physics, and applications. ChemPhysChem, 8(6), 782-803.

[55] Wiberg, N., Blank, T., Amelunxen, K., Nöth, H., Knizek, J., Habereder, T., and Wanner, M. (2001). On the Clay-polymer R* 3Ga2· and R* 4Ga3· As Well As Gallanides R* 3Ga2− and R* 4Ga3−(R*= SitBu3)− Syntheses, Characterization, Structures. European Journal of Inorganic Chemistry, 2001(7), 1719-1727.

[56] Takahashi, K., Yoshikawa, A., and Sandhu, A. (2007). Wide bandgap semiconductors. Springer-Verlag Berlin Heidelberg., 239.

[57] Richardson, H. W. Copper Compounds in Ullmann's Encyclopedia of Industrial Chemistry 2002.

[58] Baturay, S., Tombak, A., Kaya, D., Ocak, Y. S., Tokus, M., Aydemir, M., and Kilicoglu, T. (2016). Modification of electrical and optical properties of CuO thin films by Ni doping. Journal of Sol-Gel Science and Technology, 78(2), 422-429.

[59] Morales, J., Sanchez, L., Martin, F., Ramos-Barrado, J. R., and Sanchez, M. (2005). Use of low-temperature nanostructured CuO thin films deposited by spray-pyrolysis in lithium cells. Thin Solid Films, 474(1), 133-140.

[60] Forsyth, J. B., and Hull, S. (1991). The effect of hydrostatic pressure on the ambient temperature structure of CuO. Journal of Physics: Condensed Matter, 3(28), 5257- 5261.

[61] Shi, W., and Chopra, N. (2011). Surfactant-free synthesis of novel copper oxide (CuO) nanowire–cobalt oxide (Co3O4) nanoparticle heterostructures and their morphological control. Journal of Nanoparticle Research, 13(2), 851-868.

[62] J. Dwarkadas. Copper (II) oxide. Sanghvi College of Engineering, (2011).

[63] Ennas Abdul - Hussein (2012). Adsorption Studies of Certain Dyes on the Mineral Raw Materials from Aqueous Solution. Master Thesis, University of Baghdad.

[64] Cheng, Y. M., Jin, X. H., Gao, D., Xia, H. F., and Chen, J. H. (2013). Thermodynamics and kinetics of lysozyme adsorption onto two kinds of weak cation exchangers. Biotechnology and Bioprocess Engineering: BBE, 18(5), 950.

[65] Angın, D., Köse, T. E., and Selengil, U. (2013). Production and characterization of activated carbon prepared from safflower seed cake biochar and its ability to absorb reactive dyestuff. Applied Surface Science, 280, 705-710.

[66] Ali, A. H. (2013). Comparative study on removal of cadmium (II) from simulated wastewater by adsorption onto GAC, DB, and PR. Desalination and Water Treatment, 51(28-30), 5547-5558.

[67] C.H. Giles and D. Smith, J. (1974). Colloid and Interface Science, 47(3), 755.

[68] C.H. Giles, A.P. D’silva and I.A. Easton, J. (1974). Colloid and Interface Science, 47(3), 754.

[68] C.H. Giles, A.P. D'silva and I.A. Easton, J. (1974). Colloid and Interface Science, 47(3), 754.

[69] Brunauer S. (1974). The Asorption of gases and Vapours, 1, Princeton University press, Princeton.

[70] Snoeyink V. L. and Summers R. S., and Architectural, (2011). Adsorption of Organic Compounds. Chapter14, American Chemical Society.

[71] Pickering, W. F. (1986). Metal ion speciation—soils and sediments (a review). Ore Geology Reviews, 1(1), 83-146.

[72] Langmur I., (1916). The constitution of Fundamental properties of solid and liquids. Journal Ameration chemistry society, 38(11), 2221-2295.

[73] Ma, J., Guo, H.M., Lei, M., Zhou, X.Y., Li, F.L., Yu, T., Wei, R.F., Zhang, H.Z., Zhang, X. and Wu, Y. (2015). Arsenic Adsorption and its Fractions on Aquifer Sediment: Effect of pH, Arsenic Species, and Iron/Manganese Minerals. Water Air and Soil Pollution, 226, 8.

[74] Crosby D.G. (1998). Environmental Toxicology and Chemistry. Oxford University Press, Oxford, 46.

[75] Shikuku, V. O., Donato, F. F., Kowenje, C. O., Zanella, R., and Prestes, O. D. (2015). A comparison of adsorption equilibrium, kinetics and thermodynamics of aqueous phase clomazone between faujasite X and a natural zeolite from Kenya. South African Journal of Chemistry, 68, 245-252.

[76] Ozeroglu, C., and Bilgiç, O. D. (2015). Use of the crosslinked copolymer functionalized with acrylic acid for the removal of strontium ions from aqueous solutions. Journal of Radioanalytical and Nuclear

Chemistry, 305(2), 551-565.

[77] Sengupta, A., Sk, J., Boda, A., and Ali, S. M. (2016). An amide functionalized task specific carbon nanotube for the sorption of tetra and hexa valent actinides: experimental and theoretical insight. RSC Advances, 6(46), 39553-39562.

[78] Kalkan, E., Nadaroglu, H., Celebi, N., Celik, H., and Tasgin, E. (2015). Experimental Study to Remediate Acid Fuchsin Dye Using Laccase-Modified Zeolite from Aqueous Solutions. Polish Journal of Environmental Studies, 24(1), 115-124.

[79] Kumar, P. S., and Kirthika, K. (2009). Equilibrium and kinetic study of adsorption of nickel from aqueous solution onto bael tree leaf powder. Journal of Engineering Science and Technology, 4(4), 351-363.

[80] Samuel, M.S., Abigail, E.A.M. and Chidambaram, R. (2015). Isotherm Modelling, Kinetic Study and Optimization of Batch Parameters Using Response Surface Methodology for Effective Removal of Cr (VI) Using Fungal Biomass. Plos One, 10, 3.

[81] Nadaroglu, H., Kalkan, E., Celebi, N., and Tasgin, E. (2015). Removal of Reactive Black 5 from wastewater using natural clinoptilolite modified with apolaccase. Clay Minerals, 50(1), 65-76.

[82] Bohn, L. H. Mcneal, L.B. O’connor and A. George (1979). Soil Chemistry. John Wily and Sons Inc., New York, Chap.6, 185.

[83] Mondal, P., and George, S. (2015). Removal of fluoride from drinking water using novel adsorbent magnesia-hydroxyapatite. Water, Air, & Soil Pollution, 226, 8.

[84] Jayakumar, R., Rajasimman, M. and Karthikeyan, C. (2015).

Optimization, equilibrium, kinetic, thermodynamic and desorption studies on the sorption of Cu (II) from an aqueous solution using marine green algae: Halimeda gracilis. Ecotoxicology and Environmental Safety, 121, 199-210.

[85] Cui, Y. W., Li, J., Du, Z. F., and Peng, Y. Z. (2016). Cr (VI) adsorption on red mud modified by lanthanum: performance, kinetics and mechanisms. PloS one, 11(9), e0161780.

[86] Wood, G. (2001). Affinity coefficients of the Polanyi / Dubinin adsorption isotherm equations A review with compilations and correlations. Carbon, 39, 343-356.

[87] Abigail, M.E.A., Samuel, M.S. and Chidambaram, R. (2015). Hexavalent chromium biosorption studies using Penicillium griseofulvum MSR1 a novel isolate from tannery effluent site: Box-Behnken optimization, equilibrium, kinetics and thermodynamic studies. Journal of the Taiwan Institute of Chemical Engineers, 49, 156-164.

[88] Ho, Y.S. (2015), Comment on. Genetic characterization, nickel tolerance, biosorption, kinetics, and uptake mechanism of a bacterium isolated from electroplating industrial effluent. Canadian Journal of Microbiology, 61 (11), 881-882.

[89] Shahwan, T. (2015). Lagergren equation: Can maximum loading of sorption replace equilibrium loading. Chemical Engineering Research and Design, 96, 172-176.

[90] Jayakumar, R., Rajasimman, M. and Karthikeyan, C. (2015). Optimization, equilibrium, kinetic, thermodynamic and desorption studies on the sorption of Cu (II) from an aqueous solution using marine green algae: Halimeda gracilis. Ecotoxicology and Environmental Safety, 121, 199-210

[91] Haciyakupoglu, S., Orucoglu, E., Esen, A.N., Yusan, S. and Erenturk, S. (2015). Kinetic modeling of selenium (IV) adsorption for remediation of contaminated aquatic systems based on mesoscale experiments. Desalination and Water Treatment, 56 (5), 1208-1216.

[92] Douven, S., Paez, C. A., and Gommes, C. J. (2015). The range of validity of sorption kinetic models. Journal of colloid and interface science, 448, 437-450.

[93] Ho, Y.S. (2014). Using of pseudo-second-order model in adsorption. Environmental Science and Pollution Research, 21 (11), 7234-7235.

[94] Vasheghani, F.B., Rajabi, F.H., Omidi, M.H. and Shabanian, S. (2015). Kinetics, equilibrium and thermodynamics of adsorption of 2-biphenyl amine and dibenzylamine from aqueous solutions by Fe3O4/bentonite nanocomposite. Russian Journal of Physical Chemistry A, 89 (5), 876-881.

[95] Ravichandran, P., Sowmya, A., and Meenakshi, S. (2012). Equilibrium and kinetic studies on the removal of basic violet 10 from aqueous solutions using activated carbons prepared from industrial wastes. Bioremediation Journal, 16(2), 86-96.

[96] Scholar, F. N. (2015). Academic Background. Journal of Educational Development, 33(5), 510-520.

[97] Yasmin B, CH, A, (2004). Studies of dyes using clay-based and activated carbon adsorb Adsorption ents. Thesis University sains Malaysia.

[98] Khari, F.A., Khatibzadeh, M., Mahmoodi, N.M. and Gharanjig, K. (2013). Removal of anionic dyes from aqueous solution by modifiedalginate. Desalination and Water Treatment, 51 (10-12), 2253-2260.

[99] Hussain, S.N., Asghar, H.M.A., Sattar, H., Brown, N.W. and Roberts, E.P.L. (2015). Removal of Tartrazine from Water by Adsorption with Electrochemical Regeneration. ChemicalEngineeringCommunications, 202 (10), 1280-1288.

[100] Wawrzkiewicz, M., Wigniewska, M., Gun'ko, V.M. and Zarko, V.I. (2015). Adsorptive removal of acid, reactive and direct dyes from aqueous solutions and wastewater using mixed silica-alumina oxide. Powder Technology, 278, 306-315.

[101] Sandeep Keshari Bhoi (2010). Adsorption characteristics of congo red dye on to PAC and GAC based on S/N ratio: a taguchi approach. A Project, ORISSA - 769 008, INDIA.

[102] Samoila, P., Cojocaru, C., Cretescu, I., Stan, C.D., Nica, V., Sacarescu, L. and Harabagiu, V. (2015). Nanosized Spinel Ferrites Synthesized by Sol-Gel Autocombustion for Optimized Removal of Azo Dye from Aqueous Solution. Journal of Nanomaterials, Article ID 713802, 13.

[103] Prodromou, M. and Pashalidis, I. (2013). Uranium adsorption by non-treated and chemically modified cactus fibers in aqueous solutions. Journal of Radioanalytical and Nuclear Chemistry, 298 (3), 1587-1595.

[104] Tumsek, F. and Avci, O. (2013). Investigation of Kinetics and Isotherm Models for the Acid Orange 95 Adsorption from Aqueous Solution onto Natural Minerals. Journal of Chemical and Engineering Data, 58 (3), 551-559.

[105] Toytziaridis, A., and Dicko, C. (2016). Fabrication and Optimization of Stable, Optically Transparent, and Reusable pH-Responsive Silk Membranes. International journal of molecular sciences, 17(11), 1897.

[106] Fan Zhang (2013). Controlling Adsorption Structure of Eosin Y Dye on Nanocrystalline TiO_2Films for Improved Photovoltaic Performances. Journal Physical Chemistry, 117 (28), 14659–14666.

[107] Kamaraj, R., and Vasudevan, S. (2016). Facile one-pot electrosynthesis of Al (OH) 3–kinetics and equilibrium modeling for adsorption of 2, 4, 5-trichlorophenoxyacetic acid from aqueous solution. New Journal of Chemistry, 40(3), 2249-2258.

[108] Jing, L., Xu, Z., Shang, J., Sun, X., Cai, W., and Guo, H. (2002). The preparation and characterization of ZnO ultrafine particles. Materials Science and Engineering: A, 332(1), 356-361.

[109] Wang, H., Xu, J. Z., Zhu, J. J., and Chen, H. Y. (2002). Preparation of CuO nanoparticles by microwave irradiation. Journal of crystal growth, 244(1), 88-94.

[110] Zhu, J., Li, D., Chen, H., Yang, X., Lu, L., and Wang, X. (2004). Highly dispersed CuO nanoparticles prepared by a novel quick-precipitation method. Materials Letters, 58(26), 3324-3327.

[111] Purkait, M. K., DasGupta, S., and De, S. (2005). Adsorption of eosin dye on activated carbon and its surfactant based desorption. Journal of environmental management, 76(2), 135-142.

[112] Porkodi, K., and Kumar, K. V. (2007). Equilibrium, kinetics and mechanism modeling and simulation of basic and acid dyes sorption onto jute fiber carbon: Eosin yellow, malachite green and crystal violet single component systems. Journal of hazardous materials, 143(1), 311-327.

[113] Guo, Z., Liang, X., Pereira, T., Scaffaro, R., and Hahn, H. T. (2007). CuO nanoparticle filled vinyl-ester resin nanocomposites: Fabrication, characterization and property analysis. Composites Science and Technology, 67(10), 2036-2044.

[114] Martinson, C. A., and Reddy, K. J. (2009). Adsorption of arsenic (III) and arsenic (V) by cupric oxide nanoparticles. Journal of Colloid and Interface Science, 336(2), 406-411.

[115] Yiamsawas, D., Boonpavanitchakul, K., and Kangwansupamonkon, W. (2009). Preparation of ZnO nanostructures by solvothermal method. Journal of Microscopy Society of Thailand, 23(1), 75-78.

[116] Goswami, A., Raul, P. K., and Purkait, M. K. (2012). Arsenic adsorption using copper (II) oxide nanoparticles. Chemical Engineering Research and Design, 90(9), 1387-1396.

[117] Sheela, T., Nayaka, Y. A., Viswanatha, R., Basavanna, S., and Venkatesha, T. G. (2012). Kinetics and thermodynamics studies on the adsorption of Zn (II), Cd (II) and Hg (II) from aqueous solution using zinc oxide nanoparticles. Powder Technology, 217, 163-170.

[118] Zena, M. A. (2012). Preparation and characterization of some nano metal oxides and their ferrites. Master Thesis, University of Diyala.

[119] Derikvandi, H., and Nezamzadeh-Ejhieh, A. (2017). Increased photocatalytic activity of NiO and ZnO in photodegradation of a model drug aqueous solution: Effect of coupling, supporting, particles size and calcination temperature. Journal of hazardous materials, 321, 629-638.

[120] Farghali, A. A., Bahgat, M., Allah, A. E., and Khedr, M. H. (2013). Adsorption of Pb (II) ions from aqueous solutions using copper oxide nanostructures. Beni-Suef University Journal of Basic and Applied Sciences, 2(2), 61-71.

[121] Srivastava, V., Gusain, D., and Sharma, Y. C. (2013). Synthesis, characterization and application of zinc oxide nanoparticles (n-ZnO). Ceramics International, 39(8), 9803-9808.

[122] Awwad, A. M., Albiss, B. A., and Salem, N. M. (2015). Antibacterial activity of synthesized copper oxide nanoparticles using Malva sylvestris leaf extract. SMU Med J, 2(1), 91-101.

[123] Zhang, F., Lan, J., Yang, Y., Wei, T., Tan, R., and Song, W. (2013). Adsorption behavior and mechanism of methyl blue on zinc oxide nanoparticles. Journal of nanoparticle research, 15(11), 2034.

[124] Mustafa, G., Tahir, H., Sultan, M., and Akhtar, N. (2013). Synthesis and characterization of cupric oxide (CuO) nanoparticles and their application for the removal of dyes. African Journal of Biotechnology, 12(47), 6650-6660.

[125] Nithya, K., Yuvasree, P., Neelakandeswari, N., Rajasekaran, N., Uthayarani, K., Chitra, M., and Kumar, S. S. (2014). Preparation and characterization of copper oxide nanoparticles. Int. J. ChemTech Res, 6(3), 2220-2222.

[126] Ghaedi, M., Ansari, A., Habibi, M. H., and Asghari, A. R. (2014). Removal of malachite green from aqueous solution by zinc oxide nanoparticle loaded on activated carbon: kinetics and isotherm study. Journal of Industrial and Engineering Chemistry, 20(1), 17-28.

[127] Fakhri, A. (2014). Assessment of ethidium bromide and ethidium monoazide bromide removal from aqueous matrices by adsorption on cupric oxide nanoparticles. Ecotoxicology and environmental safety, 104, 386-392.

[128] Nekouei, F., Nekouei, S., Tyagi, I., and Gupta, V. K. (2015). Kinetic, thermodynamic and isotherm studies for acid blue 129 removals from liquids using copper oxide nanoparticle-modified activated carbon as a novel adsorbent. Journal of Molecular Liquids, 201, 124-133.

[129] Naghizade Asl, M., Mahmodi, N. M., Teymouri, P., Shahmoradi, B., Rezaee, R., and Maleki, A. (2016). Adsorption of organic dyes using copper oxide nanoparticles: isotherm and kinetic studies. Desalination and Water Treatment, 57(52), 25278-25287.

[130] Dashamiri, S., Ghaedi, M., Dashtian, K., Rahimi, M. R., Goudarzi, A., and Jannesar, R. (2016). Ultrasonic enhancement of the simultaneous removal of quaternary toxic organic dyes by CuO nanoparticles loaded on activated carbon: central composite design, kinetic and isotherm study. Ultrasonics sonochemistry, 31, 546-557.

[131] Karim, H., Hassan, and Eman, R. (2017). Preparation and Characterization of Copper Oxide Nanoparticles Used to Remove Nickel Ions from Aqueous Solution. Diyala Journal for Pure Science, 13(2), 217-234.

[132] Amir, F., Dawood, Abd, A., Khudheir, A, and Marwa, I., Mubarak, (2017). Study Eosin Dye Adsorption on the Surface Waste of Molasses Dates Production. Diyala Journal for Pure Science, 13(1), 22-41.

[133] Liu, M., Dong, F., Kang, W., Sun, S., Wei, H., Zhang, W., and Liu, Y. (2014). Biosorption of strontium from simulated nuclear wastewater by Scenedesmus spinosus under culture conditions: adsorption and bioaccumulation processes and models. International journal of environmental research and public health, 11(6), 6099-6118.

[134] Cottet, L., Almeida, C. A. P., Naidek, N., Viante, M. F., Lopes, M. C., and Debacher, N. A. (2014). Adsorption characteristics of montmorillonite clay modified with iron oxide with respect to methylene blue in aqueous media. Applied Clay Science, 95, 25-31.

[135] Smaranda, C., Gavrilescu, M., and Bulgariu, D. (2011). Studies on sorption of Congo red from aqueous solution onto soil. International Journal of Environmental Research, 5(1), 177-188.

[136] Baig, S. A., Sheng, T., Sun, C., Xue, X., Tan, L., and Xu, X. (2014). Arsenic removal from aqueous solutions using Fe3O4-HBC composite: effect of calcination on adsorbents performance. PloS one, 9(6), e100704.

[137] Srivastava, V. C., Swamy, M. M., Mall, I. D., Prasad, B., and Mishra, I. M. (2006). Adsorptive removal of phenol by bagasse fly ash and activated carbon: equilibrium, kinetics, and thermodynamics. Colloids and Surfaces A: Physicochemical and Engineering Aspects, 272(1), 89-104.

[138] Amir, F., Dawood, Abd, A., Khudheir, A, and Marwa, I., Mubarak, (2017). Study Eosin Dye Adsorption on the Surface Wheat Chaff. Diyala Journal for Pure Science, 13(1), 42-59.

[139] Fernandez-Garcia, M., Martinez-Arias, A., Hanson, J. C., and Rodriguez, J. A. (2004). Nanostructured oxides in chemistry: characterization and properties. Chemical Reviews, 104(9), 4063-4104.

[140] Shifu, C., Wei, Z., Sujuan, Z., and Wei, L. (2009). Preparation, characterization and photocatalytic activity of N-containing ZnO powder. Chemical Engineering Journal, 148(2-3), 263-269.

[141] Fungaro, D. A., Borrely, S. I., and Carvalho, T. E. (2013). Surfactant modified zeolite from cyclone ash as adsorbent for removal of Reactive Orange 16 from aqueous solution. American Journal of Environmental Protection, 1(1), 1-9.

[142] Chen, J. J., Ahmad, A. L., and Ooi, B. S. (2013). Poly (N-isopropylacrylamide-co-acrylic acid) hydrogels for copper ion adsorption: Equilibrium isotherms, kinetic and thermodynamic studies. Journal of Environmental Chemical Engineering, 1(3), 339-348.

المستخلّـــص

في هذا الدراسة . تم تحضير اوكسيد الخارصين (ZnO) واوكسيد النحاس (CuO) النانوية بطريقة الترسيب. تم تشخيص الاكاسيد المحضرة بتقنيات (FTIR, AFM SEM, XRD و BET). وتم استخدام حيود الاشعة السينية (XRD) لوصف التبلور للأكاسيد النانوية وتم حساب حجم الدقائق باستخدام معادلة ديباي شيرر, وكانت الحجوم للأوكسيد النحاس ولأوكسيد الخارصين (23.4 , 47,8) نانومتر على التوالي عند درجة حرارة الكلسنة 400 م^{o}. وهذا يتفق مع تقنيات (AFM ,BET,FTIR و SEM). وتم استخدام المجهر الالكتروني الماسح (SEM) ومجهر القوة الذري (AFM) لوصف تركيب الاكاسيد. اما المساحة السطحية فكانت (35,635 و 6,704) م^{2}/غم للأكاسيد (CuO و ZnO) على التوالي.

استخدمت الاكاسيد النانوية المحضرة لإزالة صبغة الايوسين من محاليلها المائية. أشتمل البحث على دارسة العوامل المؤثرة في عملية الامتزاز والتي تتضمن تأثير التركيز الابتدائي للصبغة [2-20] أجزاء لكل مليون والدالة الهيدروجينية للوسط [1-10] وزمن اتزان [10-140] دقيقة وزن المادة المازة [0,09-0,01]غم ودرجة الحرارة [20-40] م^{o} , تم اجراء تجارب الامتزاز بطريقة الوجبة.

درست ايزوثيرمات الامتزاز والحركية والدوال الثرموديناميكية لأمتزازصبغة الايوسين عند تركيز ثابت للصبغة (10) جزء في مليون ووزن السطح الماز الامثل (0,04)غم والدالة الهيدروجينية (7) عند درجات حرارية مختلفة (20-40) م^{o} . أظهرت النتائج ان افضل زمن اتزان لسطح CuO (50) دقيقة ولسطح ZnO (120) دقيقة. النسبة المئوية لإزالة صبغة الايوسين ازدادت بازدياد زمن الاتزان, بلغت النسبة المئوية لامتزاز صبغة الايوسين على سطح CuO (91,05%) وعلى سطح ZnO (40,82%).

تم تحليل نتائج امتزاز صبغة الايوسين على السطوح المازة باستخدام ايزوثيرمات لانكماير وفريندلج ودوبنين و تمكن . اعطت نتائج التحليل علاقة خطية ومعاملات ارتباط عالية لأيزوثيرم دوبنين بالنسبة لسطح CuO بينما ايزوثيرم فريندلج هو المناسب مع سطح ZnO. بالاستعانة بالنتائج التي تم الحصول عليها من دراسة الامتزاز في الدرجات الحراية المختلفة .

تم احتساب قيم الدوال الثرموديناميكية ($\Delta G, \Delta H, \Delta S$) بتطبيق معادلة فانت هوف لامتزاز صبغة الايوسين على الاسطح المازة المستخدمة . ان قيم (ΔG) السالبة لسطح CuO وZnO مؤشر الى ان الامتزاز يحصل تلقائيا. قيم (ΔH) تكون سالبة لكلا السطحين اي ان الامتزاز باعث للحرارة ومؤشر الى ان الامتزاز فيزيائي لان قيمه اقل من 40 كيلو جول /مول. فضلا عن قيم ($E <8$) كيلوجول/مول والتي تشير الى ان القوى الفيزيائية تؤثر في الامتزاز. اما قيم (ΔS) تكون سالبة لسطح CuO اي ان الجزيئات الممتزة لصبغة الايوسين تنتظم على السطح اكثر من المحلول في حين قيم (ΔS) تكون موجبة لسطح ZnO اي ان الجزيئات غير مقيدة ولاتزال في حركة مستمرة على السطح.

تم اجراء دراسة حركية الامتزاز بتطبيق المرتبة الاولى الكاذبة بأستخدام نموذج (Largergreen) والمرتبة الثانية الكاذبة واعطت نتائج الدراسة معاملات ارتباط عالية للمرتبة الثانية الكاذبة .امتزاز صبغة الايوسين على كلا السطحين يتبع حركية المرتبة الثانية الكاذبة.

وزارة التعليم العالي والبحث العلمي

جامعة ديالى

كلية العلوم

قسم الكيمياء

إزالة صبغة الايوسين من المحاليل المائية بأستخدام سطوح نانوية

رسالة

مقدمة الى مجلس كلية العلوم/ جامعة ديالى وهي جزء من متطلبات
الحصول على شهادة الماجستير في علوم الكيمياء

من قبل الطالبة

دنيا احمد عبد اللطيف

بكالوريوس علوم الكيمياء / جامعة ديالى 2015

بأشراف

أ. د. عامر فاضل داود
أ.م. د. غالب ادريس عطية

2018 م
1439 هـ